Biomaterials Translational

CONTENTS Quarterly Established in December 2020. Volume 4, Issue 2 June 28, 2023

EDITORIAL

VIEWPOINT

REVIEWS

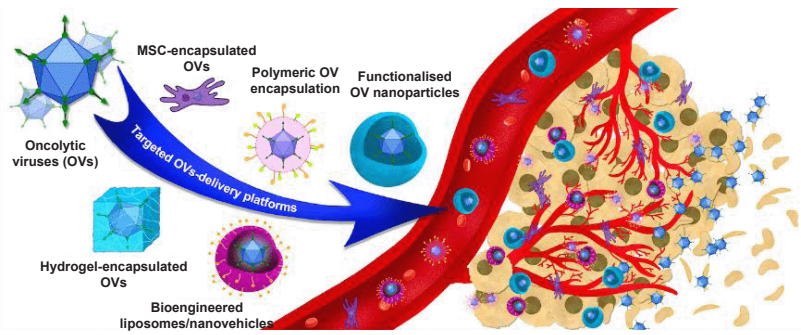

The recent progress in genetic engineering, the design of systemic delivery carriers, and targeted delivery platforms will provide more opportunities for oncolytic viruses (OVs) with enhanced anti-tumour immunity, safety, and efficacy in cancer treatment. This review will discuss the mechanism, rational design, recent clinical trials, applications, and the development of targeted delivery platforms for OVs.

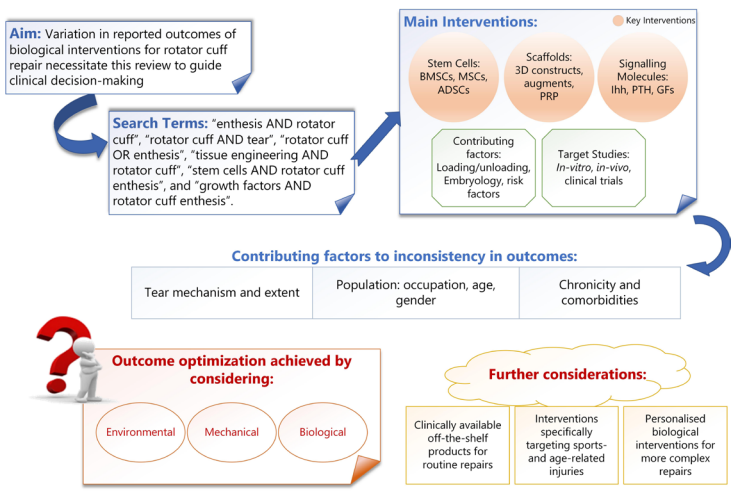

Biological methodologies for rotator cuff enthesis and their reported outcomes vary, challenging repair strategies. This review stratifies the existing literature into different categories, guiding decision-making with respect to repair approaches. Outcomes highlight the importance of tailoring interventions according to tear extent, chronicity, and the population treated.

RESEARCH ARTICLES

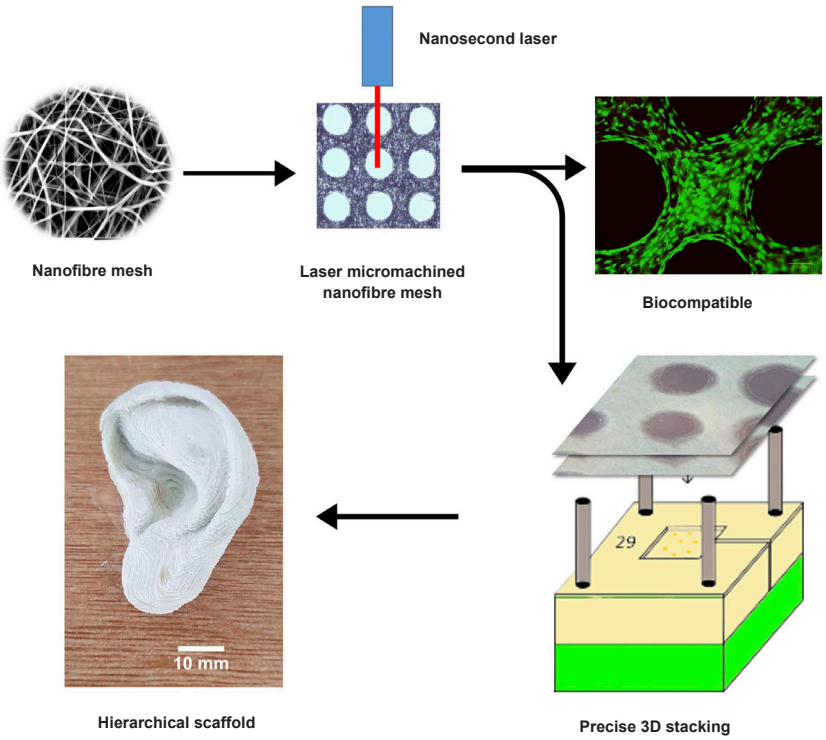

Three-dimensional (3D) biofabrication method is developed using the combined nanosecond laser micromachined nanofibre meshes and precision 3D stacking to produce the hierarchical structure of bone scaffold.

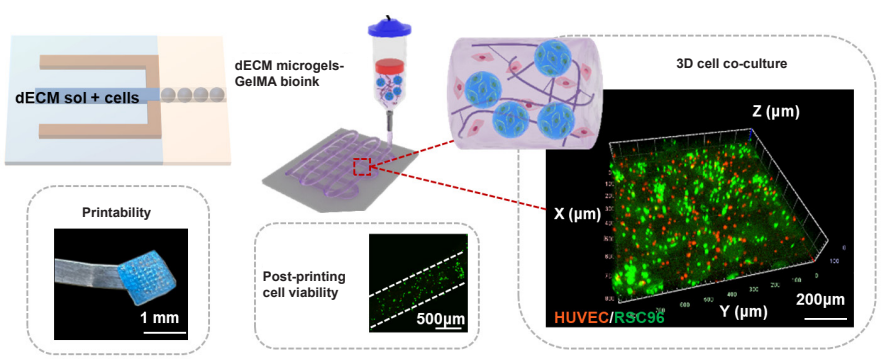

Cell-laden decellularised extracellular matrix (dECM) microgels fabricated by microfluidic emulsification were used as the discrete phase for cell protection from shear damage, and gelatin methacrylate served as the continuous phase to form modular bioinks with good printability after extrusion-based bioprinting, high post-printing cell viability, and feasibility of three-dimensional (3D) cell co-culture system.

Carrying passion in a numerical world

*Qian Wang**

We are immersed in a world where success is quantified by numbers. Whether it's salaries, signing bonuses, social media metrics, or exposure frequencies, our evaluation systems have become obsessed with various indices. As researchers, our worth is frequently measured not by the creativity and impact of our work, but rather by the awards we receive, the dollar amounts of our grants, the number of publications we have, and the citations we accumulate. Likewise, as an editor, I find myself constantly reflecting on the most objective criteria for evaluating the success of our journal.

In 2022, a historic event unfolded within the science community. For the fifth time, an individual received the Nobel Prize for the second time. This outcome did not come as a surprise to those familiar with the current chemistry literature. Predictions had long circulated that Barry Sharpless would be honored with a second Nobel Prize in Chemistry for his groundbreaking invention of the concept of "Click Chemistry".[1] This concept, without exaggeration, has revolutionised organic chemistry, chemical biology, materials sciences, and related research fields.

Learning that Barry had indeed received this prestigious recognition filled me with uncontainable elation. It wasn't solely because Barry had been one of my mentors throughout my career development. Rather, it was the privilege of witnessing how the concept of Click Chemistry was initially ridiculed, gradually recognised, suddenly popularised, and ultimately worshipped by the science community. It underscored the power of philosophical scientific thinking and how the passion of one individual can transform an entire scientific community.[2]

Among my countless interactions with Barry, one encounter stands out vividly in my memory. It occurred at the atrium of the Backman building at the Scripps Research Institute. By chance, we crossed paths, and Barry approached me with his familiar enthusiasm, eager to discuss a recent discovery in his lab: a solvent-free reaction that forms amides from acids and amines. While this reaction procedure may seem practical and "cute," it is a common organic transformation taught in Organic Chemistry, typically performed in a solvent system with a catalyst. I was struck by Barry's unwavering passion for this research question. How could a world-renowned scientist and Nobel Laureate be genuinely excited about such a "trivial" experiment?

This incident brought to my mind Irving Stone's book, "*The Agony and the Ecstasy*," which powerfully portrays Michelangelo's devotion to sculpture. Stone eloquently states, "*For him, the milky white marble was a living, breathing substance that felt, sensed, judged. He could not permit himself to be found wanting. It was not fear but reverence. In the back of his mind, a voice said: 'This is love.'*"[3] Michelangelo's dedication stemmed from a profound passion that gave him the courage to challenge the prejudice against sculpture at his time beliefs and fulfill his ultimate destiny.

Yes, passion!

When discussing my expectations for graduate students, I often express my desire for them to have a passion for learning and a genuine interest in their projects. In a world fixated on numerical measures of success, it is crucial to reevaluate our standards and embrace the enduring power of passion. The story of Barry Sharpless and his unwavering excitement for a seemingly "trivial" experiment serves as a reminder that true greatness arises not from accolades or predictions, but from an unyielding love, an unyielding passion, for one's own work.

Nearly 3 years have passed since I joined the editorial team of Biomaterials Translational, providing a unique platform for our readers. We have overcome numerous challenges and endured the hardships posed by the coronavirus

Department of Chemistry and Biochemistry, University of South Carolina, Columbia, SC, USA

***Corresponding author:** Qian Wang, Wang263@mailbox.sc.edu.

http://doi.org/10.12336/biomatertransl.2023.02.001

How to cite this article: Wang, Q. Carrying passion in a numerical world. *Biomater Transl.* **2023**, *4*(2), 63-64.

disease 2019 (COVID-19) pandemic. As I proudly serve in my role as an editor, I carry with me the profound impact of this journey and the understanding that success should not be reduced to mere numbers. Instead, it should be defined by the passionate pursuit of excellence.

In this issue of *Biomaterials Translational*, we provide one viewpoint essay,[4] two review papers[5, 6] and two research articles.[7, 8] As before, we hope these works can point the direction of this exciting research field.

Thank you for reading!

1. Kolb, H. C.; Finn, M. G.; Sharpless, K. B. Click Chemistry: Diverse Chemical Function from a Few Good Reactions. *Angew Chem Int Ed Engl.* **2001**, *40*, 2004-2021.
2. Wang, Q.; Hawker, C. Toward a few good reactions: celebrating click chemistry's first decade. *Chem Asian J.* **2011**, *6*, 2568-2569.
3. Stone, I. *The Agony and the Ecstasy: A Biographical Novel of Michelangelo.* New American Library: New York, 1963.
4. Chen, X.; Peng, Y. Wearable bioelectronic system for wound healing and management. *Biomater Transl.* **2023**, *4*, 65-66.
5. Kingsak, M.; Meethong, T.; Jongkhumkrong, J.; Cai, L.; Wang, Q. Therapeutic potential of oncolytic viruses in the era of precision oncology. *Biomater Transl.* **2023**, *4*, 67-84.
6. Abdalla, A.; Pendegrass, C. Biological approaches to the repair and regeneration of the rotator cuff tendon-bone enthesis: a literature review. *Biomater Transl.* **2023**, *4*, 85-103.
7. McWilliam, R. H.; Chang, W.; Liu, Z.; Wang, J.; Han, F.; Black, R. A.; Wu. J.; Luo, X.; Li, B.; Shu, W. Three-dimensional biofabrication of nanosecond laser micromachined nanofibre meshes for tissue engineered scaffolds. *Biomater Transl.* **2023**, *4*, 104-114.
8. Chu, H.; Zhang, K.; Rao, Z.; Song, P.; Lin, Z.; Zhou, J.; Yang, L.; Quan, D.; Bai, Y. Harnessing decellularised extracellular matrix microgels into modular bioinks for extrusion-based bioprinting with good printability and high post-printing cell viability. *Biomater Transl.* **2023**, *4*, 115-127.

Wearable bioelectronic system for wound healing and management

*Xuanzuo Chen, Yizhong Peng**

Department of Orthopaedics, Union Hospital, Tongji Medical College, Huazhong University of Science and Technology, Wuhan, Hubei Province, China

***Corresponding author:**
Yizhong Peng,
pyz5941z@163.com.

http://doi.org/10.12336/biomatertransl.2023.02.002

How to cite this article:
Chen, X.; Peng, Y. Wearable bioelectronic system for wound healing and management. *Biomater Transl.* **2023**, *4*(2), 65-66.

Chronic wounds are a significant healthcare challenge, affecting millions of people worldwide.[1] Chronic wounds do not heal within a normal time frame, which leads to severe complications such as infection, amputation, and even death.[2] Chronic wounds can be caused by a variety of factors, including diabetes, vascular disease, and pressure sores.[3] One of the treatments for infected chronic wounds is the use of antibiotics, which depends on the type of infection present.[3] In some cases, surgical debridement may also be necessary to remove infected tissue and promote healing.[1] Chronic wounds often require a multi-faceted treatment approach, and there can be challenges associated with finding the right treatment. One of the biggest challenges is the development of antibiotic resistance, which can make it difficult to treat infections.[4] Additionally, chronic wounds can be slow to heal and may require ongoing care and treatment.[1] It is important to work closely with a healthcare professional to determine the appropriate treatment plan for a chronic wound and to monitor progress regularly to ensure that the wound is healing properly.

Biomaterials such as dressings, scaffolds, and hydrogels can deliver therapeutic agents such as growth factors or antibiotics and provide a supportive environment for wound healing.[5] One promising biomaterial is biodegradable scaffolds that can provide a physical scaffold for cells to grow and proliferate.[6] These scaffolds can be designed to degrade over time, allowing for the gradual release of therapeutic agents and the eventual regeneration of new tissue.[7, 8] Another biomaterial that has shown promise is hydrogels, which can form a gel-like matrix that can hold and deliver therapeutic agents.[9] Hydrogels form a moist environment for wound healing, which is important for promoting cell migration and proliferation.[10] Biomaterials offer a promising approach to the treatment of chronic wounds. These materials provide a supportive environment for wound healing and can also deliver therapeutic agents to promote healing.

Wound management is an important aspect of healthcare, and recent advancements in technology have provided new opportunities for preventing these complications and achieving effective wound healing.[1] Wearable bioelectronic systems and biomaterials are promising solutions for the treatment of chronic wounds, offering real-time monitoring and treatment as well as supportive environments for wound healing.[11] Shirzaei Sani et al.[12] reported a wearable patch that wirelessly and continuously monitors the physiological conditions of the wound bed via a custom-developed multiplexed multimodal electrochemical biosensor array and performs noninvasive combination therapy through controlled anti-inflammatory antimicrobial treatment and electrically stimulated tissue regeneration (**Figure 1**).

Wearable bioelectronic systems have emerged as a promising solution for wound management due to their ability to constantly monitor and regulate wound conditions.[11] These systems consist of a wearable device that is placed directly on the wound and is equipped with sensors and bioelectronic components.[13] The sensors are used to monitor wound conditions such as temperature, pH, and moisture levels.[14] The bioelectronic components are then used to deliver appropriate treatments, such as electrical stimulation or drug delivery, to promote healing.[11, 15] One of the key advantages of wearable bioelectronic systems is their ability to provide real-time monitoring and treatment.[16] This allows for timely interventions and can prevent complications that may arise from delayed treatment. Additionally, these systems are non-invasive and can be worn for extended periods, allowing for continuous monitoring and treatment.[17] Wearable systems have already shown promising results in pre-clinical trials and are now being tested in clinical trials (NCT03948360). These systems have the potential to revolutionize wound management and improve patient outcomes.

In conclusion, wearable bioelectronic systems offer a promising solution for wound healing and management. These systems are non-invasive,

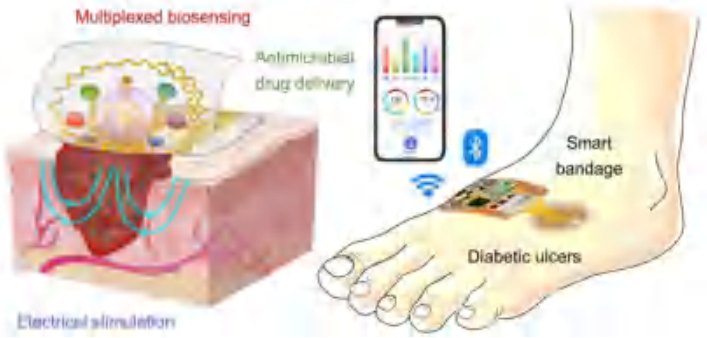

Figure 1. A wireless stretchable and wearable bioelectronic system for multiplexed monitoring and treatment of chronic wounds.[12] Copyright © 2023 Shirzaei Sani et al., some rights reserved; exclusive licensee American Association for the Advancement of Science.

and provide real-time monitoring and conditional responsive treatment for chronic wounds. As technology continues to advance, it is likely that wearable bioelectronic systems will become more widely available and have an even greater impact on healthcare.

Author contributions

YP: Conceptualization, resources, writing-review & editing, supervision, project administration; XC: writing-original draft, writing-review & editing. Both authors approved the final version of the manuscript.

Financial support

This work was supported by the National Natural Science Foundation of China, No. 82202764 and the China Postdoctoral Science Foundation, No. 2021M701331.

Acknowledgement

None.

Conflicts of interest statement

The authors declare that they have no known competing financial interests or personal relationships that could have influenced the work reported in this study.

Open access statement

This is an open access journal, and articles are distributed under the terms of the Creative Commons Attribution-NonCommercial-ShareAlike 4.0 License, which allows others to remix, tweak, and build upon the work noncommercially, as long as appropriate credit is given and the new creations are licensed under the identical terms.

1. Jones, R. E.; Foster, D. S.; Longaker, M. T. Management of chronic wounds-2018. *JAMA.* **2018**, *320*, 1481-1482.
2. Wilkinson, H. N.; Hardman, M. J. Wound healing: cellular mechanisms and pathological outcomes. *Open Biol.* **2020**, *10*, 200223.
3. Morton, L. M.; Phillips, T. J. Wound healing and treating wounds: differential diagnosis and evaluation of chronic wounds. *J Am Acad Dermatol.* **2016**, *74*, 589-605; quiz 605-606.
4. Da Silva, J.; Leal, E. C.; Carvalho, E. Bioactive antimicrobial peptides as therapeutic agents for infected diabetic foot ulcers. *Biomolecules.* **2021**, *11*, 1894.
5. Chen, T. Y.; Wen, T. K.; Dai, N. T.; Hsu, S. H. Cryogel/hydrogel biomaterials and acupuncture combined to promote diabetic skin wound healing through immunomodulation. *Biomaterials.* **2021**, *269*, 120608.
6. Nakkala, J. R.; Li, Z.; Ahmad, W.; Wang, K.; Gao, C. Immunomodulatory biomaterials and their application in therapies for chronic inflammation-related diseases. *Acta Biomater.* **2021**, *123*, 1-30.
7. Choudhury, H.; Pandey, M.; Lim, Y. Q.; Low, C. Y.; Lee, C. T.; Marilyn, T. C. L.; Loh, H. S.; Lim, Y. P.; Lee, C. F.; Bhattamishra, S. K.; Kesharwani, P.; Gorain, B. Silver nanoparticles: advanced and promising technology in diabetic wound therapy. *Mater Sci Eng C Mater Biol Appl.* **2020**, *112*, 110925.
8. Emmert, S.; Pantermehl, S.; Foth, A.; Waletzko-Hellwig, J.; Hellwig, G.; Bader, R.; Illner, S.; Grabow, N.; Bekeschus, S.; Weltmann, K. D.; Jung, O.; Boeckmann, L. Combining biocompatible and biodegradable scaffolds and cold atmospheric plasma for chronic wound regeneration. *Int J Mol Sci.* **2021**, *22*, 9199.
9. Kharaziha, M.; Baidya, A.; Annabi, N. Rational design of immunomodulatory hydrogels for chronic wound healing. *Adv Mater.* **2021**, *33*, e2100176.
10. Qian, Z.; Wang, H.; Bai, Y.; Wang, Y.; Tao, L.; Wei, Y.; Fan, Y.; Guo, X.; Liu, H. Improving chronic diabetic wound healing through an injectable and self-healing hydrogel with platelet-rich plasma release. *ACS Appl Mater Interfaces.* **2020**, *12*, 55659-55674.
11. Wang, C.; Sani, E. S.; Gao, W. Wearable bioelectronics for chronic wound management. *Adv Funct Mater.* **2022**, *32*, 2111022.
12. Shirzaei Sani, E.; Xu, C.; Wang, C.; Song, Y.; Min, J.; Tu, J.; Solomon, S. A.; Li, J.; Banks, J. L.; Armstrong, D. G.; Gao, W. A stretchable wireless wearable bioelectronic system for multiplexed monitoring and combination treatment of infected chronic wounds. *Sci Adv.* **2023**, *9*, eadf7388.
13. Pal, A.; Goswami, D.; Cuellar, H. E.; Castro, B.; Kuang, S.; Martinez, R. V. Early detection and monitoring of chronic wounds using low-cost, omniphobic paper-based smart bandages. *Biosens Bioelectron.* **2018**, *117*, 696-705.
14. Brown, M. S.; Ashley, B.; Koh, A. Wearable technology for chronic wound monitoring: current dressings, advancements, and future prospects. *Front Bioeng Biotechnol.* **2018**, *6*, 47.
15. Chen, H.; Cheng, Y.; Tian, J.; Yang, P.; Zhang, X.; Chen, Y.; Hu, Y.; Wu, J. Dissolved oxygen from microalgae-gel patch promotes chronic wound healing in diabetes. *Sci Adv.* **2020**, *6*, eaba4311.
16. Mohamed Salleh, N. A. B.; Tanaka, Y.; Sutarlie, L.; Su, X. Detecting bacterial infections in wounds: a review of biosensors and wearable sensors in comparison with conventional laboratory methods. *Analyst.* **2022**, *147*, 1756-1776.
17. Sharifuzzaman, M.; Chhetry, A.; Zahed, M. A.; Yoon, S. H.; Park, C. I.; Zhang, S.; Chandra Barman, S.; Sharma, S.; Yoon, H.; Park, J. Y. Smart bandage with integrated multifunctional sensors based on MXene-functionalized porous graphene scaffold for chronic wound care management. *Biosens Bioelectron.* **2020**, *169*, 112637.

Received: May 3, 2023
Revised: May 20, 2023
Accepted: June 16, 2023
Available online: June 28, 2023

Biomaterials Translational

Therapeutic potential of oncolytic viruses in the era of precision oncology

Monchupa Kingsak[1], Thongpon Meethong[1], Jinnawat Jongkhumkrong[1], Li Cai[2], Qian Wang[1,]*

Key Words:
anti-cancer; applications; delivery platform; genetic modification; mechanism; oncolytic virus

From the Contents

ABSTRACT

Oncolytic virus (OV) therapy has been shown to be an effective targeted cancer therapy treatment in recent years, providing an avenue of treatment that poses no damage to surrounding healthy tissues. Not only do OVs cause direct oncolysis, but they also amplify both innate and adaptive immune responses generating long-term anti-tumour immunity. Genetically engineered OVs have become the common promising strategy to enhance anti-tumour immunity, safety, and efficacy as well as targeted delivery. The studies of various OVs have been accomplished through phase I-III clinical trial studies. In addition, the uses of carrier platforms of organic materials such as polymer chains, liposomes, hydrogels, and cell carriers have played a vital role in the potentially targeted delivery of OVs. The mechanism, rational design, recent clinical trials, applications, and the development of targeted delivery platforms of OVs will be discussed in this review.

1 Department of Chemistry and Biochemistry, University of South Carolina, Columbia, SC, USA; 2 Department of Chemistry, University of South Carolina Lancaster, Lancaster, SC, USA

***Corresponding author:**
Qian Wang,
Wang263@mailbox.sc.edu.

http://doi.org/10.12336/biomatertransl.2023.02.003

How to cite this article:
Kingsak, M.; Meethong, T.; Jongkhumkrong, J.; Cai, L.; Wang, Q. Therapeutic potential of oncolytic viruses in the era of precision oncology. *Biomater Transl.* **2023**, *4*(2), 67-84.

Introduction

Cancer is a major public health problem worldwide, accounting for almost 10 million cancer deaths and over 19 million new cancer cases in 2020.[1] In 2022, the estimated numbers of new cancer cases and deaths in the United States are 1,918,030 and 609,360 people, respectively.[2] Chemotherapy is a major therapeutic approach to cancer treatment. However, success of chemotherapy has been limited due to a lack of selectivity toward cancer cells, rapid drug metabolism, and multidrug resistance, mainly resulting from increased efflux pumps in the cell membrane which transport various anti-cancer drugs out of the cells.[3,4] In addition, conventional chemotherapy may significantly damage healthy cells causing harmful side effects in patients.[5,6]

Oncolytic virus (OV) therapy has recently been recognised as a promising new therapeutic strategy in cancer treatment, which can circumvent some drawbacks of conventional chemotherapy. Due to their ability to specifically target and lyse tumour cells without harming surrounding healthy cells, as well as induce anti-tumour effects by multiple action mechanisms, OV can decrease the emergence of acquired drug resistance.[7-9] In addition to direct oncolysis, it can also amplify both innate and adaptive immune responses generating long-term anti-tumour immunity.[9-11] The targeted delivery and anti-tumour immunity are critical for potential applications of OVs in cancer therapy. However, a key challenge facing oncolytic virotherapy is the anti-viral immune responses from vaccinated patients, which may lead to viral clearance that limits the overall therapeutic efficacy of OVs. Thus extensive research efforts have been aimed to engineer OVs for improving their efficacy, safety, tumour-specific targeting, viral delivery, and anti-tumour immune evasion.[12,13] The literature retrieval strategy of this review is shown in **Additional file 1**.

Mechanism and Rational Design of Oncolytic Viruses

OVs utilise several mechanisms to preferentially enter and replicate in cancer cells. Many OVs have a natural tropism for the surface receptors

that irregularly overexpressed on cancer cell surfaces such as CD46, CD54, CD55, CD155, laminin, integrin α2β1, etc.[13-15] OVs can utilise and recognize those receptors to enter the targeted cancer cells as shown in **Table 1**. For example, adenovirus utilises coxsackievirus and adenovirus receptor (CAR) as a primary receptor to ensure attachment, and cell surface integrins (αvβ3 and αvβ5) to further facilitate viral internalization.[16] CAR expression is upregulated in basal cell carcinoma, thyroid adenoma, lung, ovarian, cervical, and laryngeal cancer cells.[17] Herpesvirus utilises herpesvirus entry mediator known as tumour necrosis factor receptor superfamily-14 for cell entry, which is overexpressed in breast cancer, gastric cancer, and hepatocellular carcinoma.[18, 19] Parvovirus H1 (H-1PV) utilises sialic acid residue presented on laminin for cell binding and enters cells via clathrin-mediated endocytosis.[20,21] In addition, a recent study found that galectin-1 also plays a key role in the cell entry of H-1PV.[22] H-1PV shows anti-cancer activity toward a variety of cancers, such as glioma, melanoma, pancreatic, breast, lung, cervical, and colon cancer.[23, 24] Coxsackievirus utilises CD54 and CD55 receptors as the primary and secondary points of viral attachment and internalization, which are overexpressed in malignant glioma, myeloma, melanoma, head and neck, lung, colon, pancreatic, and breast cancer cells.[25, 26] Poliovirus utilises the CD155 receptor, which is overexpressed in colorectal carcinoma, glioblastoma, melanoma, sarcoma, hepatocellular carcinoma, non-small-cell lung carcinoma, and pancreatic cancer cells.[27-30] Measles virus utilises CD46 receptor which is overexpressed in some cancer cells such as myeloma, hepatocellular carcinoma, colorectal, prostate, ovarian, and breast cancer cells.[14, 31] Normally, CD46 protects healthy cells from cell elimination by complement attack.[31] Vesicular stomatitis virus (VSV) utilises low-density lipoprotein receptor as a major receptor and other low-density lipoprotein receptor family members as alternatives for attachment and cell entry.[32, 33] Cancer cells that are susceptible to VSV are glioblastoma, melanoma, osteosarcoma, hepatocellular carcinoma, breast, cervical, and pancreatic cancer cells.[34] Sindbis virus enters cells through laminin receptor, which is overexpressed in uterine adenocarcinoma, melanoma, colorectal carcinoma, breast carcinoma, and non-small cell lung carcinoma.[35-39] Echovirus utilises integrin α2β1 as its cellular receptor for cell entry, which is overexpressed in ovarian, prostate, and gastric cancer cells.[40, 41] Newcastle disease virus binds to a sialic acid receptor for virus attachment to host cells, which demonstrates anti-cancer activity toward glioma and melanoma, renal cell carcinoma, ovarian, and cervical cancer.[42-45]

Table 1. The cell entry receptor and the aberrant oncogenic signalling pathway that OVs utilise to preferentially enter and replicate in cancer cells

Virus					
Genome type	Name of the OV	Enveloped	Cell entry receptors	Aberrant oncogenic signalling pathway	References
DNA	Adenovirus	N	CAR, integrins	PKR, Rb and p16	14, 16, 46
	Herpesvirus	Y	HVEM	PKR, Rb and p16	14, 18, 19, 46
	Parvovirus H1	N	Sialic acid, galectin-1	–	20-22
	Vaccinia virus	Y	–	RAS, PKR, Rb and p16, IFN-1	14, 46
RNA	Coxsackievirus	N	ICAM-1 (CD54), DAF (CD55)	–	25, 26
	Poliovirus	N	CD155	–	27-30
	Measles virus	Y	CD46	–	14, 31
	Vesicular stomatitis virus	Y	LDLR	IFN-1	14, 32, 33
	Sindbis virus	Y	LAMR	–	35-39
	Echovirus	N	Integrin a2b1	–	40, 41
	Reovirus	N	–	RAS, PKR, Rb and p16	14, 46
	Newcastle disease virus	Y	Sialic acid	Bcl-xL, IFN-1	14, 44-46, 57

Note: Bcl-xL: B-cell lymphoma-extra large; CAR: coxsackievirus and adenovirus receptor; DAF: decay-accelerating factor; HVEM: herpesvirus entry mediator; ICAM-1: intercellular adhesion molecule 1; IFN-1: type I interferon; LAMR: laminin receptor; LDLR: low-density lipoprotein receptor; N: no; p16: tumour suppressor protein; PKR: protein kinase R; RAS: rat sarcoma; Rb: retinoblastoma; Y: yes.

Furthermore, OVs exploit aberrant signalling pathways and can replicate in tumour cells, which have defects in anti-viral pathways.[13,14] Cancer cells promote their survival, proliferation, and metastasis by manipulating cellular transcriptional and signalling pathways.[46] Additionally, cell cycle and cell proliferation in tumour may be disrupted by oncogenes and the deficit of tumour suppressor genes, which allows OVs to survive longer in cancer cells.

In healthy cells, the natural cellular defense mechanisms in response to viral infection, including interferon (IFN) and protein kinase R (PKR) signalling pathways, induce infected cells to undergo apoptosis and viral clearance.[14] Type I IFN (IFN-1) is a cytokine in an early host defense that occurred prior to the immune response and possesses anti-viral activity.[47-49] Stimulating the release of IFN-1 during the viral infection triggers the intracellular signalling pathway, mainly

Janus kinase-signal transducers and activators of transcription pathway, and eventually limits viral replication and enhances the rate of viral clearance and the immune responses in infected cells.[47] Additionally, the activation of IFN-1 pathway induces PKR expression and activation.[50] PKR is a major host defense against viruses and can be activated by viral-specific RNAs.[47] The activated PKR phosphorylates the eukaryotic translation initiation factor 2, resulting in the inhibition of protein translation and synthesis, and consequently suppressing viral replication and spreading.[51] PKR also involves in cellular differentiation, proliferation, and apoptosis.[52]

In contrast, PKR and IFN in regulating viral clearance on cancer cells are impaired.[50] Rising metabolic activity of cancer cells also enhances viral replication and the rate of cell lysis compared to healthy cells.[53] These aberrant signalling pathways of carcinogenesis render cancer cells susceptible to viral infection, which is summarised in **Table 1**. Some OVs naturally exploit the aberrant expression of various proteins usually involved in the rat sarcoma (RAS) pathway. For example, the suppression of p16, a tumour suppressor, together with over-active RAS signalling in cancer cells can influence the expression of retinoblastoma and prevent it from regulating cell cycle entry and restricting cell proliferation.[54-56] In addition, over-active RAS signalling in cancer cells can inhibit PKR signalling and block cell apoptosis.[14] It has been identified that vaccinia virus and reovirus selectively target various tumours with activation of RAS signalling.[46] Some viruses such as adenovirus, herpesvirus, vaccinia virus, and reovirus utilise the defects in cell cycle regulation and anti-viral mechanisms in tumours such as PKR, retinoblastoma and p16 for viral replication and survival.[14, 46] In addition, dysregulation of IFN-1 pathway in cancer cells, which plays an important role in anti-viral and anti-tumour responses, facilitates some viruses such as vaccinia virus, VSV, and newcastle disease virus to replicate preferentially within tumours.[14] Cancers often overexpress anti-apoptotic molecules such as B-cell lymphoma (Bcl) family of proteins for cell immortality, and newcastle disease virus targets Bcl-xL-overexpressing cells, promoting viral accumulation and replication.[46, 57] OVs use the cellular machinery for their replication and protein production, while affect cell functions, stimulate oxidative stress, and activate the pathways involving autophagic process.[48]

Not only do OVs lyse cancer cells leading to tumour regression but also concurrently create and stimulate anti-tumour immunity, resulting in eradication of the disease and prevention of the recurrence.[46, 58, 59] **Figure 1** shows the anti-tumour activity of OVs associated with multiple mechanisms involving inflammation process and immunogenic cell death.[59] Following the cancer cell damage by OV-induced oncolytic cell death, viral progeny such as pathogen-associated molecular patterns and immune signs such as damage-associated molecular patterns are produced and released, which will stimulate the maturation of dendritic cells and promote the release and the expression of tumour-associated antigens and tumour-associated neoantigens to the immune cells and cancer cells.[14, 48] Antigen presentation through major histocompatibility complex class II and major

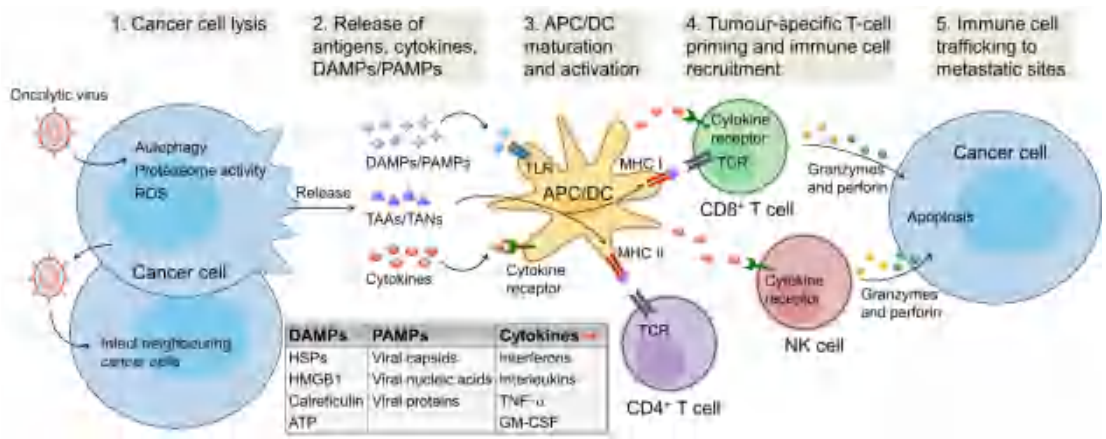

Figure 1. The generalised overview of OV-induced anti-tumour immunity. Initially, OVs infect primary cancer cells and cause direct oncolysis via inducing autophagy, increasing proteasome activity, and upregulating ROS caused by ER stress and genotoxic stress upon the infection. Subsequently, DAMPs and PAMPs trigger TLR, a major sub-family of the PRRs, and activate APCs. APC/DC uptake TAAs/TANs and express them to immune cells such as $CD8^+$ T cells and $CD4^+$ T cells through MHC I – TCR and MHC II – TCR interactions, respectively. The releasing cytokines and chemokines recruit both innate immune cells such as neutrophils, macrophages, NK cells, and DC, and adaptive immune cells such as T cells and B cells to the infected sites. In addition, APC helps stimulating and manipulating $CD8^+$ T cells and NK cells to release granzymes and perforin causing apoptosis of cancer cells. Furthermore, cytotoxic T lymphocytes can migrate to a distant tumour, recognize tumour antigens, and kill cancer cells.[9, 14, 46, 48, 59, 60] APC: antigen presenting cells; ATP: Adenosine triphosphate; DAMPs: damage-associated molecular patterns; DC: dendritic cells; ER: endoplasmic reticulum; GM-CSF: granulocyte macrophage colony-stimulating factor; HSP: heat shock protein; HMGB1: high mobility group protein; MHC: major histocompatibility complex; NK cell: natural killer cell; OV: oncolytic virus; PAMPs: pathogen-associated molecular patterns; PRR: pattern recognition receptor; ROS: reactive oxygen species; TAAs: tumour-associated antigens; TANs: tumour-associated neoantigens; TCR: T cell receptor; TLR: Toll-like receptor; TNF-α: tumour necrosis factor-α. Adapted from Kaufman et al.[14]

histocompatibility complex class I to $CD8^+$ T cells and $CD4^+$ T cells, respectively, leads to T cell priming and inflammatory responses.[60] The increase of proinflammatory cytokines such as IFN-1, interleukins (i.e. interleukin-1β, interleukin-6, interleukin-12), tumour necrosis factor-α, and granulocyte macrophage colony-stimulating factor, and the chemokines such as C-C motif chemokine ligand 2, C-C motif chemokine ligand 3, C-C motif chemokine ligand 5 and C-X-C motif chemokine 10 are beneficial for activating and recruiting both adaptive and innate immune cells against the primary tumour that is exposed to the virus and even in metastatic sites.[9, 46]

Different Strategies to Improve Oncolytic Viruses through Genetic Engineering

Manipulating viral genome has become the common strategy to apply OVs in cancer immunotherapy (**Table 2**). OVs can be genetically modified to enhance the anti-tumour immunity by employing immunostimulatory elements, and to improve the safety, efficacy, and targeted delivery of OVs.[13] Additionally, OVs can be genetically engineered to selectively target the unique receptors on the surface of cancer cells, providing greater safety for healthy cells.

Table 2. Summary of important genetic engineering in OVs

Genetic modification				
Gene deletion	**Gene insertion**	**Purpose/aim**	**Example of OVs**	**References**
ICP34.5		Selectively replicate in cancer cells, which have impaired PKR activity	Herpesvirus	61
ICP6	LacZ	Selectively replicate in cancer cells, which have sufficient level of host RR and $p16^{INK4A}$ tumour suppressor inactivation, avoid RR encoding	Herpesvirus	48, 61, 66
E1A		Restrict viral proliferation in healthy tissue	Adenovirus	61
g34.5		Restrict viral proliferation in healthy tissue and reduce neurovirulence	Herpesvirus	48, 62
a47		Increase anti-tumour immunity	Herpesvirus	63
TK		Selectively replicate in cancer cells	Vaccinia virus	68
	GM-CSF	Increase anti-tumour immunity	Herpesvirus, vaccinia virus, and adenovirus	58, 59, 64
	Endostatin	Destroy tumour vasculature and enhance therapeutic efficiency	Herpesvirus	13
	TSP1	Destroy tumour vasculature and enhance therapeutic efficiency	Herpesvirus	13
	GLAF-2	Increases anti-angiogenic and anti-tumour properties	Vaccinia virus	67

Note: GLAF-2: vascular endothelial growth factor-2; GM-CSF: granulocyte macrophage colony-stimulating factor; ICP: infected cell protein; OV: oncolytic virus; PKR: protein kinase R; RR: ribonucleotide reductase; TK: thymidine kinase; TSP1: thrombospondin-1.

For example, a deletion of ICP34.5 and ICP6 genes drives herpes simplex virus (HSV-1) to have replicative selectivity in tumour cells that show $p16^{INK4A}$ tumour suppressor inactivation, a common deficit in cancers.[61] A deletion of E1A gene, which functions to promote S-phase entry via retinoblastoma signalling pathway in adenovirus, can prevent viral replication in normal cells.[61] Furthermore, a deletion of γ34.5 gene in HSV-1 also renders the virus unable to replicate in normal cells because γ34.5 gene functions to impede a shutoff of host protein synthesis.[62] Anti-tumour immunity can also be enhanced by the deletion of viral genes such as α47 gene in HSV-1 which functions to antagonize the transporter associated with antigen presentation in host's cells.[63] The insertion of granulocyte macrophage colony-stimulating factor gene in HSV-1, vaccinia virus, and adenovirus can enhance the cytokine secretion for immune cell recruitment and stimulation.[58, 59, 64] Inserting the *Escherichia coli LacZ* gene into the ICP6 coding region in HSV-1 inactivates the ICP6 gene which encodes a viral ribonucleotide reductase function that allows viral DNA synthesis.[65] It promotes the selective viral replication within the cancer cells because the rapidly dividing cells express sufficient level of host ribonucleotide reductase.[66] To destroy tumour vasculature and enhance therapeutic efficiency, endostatin and thrombospondin-1 genes have been inserted in HSV-1 to suppress angiogenesis.[13] Vaccinia virus encoding a single-chain antibody against vascular endothelial growth factor-2 also increases anti-angiogenic and anti-tumour properties.[67] Furthermore, the deletion of the viral thymidine kinase (TK) gene in vaccinia virus increases the selectivity of OVs to cancer cells since tumour cells produce higher levels of TK.[68]

Viral Vector Systems Used for Oncolytic Therapy

Virus particles are broadly used in cancer treatment as gene delivery vehicles and as OVs.[69] The viral-based vectors for gene delivery can be used in targeted transfer of therapeutic genetic materials such as tumour suppressor genes, tumour-associated antigens, small interference RNA, pro-inflammatory factors, immune checkpoint inhibitors, and anti-angiogenic proteins.[70] Furthermore, OVs including many virus families are often additionally armed in order to enhance therapeutic efficiency and induce an anti-cancer immune response.[71] In clinical trials for cancer treatment, retrovirus (including lentivirus), adenovirus, and poxvirus vectors are commonly used.[70] Other virus vectors such as HSV, adeno-associated virus, measles virus, VSV, and poliovirus can also be found in the clinical trials.[72]

Clinical Trials and Applications of Oncolytic Viruses

The novel medical approaches including oncolytic cancer therapy inevitably need efficient tests to analyze their ability before being widely used or executed in the populations. Normally, clinical trials of various OVs would examine the safety, toxicity, efficacy, adverse effects, maximum tolerated dose, biomarkers, anti-tumour mechanism, and immune responses. These experiments could confine the effective and safe modified viruses to be used in cancer patients with fewer off-target delivery, lower rate of normal cell lysis, and less severe side effects. In addition, we could acknowledge the practical doses for patients and the mechanism of drugs towards cancer cells and the immune system against OV therapy. Here we summarize the clinical trials of OVs in different phases with various OVs in recent years. They would show the early stage of clinical proceedings, and the efficacy of the virus across many cancer types. The clinical trials included in this review were collected from published years between 2015–2023. The information of the recent clinical trials phases I,[73-88] II,[102,103] and III[89-101] are presented in **Tables 3–5**, respectively.

Various Approaches to Improve Oncolytic Virus-Delivery Specificity

Recently, viral delivery has played a vital role and extensively obtained attention in preclinical and clinical trials of biomedical fields. Owing to the specific and special properties of viruses, including great biocompatibility and biodegradation in cellular environments and minimal toxicity, viruses have been utilised as biological carriers of drugs, genes, and active chemical compounds.[104, 105] Therefore, the viral delivery platform is nowadays developed and evolved in many therapeutic applications, such as vaccines, gene therapies, immunotherapies, cancer therapies, anti-microbial therapies, cardiovascular therapies, imaging, and theranostics. Particularly, OV delivery offers efficient anti-tumour treatment and immunovirotherapies with potential advantages of high safety, specificity, selectivity, and efficacy.[20, 62, 106] On the other hand, designing the oncolytic viral delivery system is still a huge challenge and under examination due to the restrictions of bioavailability. The systematic administration of OVs usually can trigger strong host immune responses, resulting in the virus inactivation and clearance as well as weakened therapeutic anti-tumour effects by the production of neutralizing antibodies in bloodstream.[107, 108] In order to address these issues, several of the following approaches were introduced.

OVs encapsulation approaches

The encapsulation of OVs exhibits a novel alternative strategy for facilitating cellular administration against the immune system.[109] Numerous biomedical research works have been progressively reported over the past couple of years corresponding to the OVs encapsulation approaches for cancer treatment.

Bioactive polymers

Virus encapsulation using bioactive polymers and nanoparticles is a fascinating alternative to enhance protection from host immune system and improve anti-cancer therapeutic performance. [110-112] In 2021, Garofalo et al.[113] designed a viral delivery platform by coating polygalactosyl-b-agmatyl (Gal_{32}-*b*-Agm_{29}) diblock copolymer with asialoglycoprotein receptor on adenovirus Ad5/3-D24-ICOSL as OVs towards the effective hepatocellular carcinoma treatment in liver cells, as illustrated in **Figure 2**. They revealed that the polymer coated-OVs system potentially showed a significant improvement in the infectivity, viral replication, the lysis of tumour cells, and immunogenic cell death together with high safety and efficacious therapeutic effect. However, some studies revealed that synthetic polymers and nanoparticles as carriers provided unpreferred delivery efficiency and elevated toxicity triggering undesirable side responses in host surroundings and improved tumour proliferation.[114-116] The alternative designs of polymeric materials for virus delivery should focus on the biocompatible polymers and OVs' capture-release efficiency. The natural polymers or naturally derived polymers linking through dynamic covalent bonds could be utilised to deplete the mentioned downsides.

Liposome and extracellular vehicles

Lipid-based non-viral encapsulation is recognised as an attractive systematic viral delivery strategy for OVs. Liposome and extracellular vehicles containing phospholipid bilayer membranes act as protective carriers to eliminate the limited effects of immune clearance and increase cellular uptake into target cells.[117-119] In 2019, Wang and coworkers[120] utilised oncolytic alphavirus M1, an anti-tumour infector, encapsulated into liposome (M-LPO) to kill and infect zinc finger anti-viral protein-deficient tumour cells in LoVo and Hep 3B cell lines, as seen in **Figure 3**.[121] The M-LPO delivery system illustrated a well-defined cellular administration with weakened intrinsic M1 immunogenicities and the attenuated responses of neutralizing-antibody production for improving anti-cancer therapies. Besides, in the next three years, Huang and his colleagues[122] synthesised the novel viral delivery platform using cationic 1,2-dioleoyl-3-trimethylammonium-propane-folate liposomes (Df) encapsulating oncolytic-competent adenovirus (TAV255-Df) for the gene and anti-tumour therapies of the CAR-deficient tumours, such as CT26 colon carcinoma murine cells, as depicted in **Figure 4**. The TAV255-Df liposome-encapsulated platform could efficiently circumvent the requirement of coxsackievirus and CAR for cell entry and express the increment of viral transfection, tumour regression, and prolonged survival rate. However, occasionally some unencapsulated OVs could be observed as they were not loaded inside liposomes and remained in suspension. Thus, the purification of OVs from the liposome-encapsulated OVs is still a challenge for this delivery platform.[123, 124]

Nanohydrogels

As a nano-scale delivery system, nanohydrogels combine the advantages of the hydrogel system and nanoparticles, including tissue-like mechanical properties, great biocompatibility and biodegradability, potential surface reactivity, and probability for efficient cellular entry.[125, 126] Hence, nanohydrogels have been considered as an attractive candidate for protective OVs

Table 3. Summary of major oncolytic virus recently under clinical trials: phase I study

Virus type	Name (published year)	Cancer	Location	Patients number	Measurement	Route of administration	Study conclusion
Herpes virus	G207[73] (2022)	Glioblastoma	USA	6	Correlated gene analysis	Intratumoural stereotactic injection	The results have shown approximately 500 tumour-associated genes expression correlating to the patient's survival rate. The enhancement of T-cell and IFN production also affected the immune system. In the longest survival patient, there was the highest T-cell-related gene expression.
	OrienX010[74] (2022)	Melanoma	China	26	Safety, tolerability, efficacy, and phase II dose level	Intratumoural injection	The oncolytic OrienX010 was safe and well-tolerated in patients with melanoma. This therapeutic method exhibited significant anti-tumour activity. The recommended dose for phase II clinical trials without severe AEs was 10 mL of 8×10^7 pfu/mL every 2 weeks.
Adenovirus	ICOVIR-5[75] (2019)	Cutaneous and uveal melanoma	Spain	12	Toxicity and efficacy	Intravenous injection	Tumour targeting is possible but more efficient tumour debulking is needed via oncolysis due to the immune system leading to low anti-tumour efficacy. The toxicity was very short without inflammatory response syndrome.
	DNX-2401[76] (2018)	Malignant glioma	USA	25	Safety, efficacy, and biologic effects	Intravenous injection	25% of patients with single DNX-2401 survived more than 3 years and 95% decrease in tumour volumes was observed in three patients. This is due to oncolytic effects and emerging immune-mediated anti-glioma response
Coxsackie virus	CVA21[77] (2019)	AML	UK	16	Anti-tumour ability and cellular mechanism responsible	Intravenous delivery	CVA21 can activate the immune system for anti-tumour activity comprising cytokine-mediated bystander killing, enhancing of natural killer cell-mediated cellular cytotoxicity and tumour-specific cytotoxic T lymphocytes. Type I IFN and NK cell activation was observed. Moreover, the crucial mediators are ICAM-1 and plasmacytoid dendritic cells.
	CVA21[78] (2019)	Non-muscle invasive bladder cancer (NMIBC)	UK	15	Safety, MTD, evidence of viral replication, induction of inflammatory cytokines, anti-tumour activity, and viral-induced changes in resected tissue	Intravesical administration	All patients showed no sign of toxicity in both virus and virus with subtherapeutic dose mitomycin C. Inflammation of NMIBC tissues was observed with the increasing immune checkpoint inhibitory genes (PD-L1 and LAG3) and Th1-associated chemokines.
Measles virus	MV-NIS[79] (2017)	Myeloma	USA	32	MTD,	Intravenous delivery	The maximum tolerated dose of the patient with MV-NIS was not reached. Phase II with TCID50 1011 will be evaluated. MV-NIS is capable of replicating before being cleared by the immune system.
Poliovirus	PVSRIPO[80] (2021)	Melanoma	USA	12	Safety and tolerability	Intratumoural injection	The study showed well-tolerated with no SAEs or DLTs
	PVSRIPO[81] (2022)	Melanoma	USA	12	Immunologic effects in the TME	Intratumoural injection	Patients with lerapolturev and anti-PD-1 therapy have a median PFS of 2.3 years and had higher $CD8^+$ T cell infiltrates in prelerapolturev tumour biopsies.
Vaccinia virus	GL-ONC1[82] (2018)	Peritoneal cancer	Germany	9	Safety assessment, MTD, anti-tumour activity, viral replication, clinical efficacy, and biological effects in real-time study	intraperitoneal injection	GL-ONC1 administration into the peritoneal cavity was tolerated in advanced stage peritoneal carcinomatosis patients. There were limited efficient tumour cell infection, virus replication, and oncolysis.
	ACAM2000[83] (2019)	AML	USA	26	safety and feasibility	Intravenous, intratumoural, and intraperitoneal injections	ACAM2000 treatment delivered by autologous adipose SVF cells in AML patients was safe and well tolerated. Many patients showed great signals of anti-cancer effect.
	Olvi-Vec[84] (2021)	Platinum-resistant/ refractory ovarian cancer (PRROC)	USA	12	Safety, adverse events assessments,	intraperitoneal injection	Intraperitoneal Olvi-Vec oncolytic viral therapy illustrated well safety, clinical activities, and immune activation in PRROC patients.
Reovirus	PD-L1 with pelareorep and pembrolizumab[85] (2022)	PDAC	USA	11	Safety, DLT, tumour response, reovirus replication, and immune analysis	Intravenous injection	Chemotherapy of pelareorep and pembrolizumab showed no toxicity and provided great efficacy. The pelareorep and anti–PD-1 therapy evaluation was ongoing.
	Reovirus[86] (2020)	Metastatic CRC	USA	8	Immune response, cytokine expression pattern in peripheral circulation, exosomal and cellular microRNA levels, and effects of reovirus on leukocyte transcriptome	Intravenous infusion	Reovirus as an oncolytic agent provided multi-layered effects in tumour patients. Reovirus can function in immune stimulants, including immuno-chemo-therapeutic drugs and an oncolytic agent efficacy. Reovirus caused lysis of tumour cells, and facilitator of immune-mediated recognition.

Table 3. Continued

Virus type	Name (published year)	Cancer	Location	Patients number	Measurement	Route of administration	Study conclusion
Parvovirus	H-1PV[87] (2017)	Glioblastoma	Germany		Safety and tolerability, virus distribution, and MTD	Intratumoural or intravenous injection	H-1PV treatment was safe and well tolerated, and no reached MTD. The virus could cross the blood-brain/tumour barrier and spread through the tumour.
Seneca Valley virus	NTX-010 with cyclophosphamide[88] (2015)	Relapsed/refractory neuroblastoma, rhabdomyosarcoma, carcinoid tumour, and adrenocorticocarcinoma	USA	13	MTD and recommended phase II dose	Intravenous injection	NTX-010 is well tolerable at the dose levels in relapsed/refractory solid tumours pediatric patients. The addition of cyclophosphamide showed limited applicability.

Note: AE: adverse event; AML: acute myeloid leukemia; CRC: colorectal cancer; DLT: dose-limiting toxicity; ICAM-1: intercellular adhesion molecule 1; IFN: type I interferon; MTD: maximum tolerated dose; NK cell: natural killer cell; ORR: response rate; PDAC: pancreatic ductal adenocarcinoma; PFS: progression-free survival; SAE: serious adverse event; SVF: stromal vascular fraction; TCID50: 50% tissue culture infectious dose; Th: T helper; TME: tumour microenvironment.

Table 4. Summary of major oncolytic virus recently under clinical trials: phase II study

Virus type	Name (published year)	Cancer	Location	Patient number	Measurement	Route of administration	Study conclusion
Herpes virus	OH2[89] (2021)	Various	China	40	Safety and tolerability	Intratumoural injection	This phase I/II study showed that the oncolytic virus OH2 was safe and well-tolerated in patients with solid tumours. The durability of anti-tumour activity was significantly remarkable in patients with metastatic esophageal and rectal cancer.
	G47Δ[90,91] (2022)	Glioblastoma	Japan	13	Safety and tumour response	Intratumoural injection	Study showed safety of G47Δ up to 1×10^9 pfu/dose for two doses within 14 days. It could cause immediate infiltration of lymphocytes that directed towards tumour cells. Three of 13 patients had long-term survival (> 46 months) from the delayed effect of anti-tumour immunity.
				19	Efficacy	Intratumoural injection	The study showed the overall response in 2 years, partial response in 1 patient and stable disease in 18 patients. The number of tumour-infiltrating $CD4^+/CD8^+$ lymphocytes and persistent low numbers of $Foxp3^+$ cells increased which was evidenced by biopsies. It also showed that G47Δ was safe for oncolytic cancer therapy.
Herpes virus	T-VEC[92,93] (2021)	Breast cancer	USA	35	Efficacy, overall response rate ORR, rates of local overall response/disease, control rate, PFS, and OS	Intratumoural injection	In patients with inoperable locoregional recurrence of breast cancer, intratumoural T-VEC as monotherapy was not therapeutically desirable owing to uncontrolled disease progression.
		STS	USA	30	Safety, tolerability, and efficacy	Intratumoural injection	The incorporation of TVEC and EBRT provided safety and good tolerability towards STS treatment. These can also increase the immune response without necrosis. The result also evidenced that Caspase-3 could be a biomarker relating to a positive effect of TVEC.
Adenovirus	CG0070[94] (2017)	NMIBC	USA	45	Safety and efficacy in patients with high-risk BCG-unresponsive NMIBC	Intravesical injection	The toxicity of virotherapy was relatively low. There was 47% CR of patients with high-risk BCG-unresponsive NMIBC, 58% CR of patients with CIS, and 50% of patients with CIS-containing tumours.
Coxsackie virus	V937[95] (2021)	Melanoma	USA	57	Efficacy and safety in patients with unresectable stage IIIC or IV melanoma	Intratumoural injection	V937 was well tolerated and warrants further investigation for treatment of patients with unresectable melanoma without additional toxicities. The primary efficacy endpoint was 38.6% and durable response rate was 21.1%. 12-month PFS was 32.9% and 12-month OS was 75.4%
Vaccinia virus	JX-594[96] (2022)	Soft-tissue sarcoma	France	20	The 6-month non-progression rate, efficacy, immune response, and therapeutic potential	Intravenous injection	The administration of JX-594 oncolytic virus was safe in advanced STS patients. The role of immune-oncology agent combination and the patient population identification who received benefit from this approach were questions from major interest.

Table 4. Continued

Virus type	Name (published year)	Cancer	Location	Patient number	Measurement	Route of administration	Study conclusion
Reovirus	FOLFOX/BEV with pelareorep[97] (2018)	Metastatic colorectal cancer	Canada	103	PFS, OS, ORR, and correlative analyses.	Intravenous injection	FOLFOX/BEV with pelareorep was increased ORR, but PFS was reduced. Reduction of treatment intensity with standard agents provided the lack of pelareorep benefit.
	Pelareorep (reolysin) with pemetrexed or docetaxel[98] (2018)	NSCLC	Canada	166	PFS, OS, ORR, and exploratory translational analyses.	Intravenous injection	No improvement of PFS in NSCLC patients was demonstrated in pelareorep chemotherapy.
	Paclitaxel/ Pelareorep[99] (2018)	mBC	Canada	81	PFS, response rate, OS, circulating tumour cell counts, safety, and exploratory correlative analyses	Intravenous injection	This randomised phase II study of pelareorep and paclitaxel was not different in PFS for treated mBC patients. Pelareorep/paclitaxel combination revealed longer OS.
Parvovirus	H-1PV (ParvOryx)[100] (2021)	metastatic PDAC	Germany	7	Safety, clinical efficacy, virus pharmacokinetics, shedding, and immune response	Intravenous injection	No environmental risks were indicated immune modulation once ParvOryx injection. H-1PV was systematic clinical development with immunomodulatory compounds.
Seneca Valley virus	NTX-010[101] (2019)	ES SCLC	USA	50	PFS, prespecified interim analysis for futility, viral clearance, and the development of neutralizing antibodies	Intravenous injection	NTX-010 treatment had no benefit with ES SCLC patients. Persistence of NTX-010 was related a short PFS. There was no outcome improvement of NTX010 treatment in ES SCLC patients after platinum-based chemotherapy.

Note: BCG: Bacillus Calmette-Guerin; CR: complete response; EBRT: external beam radiation therapy; ES SCLC: extensive-stage small cell lung cancer; mBC: metastatic breast cancer; NMIBC: non-muscle invasive bladder cancer; NSCLC: non-small cell lung cancer; ORR: objective response rate; OS: overall survival; PDAC: pancreatic ductal adenocarcinoma; PFS: progression-free survival; STS: soft-tissue sarcoma.

Table 5. Summary of major oncolytic virus recently under clinical trials: phase III study

Virus type	Name (published year)	Cancer	Location	Patients number	Measurement	Route of administration	Study conclusion
Herpes virus	T-VEC[102] (2017)	Melanoma	UK	437	Efficacy	Intratumoural delivery	Patients with early metastatic melanoma (stage IIIB–IVM1a) had a high CR rate and durability with T-VEC administration. The results still showed the well-tolerated ability of T-VEC and also exposed the association between the virus and the survival rate.
	T-VEC[103] (2019)	Melanoma	USA	41	Safety	Intralesional injection	The results showed consistent safety as previous research of T-VEC. Only influenza-like symptoms were observed which are mild or moderate AEs

Note: AE: adverse event; CR: complete response.

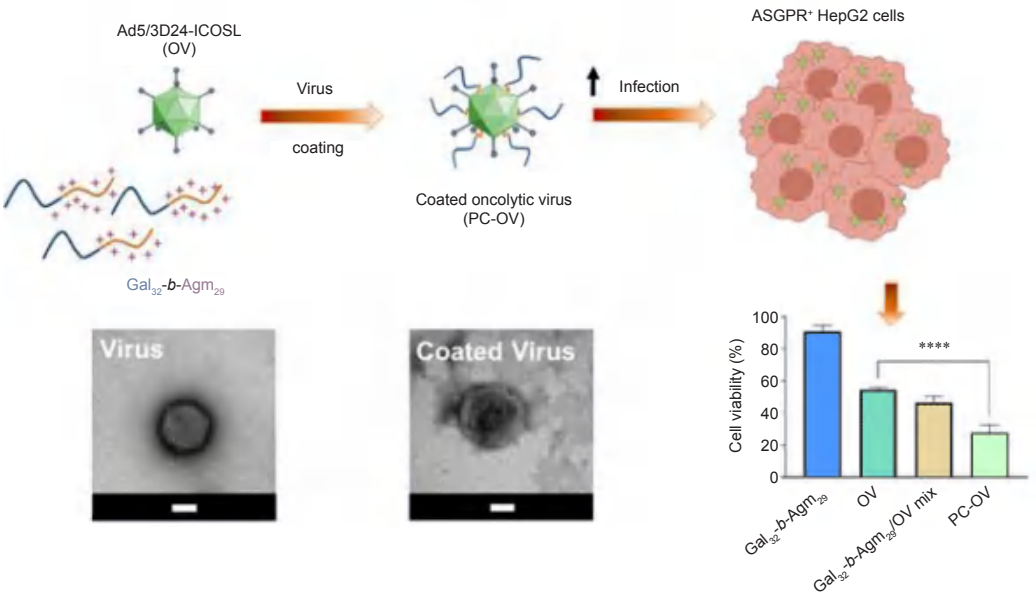

Figure 2. The design of a high potential therapeutic polymer-coated oncolytic viruses (PC-OVs) delivery system which is coated by electrostatic polygalactosyl-b-agmatyl (Gal_{32}-*b*-Agm_{29}) diblock copolymer with asialoglycoprotein receptor (ASGPR) for diagnosis of hepatocellular carcinoma in human hepatoma cell line HepG2 as a model. ****$P < 0.0001$. Reprinted from Garofalo et al.[113] OV: oncolytic virus; PC: polymer-coated.

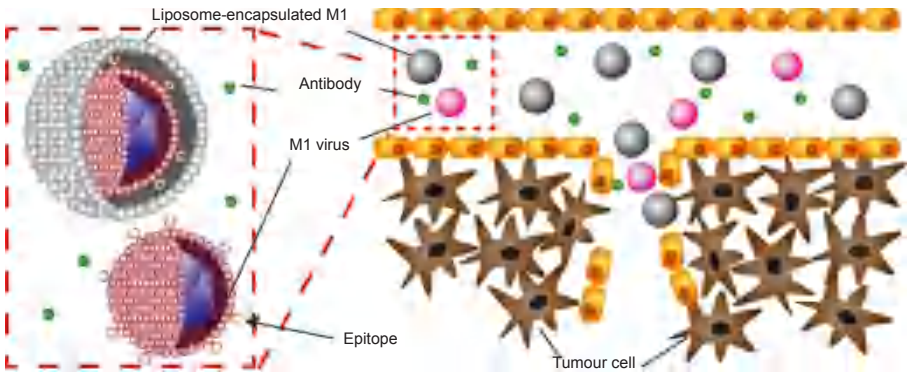

Figure 3. Schematic illustration of the fabrication of a liposome-encapsulated M1 virus platform (M-LPO) for tumour therapy in LoVo and Hep 3B cell lines. Reprinted with permission from Wang et al.[120] Copyright 2019 American Chemical Society.

delivery. In 2021, Deng and coworkers[127] developed an OV delivery system employing a prostate-specific adenovirus [I/PPT-E1A] (DNA virus) and echovirus Rigvir® ECHO-7 (RNA virus)-encapsulated hyaluronic acid-based redox responsive nanohydrogels for anti-tumour therapies (**Figure 5**). The OVs-loaded nanohydrogel platform could promote systematic cellular administration and viral releasability equipped with redox stimulation in cancer cells with highly promising safety and efficacy. Furthermore, this platform illustrated the limited anti-virus neutralizing antibody and reduced immune response.

Carrier cell-based delivery approaches

Carrier cell-based delivery is a process of using a suitable cell as a viral carrier to facilitate the ferrying. These cells should protect the therapeutic substances from inevitable biodegradation, increase the density of viral agglomeration at tumour cells and reduce the side effects of cancer therapy. Stem cells have been broadly used as carriers for numerous therapeutic agents as well as OVs because these carriers would not be filtered by the liver and neutralised via the immune system. Therefore, they could directly access the tumour cells and release the curing viruses after their replication. In this section, the strategies for utilizing mesenchymal stem cells (MSCs), neural stem cells (NSCs), menstrual blood-derived stem cells, tumour-infiltrating lymphocytes, and cryo-shocked cancer cells as carriers for the OVs will be discussed.

Mesenchymal stem cells

MSCs are multipotent stem cells that can be found in various sources in the body such as adipose tissue, umbilical cord, placental tissue, and bone marrow. MSCs have the ability to differentiate and express tumour-associated chemokines, which can benefit tumour targeting and accumulation. Moreover,

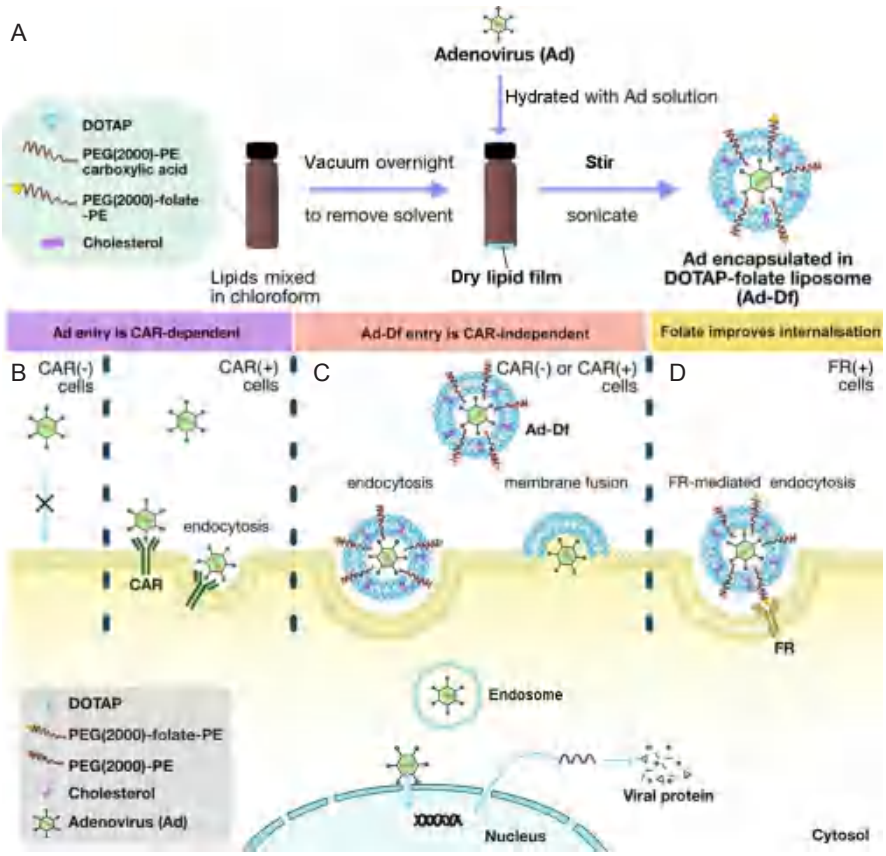

Figure 4. (A) The synthesis of adenovirus encapsulating cationic 1,2-dioleoyl-3-trimethylammonium-propane (DOTAP)-folate liposomes (Ad-Df). (B) The cellular penetration approaches of Ad-Df viral platform in various coxsackievirus and adenovirus receptor (CAR)-deficient cell lines. (C) Ad-Df is capable of entering the cells via endocytosis during no expression of CAR of the target cells, leading to transfect CAR-positive and -negative cells. (D) The cellular uptake into FR-positive cells can be enhanced by Ad-Df containing folate-conjugated lipid through FR-mediated endocytosis. Reprinted with permission from Huang et al.[122] Copyright 2022 American Chemical Society. FR: Folate receptor; PEG(2000)-PE: 1,2-distearoyl-*sn*-glycero-3-phosphoethanolamine-*N*-[methoxy(poly-ethylene glycol)-2000].

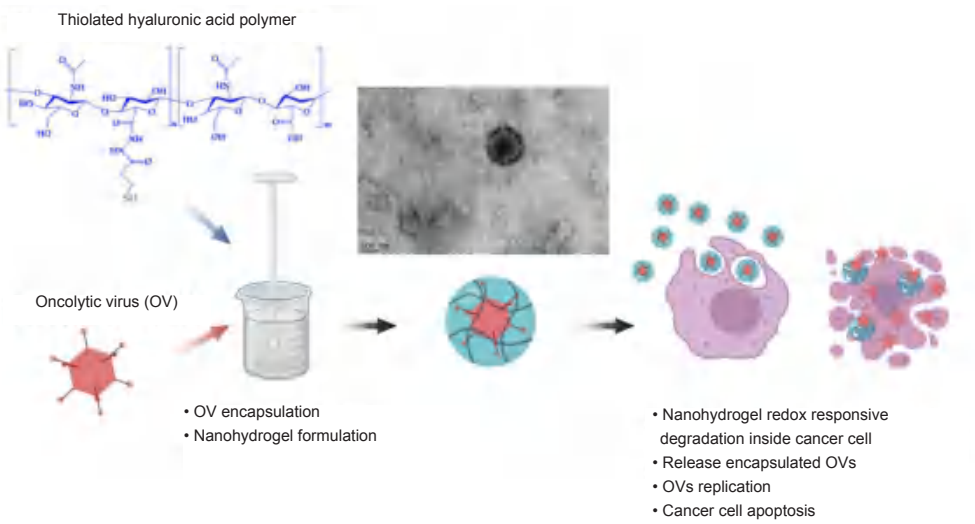

Figure 5. A hyaluronic acid-based nanohydrogel formulation for oncolytic viral delivery for anti-cancer therapy. Reprinted from Deng et al.[127]

MSCs can exhibit the tolerogenic microenvironment through the T-cell unresponsiveness or apoptosis induction and suppress the activity of natural killers, $CD8^+$ and $CD4^+$ cells, by releasing prostaglandins and interleukins) in blood. Therefore, MSCs could be employed as a carrier for OV delivery, as depicted in **Figure 6**.[128]

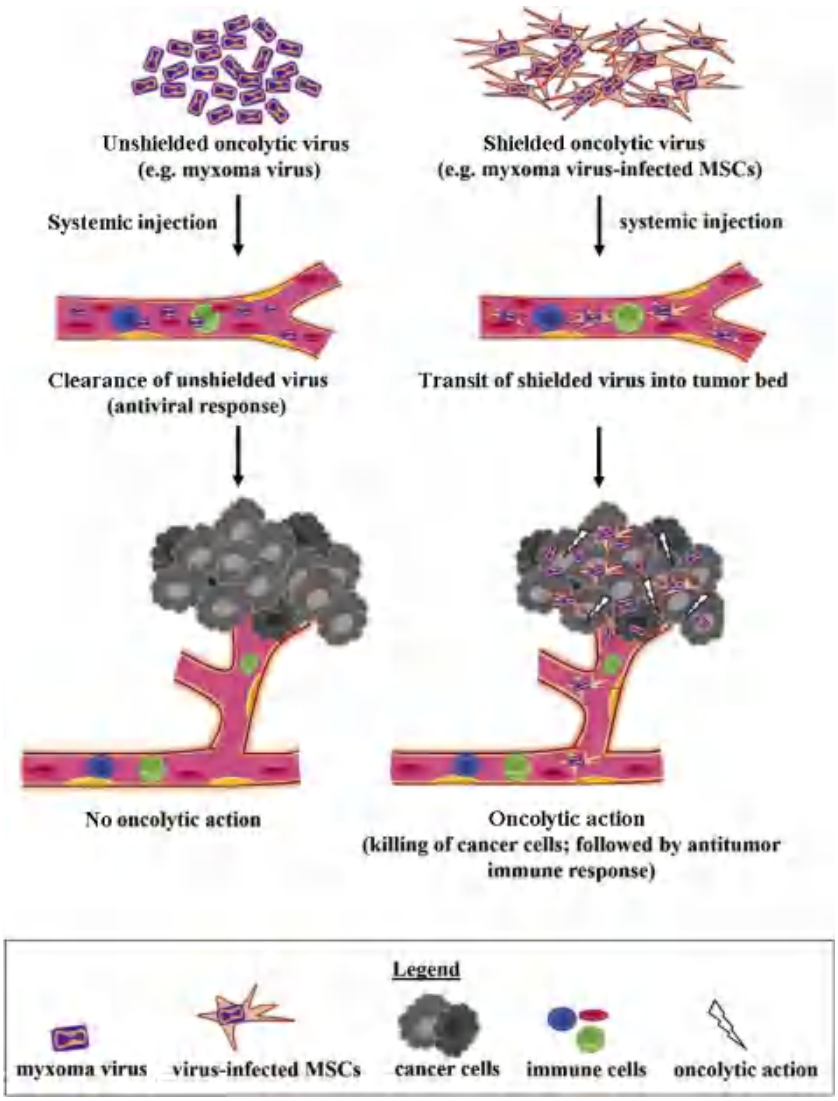

Figure 6. Application of myxoma virus-loaded mesenchymal stem cells (MSCs) for pulmonary melanoma treatment. Reprinted from Hadryś et al.[128]

Interleukin-15 derived-oncolytic myxoma cells carrying myxoma virus were delivered through intravenous administration via the bone marrow-derived MSCs as a viral carrier in order to treat pulmonary melanoma in mice.[129] The results of bioluminescence imaging showed the high tumour infectivity of the delivery process and enhanced oncolytic activity due to the immune response compared to blood and lungs. The levels of $CD8^+$ and $CD4^+$ in blood did not significantly increase at the endpoint of the experiment on the 21st day whereas those percentages were higher in the lung. In addition, the survival rate tended to be longer in mice that were injected with two doses of MSC-shielded carrying myxoma virus in comparison to MSC and unshielded carrying myxoma virus.

Neural stem cells

Malignant glioma, a brain and/or spinal cord cancer, is another severe disease that is rarely curable these days due to the rapid growth rate of the tumour cells and the prevention of chemotherapeutic agents by the blood-brain barrier. NSCs can serve as an effective vehicle for oncolytic therapy as they could penetrate blood-brain barrier, migrate to the tumour site, and distribute among the glioma cells. One recent study reported that the engineered oncolytic adenovirus, CRAd-S-pk7, delivered by NSCs had a longer survival rate of 50% in mice compared to the virus alone.[130] The clinical trial phase I treatment of NSC-CRAd-S-pk7 injected through the walls of the resection cavity affirmed the safety and feasibility of glioma therapy without formal dose-limiting toxicity.

In another study, oncolytic chimeric orthopoxvirus was chosen as a candidate for ovarian cancer treatment. CF33, a mutated chimeric orthopoxvirus in the J2R (TK) gene was delivered via the HB1.F3.CD21 clonal NSCs.[131] The precision of tumour targeting increased as the deficiency of TK in the CF33 could lead the NSCs loaded CF33 to the overexpressing TK area of tumour cells and thus, CF33 could infect, replicate, and kill the cancer cells. Another research showed the use of NSC.CRAd-S-pk7, NSCs that are transfected with glioma-tropic oncolytic adenovirus, to treat ovarian cancer (OVCAR8).[132] The number of tumours was reduced by more than 9-fold in 14 days in culture although the ratio of NSC.CRAd-S-pk7: OVCAR8 was 1:1000.

Menstrual blood derived MSCs

Menstrual blood contains MSCs which possess target tropism and low immunity. Menstrual blood therefore can be used to obtain menstrual blood derived MSCs, which are abundant and have a rapid growth profile. Guo et al.[133] reported that menstrual blood derived MSCs could be used to deliver engineered CRAd5/F11 chimeric oncolytic adenovirus, which could provide a large number of viruses within the colorectal cancer tumour area that efficiently expressed the tumour inhibitory activity within 7 days after injection. This could serve as a promising new source of stem cell carriers that successfully loaded and transferred the OVs to the desired targets.

Tumour-infiltrating lymphocytes/T cells

Tumour-infiltrating lymphocytes/T cell (TIL) therapy has been introduced to synergistically used as an anti-tumour agent with the oncolytic adenovirus.[134] The combination of those could enhance the treatment's ability to target by prevention of neutralization and kill the cancer cell. Oncolytic adenovirus coding for tumour necrosis factor-α and interleukin-2 (TILT-23) was intravenously and intratumourally delivered via TIL into tumours in mice. However, the relevant aspects of humans are still questionable and need further clarification.

Cryo-shocked cancer cells

Another state-of-the-art OV carrier is the cryo-shocked cancer cells in **Figure 7A**. The cancer cells were infected by an OV before treating with liquid nitrogen to eliminate the proliferation capacity and pathogenicity of the tumour cells.[135] After intratumoural injection as demonstrated in **Figure 7B**, the OV-loaded cancer cells could still release the targeting agent and have antitumour activity inside the tumour area. Moreover, the infiltration of $CD8^+$ was then increased by the activation of dendritic cells which could elevate the amount of anti-tumour cytokine and reduce the infiltration of regulatory T cells in tumours.

Conclusions and Perspectives

OVs utilise extensive mechanisms to preferentially infect and destroy cancer cells, including the specific replication in cancer cells causing direct oncolysis, the induction and stimulation of immunogenic cell death and anti-tumour immunity, and tumour vasculature which can be damaged by the infection of engineered OVs to tumour-associated vascular endothelial cells, leading to tumour necrosis and the infiltration of immune cells.[136] Genetically, engineered OVs have become the common promising strategy to enhance anti-tumour immunity, safety, and efficacy as well as targeted delivery, such as the deletion of ICP34.5, ICP6, E1A, γ34.5, α47, and TK gene, and the insertion of LacZ gene into the ICP6 coding region, and granulocyte macrophage colony-stimulating factor gene.

In the field of engineered OVs as anti-tumour agents, the major challenge for oncolytic virotherapy is the rapid viral clearance due to the host's immune response towards anti-viral immunity, as the primary results of the various physical and immunological defense mechanisms of the host cells, which are capable of virus inactivation and elimination. Manipulating the host immune system to minimize anti-viral responses and viral clearance, while immune-mediated tumour destruction is promoted, is a key to efficient oncolytic virotherapy. Hence, the design of systemic delivery carriers is of great significance and considerable effort has been made to obtain a novel and efficient platform for delivering OVs to targeted cells. An effective delivery method should minimize the viral clearance, reduce the off-target toxicity and enhance the tumour-specific responses. Numerous strategies have been developed to improve viral administration efficiency in preclinical and clinical settings, for instance, the encapsulation of OVs in polymeric scaffolds, nanoparticles, liposomes, extracellular vehicles, nanohydrogels, and carrier cells. The recent progress in genetic engineering and targeted delivery platforms will provide more opportunities for OVs with enhanced anti-tumour immunity, safety, and efficacy in cancer treatment and overcome clinical challenges.

The limitation of this review paper is that it provides information based on computerised or electronic databases. The hand-searching (manual process of screening) of journals, conference proceedings, and other publications was not included in the literature search process of this review.

Author contributions

Conceptualization and outline design of the paper: QW, MK; funding acquisition: QW, LC; manuscript review and editing: MK, TM, JJ, LC, QW. All authors approved the final version of this manuscript.

Financial support

The work was financial supported by the National Science Foundation and South Carolina Experimental Program to Stimulate Competitive Research and Institutional Development Awards (SC EPSCoR IDeA) program under NSF Award.

Acknowledgement

We wish to acknowledge the work of Ryan Lucas, an undergraduate student in biochemistry and molecular biology major at the University of South Carolina, for his contribution to the related literature survey.

Conflicts of interest statement

The authors declare no conflict of interest.

Editor note: Qian Wang is an Editorial Board member of *Biomaterials Translational*. He was blinded from reviewing or making decisions on the manuscript. The article was subject to the journal's standard procedures, with peer review handled independently of this Editorial Board member and his research group.

Open access statement

This is an open access journal, and articles are distributed under the terms of the Creative Commons Attribution-NonCommercial-ShareAlike 4.0

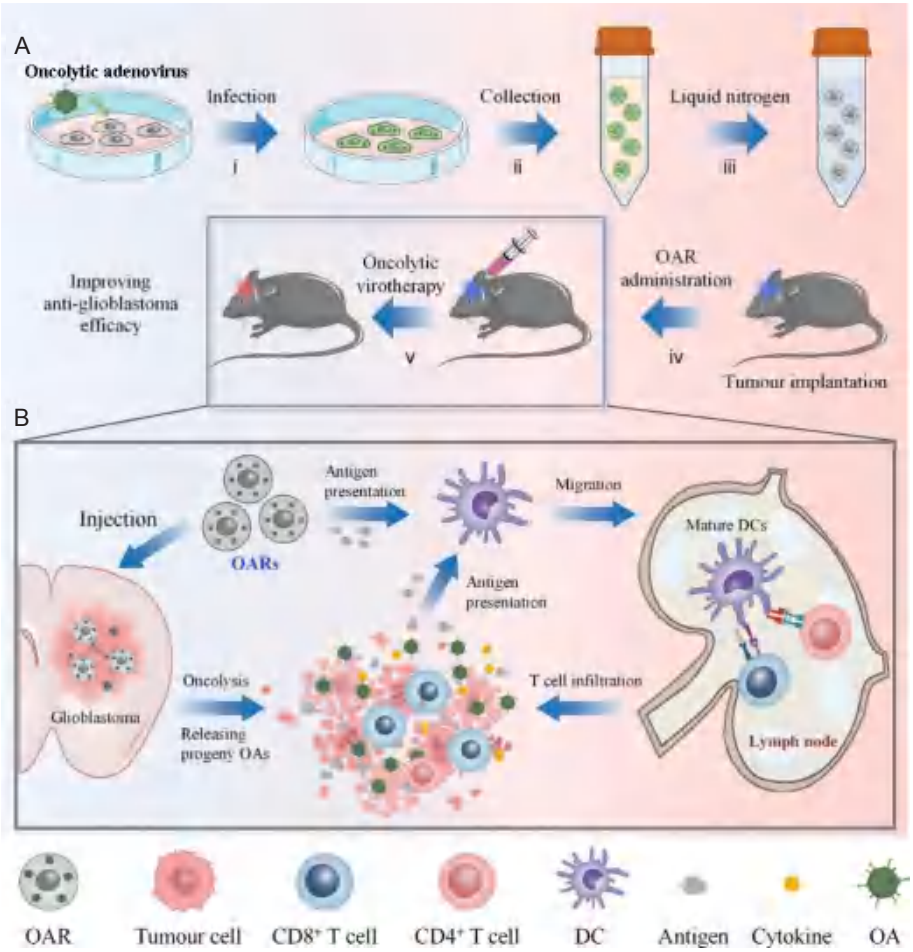

Figure 7. (A) Illustration of the preparation and *in vivo* experimental processes of cryo-shocked cancer cells as oncolytic adenovirus reservoir (OARs) for glioblastoma immunotherapy in a mouse glioblastoma model. (B) The administration mechanism of OARs via intratumoural injection. Reprinted with permission from Liu et al.[135] Copyright 2022 American Chemical Society. DC: dendritic cell; OA: oncolytic adenovirus.

License, which allows others to remix, tweak, and build upon the work non-commercially, as long as appropriate credit is given and the new creations are licensed under the identical terms.

Additional file

Additional file 1: Literature retrieval strategy.

1. Sung, H.; Ferlay, J.; Siegel, R. L.; Laversanne, M.; Soerjomataram, I.; Jemal, A.; Bray, F. Global Cancer Statistics 2020: GLOBOCAN estimates of incidence and mortality worldwide for 36 cancers in 185 countries. *CA Cancer J Clin.* **2021**, *71*, 209-249.
2. Siegel, R. L.; Miller, K. D.; Fuchs, H. E.; Jemal, A. Cancer statistics, 2022. *CA Cancer J Clin.* **2022**, *72*, 7-33.
3. Mondal, J.; Panigrahi, A. K.; Khuda-Bukhsh, A. R. Conventional chemotherapy: problems and scope for combined therapies with certain herbal products and dietary supplements. *Austin J Mol Cell Biol.* **2014**, *1*, 10.
4. Carvalho, A.; Fernandes, A. R.; Baptista, P. V. Chapter 10 - Nanoparticles as delivery systems in cancer therapy: focus on gold nanoparticles and drugs. In *Applications of targeted nano drugs and delivery systems*, Mohapatra, S. S.; Ranjan, S.; Dasgupta, N.; Mishra, R. K.; Thomas, S., eds.; Elsevier: 2019; pp 257-295.
5. Chidambaram, M.; Manavalan, R.; Kathiresan, K. Nanotherapeutics to overcome conventional cancer chemotherapy limitations. *J Pharm Pharm Sci.* **2011**, *14*, 67-77.
6. Choi, C. H. ABC transporters as multidrug resistance mechanisms and the development of chemosensitizers for their reversal. *Cancer Cell Int.* **2005**, *5*, 30.
7. Rahman, M. M.; McFadden, G. Oncolytic viruses: newest frontier for cancer immunotherapy. *Cancers (Basel).* **2021**, *13*, 5452.
8. Truong, C. S.; Yoo, S. Y. Oncolytic vaccinia virus in lung cancer vaccines. *Vaccines.* **2022**, *10*, 240.
9. Tian, Y.; Xie, D.; Yang, L. Engineering strategies to enhance oncolytic viruses in cancer immunotherapy. *Signal Transduct Target Ther.* **2022**, *7*, 117.
10. Lemos de Matos, A.; Franco, L. S.; McFadden, G. Oncolytic viruses and the immune system: the dynamic duo. *Mol Ther Methods Clin Dev.* **2020**, *17*, 349-358.
11. Filley, A. C.; Dey, M. Immune system, friend or foe of oncolytic virotherapy? *Front Oncol.* **2017**, *7*, 106.
12. Maroun, J.; Muñoz-Alía, M.; Ammayappan, A.; Schulze, A.; Peng, K. W.; Russell, S. Designing and building oncolytic viruses. *Future Virol.* **2017**, *12*, 193-213.
13. Jin, K. T.; Du, W. L.; Liu, Y. Y.; Lan, H. R.; Si, J. X.; Mou, X. Z. Oncolytic virotherapy in solid tumors: the challenges and achievements.

Cancers (Basel). **2021**, *13*, 588.

14. Kaufman, H. L.; Kohlhapp, F. J.; Zloza, A. Oncolytic viruses: a new class of immunotherapy drugs. *Nat Rev Drug Discov.* **2015**, *14*, 642-662.
15. Martini, V.; D'Avanzo, F.; Maggiora, P. M.; Varughese, F. M.; Sica, A.; Gennari, A. Oncolytic virotherapy: new weapon for breast cancer treatment. *Ecancermedicalscience.* **2020**, *14*, 1149.
16. You, Z.; Fischer, D. C.; Tong, X.; Hasenburg, A.; Aguilar-Cordova, E.; Kieback, D. G. Coxsackievirus-adenovirus receptor expression in ovarian cancer cell lines is associated with increased adenovirus transduction efficiency and transgene expression. *Cancer Gene Ther.* **2001**, *8*, 168-175.
17. Hensen, L. C. M.; Hoeben, R. C.; Bots, S. T. F. Adenovirus receptor expression in cancer and its multifaceted role in oncolytic adenovirus therapy. *Int J Mol Sci.* **2020**, *21*, 6828.
18. Cheng, T.; Bai, J.; Chung, C. S.; Chen, Y.; Fallon, E. A.; Ayala, A. Herpes virus entry mediator (HVEM) expression promotes inflammation/organ injury in response to experimental indirect-acute lung injury. *Shock.* **2019**, *51*, 487-494.
19. Tang, M.; Cao, X.; Li, Y.; Li, G. Q.; He, Q. H.; Li, S. J.; Chen, J.; Xu, G. L.; Zhang, K. Q. High expression of herpes virus entry mediator is associated with poor prognosis in clear cell renal cell carcinoma. *Am J Cancer Res.* **2019**, *9*, 975-987.
20. Ferreira, T.; Kulkarni, A.; Bretscher, C.; Richter, K.; Ehrlich, M.; Marchini, A. Oncolytic H-1 parvovirus enters cancer cells through clathrin-mediated endocytosis. *Viruses.* **2020**, *12*, 1199.
21. Nettelbeck, D. M.; Leber, M. F.; Altomonte, J.; Angelova, A.; Beil, J.; Berchtold, S.; Delic, M.; Eberle, J.; Ehrhardt, A.; Engeland, C. E.; Fechner, H.; Geletneky, K.; Goepfert, K.; Holm, P. S.; Kochanek, S.; Kreppel, F.; Krutzke, L.; Kühnel, F.; Lang, K. S.; Marchini, A.; Moehler, M.; Mühlebach, M. D.; Naumann, U.; Nawroth, R.; Nüesch, J.; Rommelaere, J.; Lauer, U. M.; Ungerechts, G. Virotherapy in Germany-recent activities in virus engineering, preclinical development, and clinical studies. *Viruses.* **2021**, *13*, 1420.
22. Ferreira, T.; Kulkarni, A.; Bretscher, C.; Nazarov, P. V.; Hossain, J. A.; Ystaas, L. A. R.; Miletic, H.; Röth, R.; Niesler, B.; Marchini, A. Oncolytic H-1 parvovirus hijacks galectin-1 to enter cancer cells. *Viruses.* **2022**, *14*, 1018.
23. Bretscher, C.; Marchini, A. H-1 parvovirus as a cancer-killing agent: past, present, and future. *Viruses.* **2019**, *11*, 562.
24. Marchini, A.; Bonifati, S.; Scott, E. M.; Angelova, A. L.; Rommelaere, J. Oncolytic parvoviruses: from basic virology to clinical applications. *Virol J.* **2015**, *12*, 6.
25. Bradley, S.; Jakes, A. D.; Harrington, K.; Pandha, H.; Melcher, A.; Errington-Mais, F. Applications of coxsackievirus A21 in oncology. *Oncolytic Virother.* **2014**, *3*, 47-55.
26. Au, G. G.; Lincz, L. F.; Enno, A.; Shafren, D. R. Oncolytic coxsackievirus A21 as a novel therapy for multiple myeloma. *Br J Haematol.* **2007**, *137*, 133-141.
27. Li, Y. C.; Zhou, Q.; Song, Q. K.; Wang, R. B.; Lyu, S.; Guan, X.; Zhao, Y. J.; Wu, J. P. Overexpression of an immune checkpoint (CD155) in breast cancer associated with prognostic significance and exhausted tumor-infiltrating lymphocytes: a cohort study. *J Immunol Res.* **2020**, *2020*, 3948928.
28. Lupo, K. B.; Matosevic, S. CD155 immunoregulation as a target for natural killer cell immunotherapy in glioblastoma. *J Hematol Oncol.* **2020**, *13*, 76.
29. Masson, D.; Jarry, A.; Baury, B.; Blanchardie, P.; Laboisse, C.; Lustenberger, P.; Denis, M. G. Overexpression of the CD155 gene in human colorectal carcinoma. *Gut.* **2001**, *49*, 236-240.
30. Huang, D. W.; Huang, M.; Lin, X. S.; Huang, Q. CD155 expression and its correlation with clinicopathologic characteristics, angiogenesis, and prognosis in human cholangiocarcinoma. *Onco Targets Ther.* **2017**, *10*, 3817-3825.
31. Elvington, M.; Liszewski, M. K.; Atkinson, J. P. CD46 and oncologic interactions: friendly fire against cancer. *Antibodies (Basel).* **2020**, *9*, 59.
32. Russell, L.; Peng, K. W. The emerging role of oncolytic virus therapy against cancer. *Chin Clin Oncol.* **2018**, *7*, 16.
33. Nikolic, J.; Belot, L.; Raux, H.; Legrand, P.; Gaudin, Y.; A, A. A. Structural basis for the recognition of LDL-receptor family members by VSV glycoprotein. *Nat Commun.* **2018**, *9*, 1029.
34. Zhang, Y.; Nagalo, B. M. Immunovirotherapy based on recombinant vesicular stomatitis virus: where are we? *Front Immunol.* **2022**, *13*, 898631.
35. Martignone, S.; Ménard, S.; Bufalino, R.; Cascinelli, N.; Pellegrini, R.; Tagliabue, E.; Andreola, S.; Rilke, F.; Colnaghi, M. I. Prognostic significance of the 67-kilodalton laminin receptor expression in human breast carcinomas. *J Natl Cancer Inst.* **1993**, *85*, 398-402.
36. Fontanini, G.; Vignati, S.; Chiné, S.; Lucchi, M.; Mussi, A.; Angeletti, C. A.; Ménard, S.; Castronovo, V.; Bevilacqua, G. 67-Kilodalton laminin receptor expression correlates with worse prognostic indicators in non-small cell lung carcinomas. *Clin Cancer Res.* **1997**, *3*, 227-231.
37. Sanjuán, X.; Fernández, P. L.; Miquel, R.; Muñoz, J.; Castronovo, V.; Ménard, S.; Palacín, A.; Cardesa, A.; Campo, E. Overexpression of the 67-kD laminin receptor correlates with tumour progression in human colorectal carcinoma. *J Pathol.* **1996**, *179*, 376-380.
38. Taraboletti, G.; Belotti, D.; Giavazzi, R.; Sobel, M. E.; Castronovo, V. Enhancement of metastatic potential of murine and human melanoma cells by laminin receptor peptide G: attachment of cancer cells to subendothelial matrix as a pathway for hematogenous metastasis. *J Natl Cancer Inst.* **1993**, *85*, 235-240.
39. van den Brule, F. A.; Buicu, C.; Berchuck, A.; Bast, R. C.; Deprez, M.; Liu, F. T.; Cooper, D. N.; Pieters, C.; Sobel, M. E.; Castronovo, V. Expression of the 67-kD laminin receptor, galectin-1, and galectin-3 in advanced human uterine adenocarcinoma. *Hum Pathol.* **1996**, *27*, 1185-1191.
40. Xing, L.; Huhtala, M.; Pietiäinen, V.; Käpylä, J.; Vuorinen, K.; Marjomäki, V.; Heino, J.; Johnson, M. S.; Hyypiä, T.; Cheng, R. H. Structural and functional analysis of integrin alpha2I domain interaction with echovirus 1. *J Biol Chem.* **2004**, *279*, 11632-11638.
41. Haley, E. S.; Au, G. G.; Carlton, B. R.; Barry, R. D.; Shafren, D. R. Regional administration of oncolytic Echovirus 1 as a novel therapy for the peritoneal dissemination of gastric cancer. *J Mol Med (Berl).* **2009**, *87*, 385-399.
42. García-Romero, N.; Palacín-Aliana, I.; Esteban-Rubio, S.; Madurga, R.; Rius-Rocabert, S.; Carrión-Navarro, J.; Presa, J.; Cuadrado-Castano, S.; Sánchez-Gómez, P.; García-Sastre, A.; Nistal-Villan, E.; Ayuso-Sacido, A. Newcastle disease virus (NDV) oncolytic activity in human glioma tumors is dependent on CDKN2A-type I IFN gene cluster codeletion. *Cells.* **2020**, *9*, 1405.
43. Keshavarz, M.; Nejad, A. S. M.; Esghaei, M.; Bokharaei-Salim, F.; Dianat-Moghadam, H.; Keyvani, H.; Ghaemi, A. Oncolytic Newcastle disease virus reduces growth of cervical cancer cell by inducing apoptosis. *Saudi J Biol Sci.* **2020**, *27*, 47-52.
44. Yuan, P.; Swanson, K. A.; Leser, G. P.; Paterson, R. G.; Lamb, R. A.; Jardetzky, T. S. Structure of the Newcastle disease virus hemagglutinin-neuraminidase (HN) ectodomain reveals a four-helix bundle stalk. *Proc*

Natl Acad Sci U S A. **2011**, *108*, 14920-14925.
45. Chu, Z.; Gao, X.; Liu, H.; Ma, J.; Wang, C.; Lu, K.; Han, Q.; Wang, Y.; Wang, C.; Adam, F. E. A.; Wang, X.; Xiao, S.; Yang, Z. Newcastle disease virus selectively infects dividing cells and promotes viral proliferation. *Vet Res.* **2019**, *50*, 27.
46. Jhawar, S. R.; Thandoni, A.; Bommareddy, P. K.; Hassan, S.; Kohlhapp, F. J.; Goyal, S.; Schenkel, J. M.; Silk, A. W.; Zloza, A. Oncolytic viruses-natural and genetically engineered cancer immunotherapies. *Front Oncol.* **2017**, *7*, 202.
47. Katze, M. G.; He, Y.; Gale, M., Jr. Viruses and interferon: a fight for supremacy. *Nat Rev Immunol.* **2002**, *2*, 675-687.
48. Santos Apolonio, J.; Lima de Souza Gonçalves, V.; Cordeiro Santos, M. L.; Silva Luz, M.; Silva Souza, J. V.; Rocha Pinheiro, S. L.; de Souza, W. R.; Sande Loureiro, M.; de Melo, F. F. Oncolytic virus therapy in cancer: a current review. *World J Virol.* **2021**, *10*, 229-255.
49. Samuel, C. E. Antiviral actions of interferons. *Clin Microbiol Rev.* **2001**, *14*, 778-809, table of contents.
50. Fernandes, J. Oncogenes: the passport for viral oncolysis through PKR inhibition. *Biomark Cancer.* **2016**, *8*, 101-110.
51. Balachandran, S.; Kim, C. N.; Yeh, W. C.; Mak, T. W.; Bhalla, K.; Barber, G. N. Activation of the dsRNA-dependent protein kinase, PKR, induces apoptosis through FADD-mediated death signaling. *EMBO J.* **1998**, *17*, 6888-6902.
52. Nakayama, Y.; Plisch, E. H.; Sullivan, J.; Thomas, C.; Czuprynski, C. J.; Williams, B. R.; Suresh, M. Role of PKR and Type I IFNs in viral control during primary and secondary infection. *PLoS Pathog.* **2010**, *6*, e1000966.
53. Cook, M.; Chauhan, A. Clinical application of oncolytic viruses: a systematic review. *Int J Mol Sci.* **2020**, *21*, 7505.
54. Ahlander, J.; Bosco, G. The RB/E2F pathway and regulation of RNA processing. *Biochem Biophys Res Commun.* **2009**, *384*, 280-283.
55. Topacio, B. R.; Zatulovskiy, E.; Cristea, S.; Xie, S.; Tambo, C. S.; Rubin, S. M.; Sage, J.; Kõivomägi, M.; Skotheim, J. M. Cyclin D-Cdk4,6 drives cell-cycle progression via the retinoblastoma protein's C-terminal helix. *Mol Cell.* **2019**, *74*:758-770.e4.
56. Fernández-Medarde, A.; Santos, E. Ras in cancer and developmental diseases. *Genes Cancer.* **2011**, *2*, 344-358.
57. Mansour, M.; Palese, P.; Zamarin, D. Oncolytic specificity of Newcastle disease virus is mediated by selectivity for apoptosis-resistant cells. *J Virol.* **2011**, *85*, 6015-6023.
58. Aurelian, L. Oncolytic viruses as immunotherapy: progress and remaining challenges. *Onco Targets Ther.* **2016**, *9*, 2627-2637.
59. Chiocca, E. A.; Rabkin, S. D. Oncolytic viruses and their application to cancer immunotherapy. *Cancer Immunol Res.* **2014**, *2*, 295-300.
60. Bommareddy, P. K.; Shettigar, M.; Kaufman, H. L. Integrating oncolytic viruses in combination cancer immunotherapy. *Nat Rev Immunol.* **2018**, *18*, 498-513.
61. Lawler, S. E.; Speranza, M. C.; Cho, C. F.; Chiocca, E. A. Oncolytic viruses in cancer treatment: a review. *JAMA Oncol.* **2017**, *3*, 841-849.
62. Fukuhara, H.; Ino, Y.; Todo, T. Oncolytic virus therapy: a new era of cancer treatment at dawn. *Cancer Sci.* **2016**, *107*, 1373-1379.
63. Uchihashi, T.; Nakahara, H.; Fukuhara, H.; Iwai, M.; Ito, H.; Sugauchi, A.; Tanaka, M.; Kogo, M.; Todo, T. Oncolytic herpes virus G47Δ injected into tongue cancer swiftly traffics in lymphatics and suppresses metastasis. *Mol Ther Oncolytics.* **2021**, *22*, 388-398.
64. Woller, N.; Gürlevik, E.; Ureche, C. I.; Schumacher, A.; Kühnel, F. Oncolytic viruses as anticancer vaccines. *Front Oncol.* **2014**, *4*, 188.
65. Todo, T.; Martuza, R. L.; Rabkin, S. D.; Johnson, P. A. Oncolytic herpes simplex virus vector with enhanced MHC class I presentation and tumor cell killing. *Proc Natl Acad Sci U S A.* **2001**, *98*, 6396-6401.
66. Goldstein, D. J.; Weller, S. K. Herpes simplex virus type 1-induced ribonucleotide reductase activity is dispensable for virus growth and DNA synthesis: isolation and characterization of an ICP6 lacZ insertion mutant. *J Virol.* **1988**, *62*, 196-205.
67. Gholami, S.; Marano, A.; Chen, N. G.; Aguilar, R. J.; Frentzen, A.; Chen, C. H.; Lou, E.; Fujisawa, S.; Eveno, C.; Belin, L.; Zanzonico, P.; Szalay, A.; Fong, Y. A novel vaccinia virus with dual oncolytic and anti-angiogenic therapeutic effects against triple-negative breast cancer. *Breast Cancer Res Treat.* **2014**, *148*, 489-499.
68. Howells, A.; Marelli, G.; Lemoine, N. R.; Wang, Y. Oncolytic viruses-interaction of virus and tumor cells in the battle to eliminate cancer. *Front Oncol.* **2017**, *7*, 195.
69. Bulcha, J. T.; Wang, Y.; Ma, H.; Tai, P. W. L.; Gao, G. Viral vector platforms within the gene therapy landscape. *Signal Transduct Target Ther.* **2021**, *6*, 53.
70. Bezeljak, U. Cancer gene therapy goes viral: viral vector platforms come of age. *Radiol Oncol.* **2022**, *56*, 1-13.
71. Cross, D.; Burmester, J. K. Gene therapy for cancer treatment: past, present and future. *Clin Med Res.* **2006**, *4*, 218-227.
72. Ginn, S. L.; Amaya, A. K.; Alexander, I. E.; Edelstein, M.; Abedi, M. R. Gene therapy clinical trials worldwide to 2017: an update. *J Gene Med.* **2018**, *20*, e3015.
73. Miller, K. E.; Cassady, K. A.; Roth, J. C.; Clements, J.; Schieffer, K. M.; Leraas, K.; Miller, A. R.; Prasad, N.; Leavenworth, J. W.; Aban, I. B.; Whitley, R. J.; Gillespie, G. Y.; Mardis, E. R.; Markert, J. M. Immune activity and response differences of oncolytic viral therapy in recurrent glioblastoma: gene expression analyses of a phase IB study. *Clin Cancer Res.* **2022**, *28*, 498-506.
74. Cui, C.; Wang, X.; Lian, B.; Ji, Q.; Zhou, L.; Chi, Z.; Si, L.; Sheng, X.; Kong, Y.; Yu, J.; Li, S.; Mao, L.; Tang, B.; Dai, J.; Yan, X.; Bai, X.; Andtbacka, R.; Guo, J. OrienX010, an oncolytic virus, in patients with unresectable stage IIIC-IV melanoma: a phase Ib study. *J Immunother Cancer.* **2022**, *10*, e004307.
75. García, M.; Moreno, R.; Gil-Martin, M.; Cascallò, M.; de Olza, M. O.; Cuadra, C.; Piulats, J. M.; Navarro, V.; Domenech, M.; Alemany, R.; Salazar, R. A phase 1 trial of oncolytic adenovirus ICOVIR-5 administered intravenously to cutaneous and uveal melanoma patients. *Hum Gene Ther.* **2019**, *30*, 352-364.
76. Lang, F. F.; Conrad, C.; Gomez-Manzano, C.; Yung, W. K. A.; Sawaya, R.; Weinberg, J. S.; Prabhu, S. S.; Rao, G.; Fuller, G. N.; Aldape, K. D.; Gumin, J.; Vence, L. M.; Wistuba, I.; Rodriguez-Canales, J.; Villalobos, P. A.; Dirven, C. M. F.; Tejada, S.; Valle, R. D.; Alonso, M. M.; Ewald, B.; Peterkin, J. J.; Tufaro, F.; Fueyo, J. Phase I study of DNX-2401 (Delta-24-RGD) oncolytic adenovirus: replication and immunotherapeutic effects in recurrent malignant glioma. *J Clin Oncol.* **2018**, *36*, 1419-1427.
77. Müller, L. M. E.; Holmes, M.; Michael, J. L.; Scott, G. B.; West, E. J.; Scott, K. J.; Parrish, C.; Hall, K.; Stäble, S.; Jennings, V. A.; Cullen, M.; McConnell, S.; Langton, C.; Tidswell, E. L.; Shafren, D.; Samson, A.; Harrington, K. J.; Pandha, H.; Ralph, C.; Kelly, R. J.; Cook, G.; Melcher, A. A.; Errington-Mais, F. Plasmacytoid dendritic cells orchestrate innate and adaptive anti-tumor immunity induced by oncolytic coxsackievirus A21. *J Immunother Cancer.* **2019**, *7*, 164.
78. Annels, N. E.; Mansfield, D.; Arif, M.; Ballesteros-Merino, C.; Simpson, G. R.; Denyer, M.; Sandhu, S. S.; Melcher, A. A.; Harrington, K. J.; Davies, B.; Au, G.; Grose, M.; Bagwan, I.; Fox, B.; Vile, R.; Mostafid,

H.; Shafren, D.; Pandha, H. S. Phase I trial of an ICAM-1-targeted immunotherapeutic-coxsackievirus A21 (CVA21) as an oncolytic agent against non muscle-invasive bladder cancer. *Clin Cancer Res.* **2019**, *25*, 5818-5831.

79. Dispenzieri, A.; Tong, C.; LaPlant, B.; Lacy, M. Q.; Laumann, K.; Dingli, D.; Zhou, Y.; Federspiel, M. J.; Gertz, M. A.; Hayman, S.; Buadi, F.; O'Connor, M.; Lowe, V. J.; Peng, K. W.; Russell, S. J. Phase I trial of systemic administration of Edmonston strain of measles virus genetically engineered to express the sodium iodide symporter in patients with recurrent or refractory multiple myeloma. *Leukemia.* **2017**, *31*, 2791-2798.
80. Beasley, G. M.; Nair, S. K.; Farrow, N. E.; Landa, K.; Selim, M. A.; Wiggs, C. A.; Jung, S. H.; Bigner, D. D.; True Kelly, A.; Gromeier, M.; Salama, A. K. Phase I trial of intratumoral PVSRIPO in patients with unresectable, treatment-refractory melanoma. *J Immunother Cancer.* **2021**, *9*, e002203.
81. Beasley, G. M.; Brown, M. C.; Farrow, N. E.; Landa, K.; Al-Rohil, R. N.; Selim, M. A.; Therien, A. D.; Jung, S. H.; Gao, J.; Boczkowski, D.; Holl, E. K.; Salama, A. K. S.; Bigner, D. D.; Gromeier, M.; Nair, S. K. Multimodality analysis confers a prognostic benefit of a T-cell infiltrated tumor microenvironment and peripheral immune status in patients with melanoma. *J Immunother Cancer.* **2022**, *10*, e005052.
82. Lauer, U. M.; Schell, M.; Beil, J.; Berchtold, S.; Koppenhöfer, U.; Glatzle, J.; Königsrainer, A.; Möhle, R.; Nann, D.; Fend, F.; Pfannenberg, C.; Bitzer, M.; Malek, N. P. Phase I study of oncolytic vaccinia virus GL-ONC1 in patients with peritoneal carcinomatosis. *Clin Cancer Res.* **2018**, *24*, 4388-4398.
83. Minev, B. R.; Lander, E.; Feller, J. F.; Berman, M.; Greenwood, B. M.; Minev, I.; Santidrian, A. F.; Nguyen, D.; Draganov, D.; Killinc, M. O.; Vyalkova, A.; Kesari, S.; McClay, E.; Carabulea, G.; Marincola, F. M.; Butterfield, L. H.; Szalay, A. A. First-in-human study of TK-positive oncolytic vaccinia virus delivered by adipose stromal vascular fraction cells. *J Transl Med.* **2019**, *17*, 271.
84. Manyam, M.; Stephens, A. J.; Kennard, J. A.; LeBlanc, J.; Ahmad, S.; Kendrick, J. E.; Holloway, R. W. A phase 1b study of intraperitoneal oncolytic viral immunotherapy in platinum-resistant or refractory ovarian cancer. *Gynecol Oncol.* **2021**, *163*, 481-489.
85. Mahalingam, D.; Wilkinson, G. A.; Eng, K. H.; Fields, P.; Raber, P.; Moseley, J. L.; Cheetham, K.; Coffey, M.; Nuovo, G.; Kalinski, P.; Zhang, B.; Arora, S. P.; Fountzilas, C. Pembrolizumab in combination with the oncolytic virus pelareorep and chemotherapy in patients with advanced pancreatic adenocarcinoma: a phase ib study. *Clin Cancer Res.* **2020**, *26*, 71-81.
86. Parakrama, R.; Fogel, E.; Chandy, C.; Augustine, T.; Coffey, M.; Tesfa, L.; Goel, S.; Maitra, R. Immune characterization of metastatic colorectal cancer patients post reovirus administration. *BMC Cancer.* **2020**, *20*, 569.
87. Geletneky, K.; Hajda, J.; Angelova, A. L.; Leuchs, B.; Capper, D.; Bartsch, A. J.; Neumann, J. O.; Schöning, T.; Hüsing, J.; Beelte, B.; Kiprianova, I.; Roscher, M.; Bhat, R.; von Deimling, A.; Brück, W.; Just, A.; Frehtman, V.; Löbhard, S.; Terletskaia-Ladwig, E.; Fry, J.; Jochims, K.; Daniel, V.; Krebs, O.; Dahm, M.; Huber, B.; Unterberg, A.; Rommelaere, J. Oncolytic H-1 parvovirus shows safety and signs of immunogenic activity in a first phase I/IIa glioblastoma trial. *Mol Ther.* **2017**, *25*, 2620-2634.
88. Burke, M. J.; Ahern, C.; Weigel, B. J.; Poirier, J. T.; Rudin, C. M.; Chen, Y.; Cripe, T. P.; Bernhardt, M. B.; Blaney, S. M. Phase I trial of Seneca Valley Virus (NTX-010) in children with relapsed/refractory solid tumors: a report of the Children's Oncology Group. *Pediatr Blood Cancer.* **2015**, *62*, 743-750.
89. Zhang, B.; Huang, J.; Tang, J.; Hu, S.; Luo, S.; Luo, Z.; Zhou, F.; Tan, S.; Ying, J.; Chang, Q.; Zhang, R.; Geng, C.; Wu, D.; Gu, X.; Liu, B. Intratumoral OH2, an oncolytic herpes simplex virus 2, in patients with advanced solid tumors: a multicenter, phase I/II clinical trial. *J Immunother Cancer.* **2021**, *9*, e002224.
90. Todo, T.; Ino, Y.; Ohtsu, H.; Shibahara, J.; Tanaka, M. A phase I/II study of triple-mutated oncolytic herpes virus G47Δ in patients with progressive glioblastoma. *Nat Commun.* **2022**, *13*, 4119.
91. Todo, T.; Ito, H.; Ino, Y.; Ohtsu, H.; Ota, Y.; Shibahara, J.; Tanaka, M. Intratumoral oncolytic herpes virus G47Δ for residual or recurrent glioblastoma: a phase 2 trial. *Nat Med.* **2022**, *28*, 1630-1639.
92. Monga, V.; Miller, B. J.; Tanas, M.; Boukhar, S.; Allen, B.; Anderson, C.; Stephens, L.; Hartwig, S.; Varga, S.; Houtman, J.; Wang, L.; Zhang, W.; Jaber, O.; Thomason, J.; Kuehn, D.; Rajput, M.; Metz, C.; Zamba, K. D.; Mott, S.; Abanonu, C.; Bhatia, S.; Milhem, M. Intratumoral talimogene laherparepvec injection with concurrent preoperative radiation in patients with locally advanced soft-tissue sarcoma of the trunk and extremities: phase IB/II trial. *J Immunother Cancer.* **2021**, *9*, e003119.
93. Kai, M.; Marx, A. N.; Liu, D. D.; Shen, Y.; Gao, H.; Reuben, J. M.; Whitman, G.; Krishnamurthy, S.; Ross, M. I.; Litton, J. K.; Lim, B.; Ibrahim, N.; Kogawa, T.; Ueno, N. T. A phase II study of talimogene laherparepvec for patients with inoperable locoregional recurrence of breast cancer. *Sci Rep.* **2021**, *11*, 22242.
94. Packiam, V. T.; Lamm, D. L.; Barocas, D. A.; Trainer, A.; Fand, B.; Davis, R. L., 3rd; Clark, W.; Kroeger, M.; Dumbadze, I.; Chamie, K.; Kader, A. K.; Curran, D.; Gutheil, J.; Kuan, A.; Yeung, A. W.; Steinberg, G. D. An open label, single-arm, phase II multicenter study of the safety and efficacy of CG0070 oncolytic vector regimen in patients with BCG-unresponsive non-muscle-invasive bladder cancer: Interim results. *Urol Oncol.* **2018**, *36*, 440-447.
95. Andtbacka, R. H. I.; Curti, B.; Daniels, G. A.; Hallmeyer, S.; Whitman, E. D.; Lutzky, J.; Spitler, L. E.; Zhou, K.; Bommareddy, P. K.; Grose, M.; Wang, M.; Wu, C.; Kaufman, H. L. Clinical responses of oncolytic coxsackievirus A21 (V937) in patients with unresectable melanoma. *J Clin Oncol.* **2021**, *39*, 3829-3838.
96. Toulmonde, M.; Cousin, S.; Kind, M.; Guegan, J. P.; Bessede, A.; Le Loarer, F.; Perret, R.; Cantarel, C.; Bellera, C.; Italiano, A. Randomized phase 2 trial of intravenous oncolytic virus JX-594 combined with low-dose cyclophosphamide in patients with advanced soft-tissue sarcoma. *J Hematol Oncol.* **2022**, *15*, 149.
97. Jonker, D. J.; Tang, P. A.; Kennecke, H.; Welch, S. A.; Cripps, M. C.; Asmis, T.; Chalchal, H.; Tomiak, A.; Lim, H.; Ko, Y. J.; Chen, E. X.; Alcindor, T.; Goffin, J. R.; Korpanty, G. J.; Feilotter, H.; Tsao, M. S.; Theis, A.; Tu, D.; Seymour, L. A randomized phase II study of FOLFOX6/Bevacizumab with or without pelareorep in patients with metastatic colorectal cancer: IND.210, a Canadian Cancer Trials Group Trial. *Clin Colorectal Cancer.* **2018**, *17*:231-239.e7.
98. Bradbury, P. A.; Morris, D. G.; Nicholas, G.; Tu, D.; Tehfe, M.; Goffin, J. R.; Shepherd, F. A.; Gregg, R. W.; Rothenstein, J.; Lee, C.; Kuruvilla, S.; Keith, B. D.; Torri, V.; Blais, N.; Hao, D.; Korpanty, G. J.; Goss, G.; Melosky, B. L.; Mates, M.; Leighl, N.; Ayoub, J. P.; Sederias, J.; Feilotter, H.; Seymour, L.; Laurie, S. A. Canadian Cancer Trials Group (CCTG) IND211: A randomized trial of pelareorep (Reolysin) in patients with previously treated advanced or metastatic non-small cell lung cancer receiving standard salvage therapy. *Lung Cancer.* **2018**, *120*, 142-148.

99. Bernstein, V.; Ellard, S. L.; Dent, S. F.; Tu, D.; Mates, M.; Dhesy-Thind, S. K.; Panasci, L.; Gelmon, K. A.; Salim, M.; Song, X.; Clemons, M.; Ksienski, D.; Verma, S.; Simmons, C.; Lui, H.; Chi, K.; Feilotter, H.; Hagerman, L. J.; Seymour, L. A randomized phase II study of weekly paclitaxel with or without pelareorep in patients with metastatic breast cancer: final analysis of Canadian Cancer Trials Group IND.213. *Breast Cancer Res Treat.* **2018**, *167*, 485-493.
100. Hajda, J.; Leuchs, B.; Angelova, A. L.; Frehtman, V.; Rommelaere, J.; Mertens, M.; Pilz, M.; Kieser, M.; Krebs, O.; Dahm, M.; Huber, B.; Engeland, C. E.; Mavratzas, A.; Hohmann, N.; Schreiber, J.; Jäger, D.; Halama, N.; Sedlaczek, O.; Gaida, M. M.; Daniel, V.; Springfeld, C.; Ungerechts, G. Phase 2 trial of oncolytic H-1 parvovirus therapy shows safety and signs of immune system activation in patients with metastatic pancreatic ductal adenocarcinoma. *Clin Cancer Res.* **2021**, *27*, 5546-5556.
101. Schenk, E. L.; Mandrekar, S. J.; Dy, G. K.; Aubry, M. C.; Tan, A. D.; Dakhil, S. R.; Sachs, B. A.; Nieva, J. J.; Bertino, E.; Lee Hann, C.; Schild, S. E.; Wadsworth, T. W.; Adjei, A. A.; Molina, J. R. A Randomized Double-Blind Phase II Study of the Seneca Valley Virus (NTX-010) versus Placebo for Patients with Extensive-Stage SCLC (ES SCLC) who were stable or responding after at least four cycles of platinum-based chemotherapy: North Central Cancer Treatment Group (Alliance) N0923 Study. *J Thorac Oncol.* **2020**, *15*, 110-119.
102. Andtbacka, R. H. I.; Collichio, F.; Harrington, K. J.; Middleton, M. R.; Downey, G.; Öhrling, K.; Kaufman, H. L. Final analyses of OPTiM: a randomized phase III trial of talimogene laherparepvec versus granulocyte-macrophage colony-stimulating factor in unresectable stage III-IV melanoma. *J Immunother Cancer.* **2019**, *7*, 145.
103. Chesney, J.; Awasthi, S.; Curti, B.; Hutchins, L.; Linette, G.; Triozzi, P.; Tan, M. C. B.; Brown, R. E.; Nemunaitis, J.; Whitman, E.; Windham, C.; Lutzky, J.; Downey, G. F.; Batty, N.; Amatruda, T. Phase IIIb safety results from an expanded-access protocol of talimogene laherparepvec for patients with unresected, stage IIIB-IVM1c melanoma. *Melanoma Res.* **2018**, *28*, 44-51.
104. Chung, Y. H.; Cai, H.; Steinmetz, N. F. Viral nanoparticles for drug delivery, imaging, immunotherapy, and theranostic applications. *Adv Drug Deliv Rev.* **2020**, *156*, 214-235.
105. Steinmetz, N. F. Biological and evolutionary concepts for nanoscale engineering: Viruses as natural nanoparticles have great potential for a wide range of nanoscale products. *EMBO Rep.* **2019**, *20*, e48806.
106. Bai, Y.; Hui, P.; Du, X.; Su, X. Updates to the antitumor mechanism of oncolytic virus. *Thoracic cancer.* **2019**, *10*, 1031-1035.
107. Pesonen, S.; Kangasniemi, L.; Hemminki, A. Oncolytic adenoviruses for the treatment of human cancer: focus on translational and clinical data. *Mol Pharm.* **2011**, *8*, 12-28.
108. Barnard, A. S. Nanohazards: knowledge is our first defence. *Nat Mater.* **2006**, *5*, 245-248.
109. Ran, L.; Tan, X.; Li, Y.; Zhang, H.; Ma, R.; Ji, T.; Dong, W.; Tong, T.; Liu, Y.; Chen, D.; Yin, X.; Liang, X.; Tang, K.; Ma, J.; Zhang, Y.; Cao, X.; Hu, Z.; Qin, X.; Huang, B. Delivery of oncolytic adenovirus into the nucleus of tumorigenic cells by tumor microparticles for virotherapy. *Biomaterials.* **2016**, *89*, 56-66.
110. Hong, J.; Yun, C. O. Overcoming the limitations of locally administered oncolytic virotherapy. *BMC Biomed Eng.* **2019**, *1*, 17.
111. Francini, N.; Cochrane, D.; Illingworth, S.; Purdie, L.; Mantovani, G.; Fisher, K.; Seymour, L. W.; Spain, S. G.; Alexander, C. Polyvalent diazonium polymers provide efficient protection of oncolytic adenovirus enadenotucirev from neutralizing antibodies while maintaining biological activity in vitro and in vivo. *Bioconjug Chem.* **2019**, *30*, 1244-1257.
112. Green, N. K.; Hale, A.; Cawood, R.; Illingworth, S.; Herbert, C.; Hermiston, T.; Subr, V.; Ulbrich, K.; van Rooijen, N.; Seymour, L. W.; Fisher, K. D. Tropism ablation and stealthing of oncolytic adenovirus enhances systemic delivery to tumors and improves virotherapy of cancer. *Nanomedicine (Lond).* **2012**, *7*, 1683-1695.
113. Garofalo, M.; Bellato, F.; Magliocca, S.; Malfanti, A.; Kuryk, L.; Rinner, B.; Negro, S.; Salmaso, S.; Caliceti, P.; Mastrotto, F. Polymer coated oncolytic adenovirus to selectively target hepatocellular carcinoma cells. *Pharmaceutics.* **2021**, *13*, 949.
114. Semashko, V. V.; Pudovkin, M. S.; Cefalas, A. C.; Zelenikhin, P. V.; Gavriil, V. E.; Nizamutdinov, A. S.; Kollia, Z.; Ferraro, A.; Sarantopoulou, E. Tiny rare-earth fluoride nanoparticles activate tumour cell growth via electrical polar interactions. *Nanoscale Res Lett.* **2018**, *13*, 370.
115. Choi, Y. J.; Kang, S. J.; Kim, Y. J.; Lim, Y. B.; Chung, H. W. Comparative studies on the genotoxicity and cytotoxicity of polymeric gene carriers polyethylenimine (PEI) and polyamidoamine (PAMAM) dendrimer in Jurkat T-cells. *Drug Chem Toxicol.* **2010**, *33*, 357-366.
116. Yang, C.; Cheng, W.; Teo, P. Y.; Engler, A. C.; Coady, D. J.; Hedrick, J. L.; Yang, Y. Y. Mitigated cytotoxicity and tremendously enhanced gene transfection efficiency of PEI through facile one-step carbamate modification. *Adv Healthc Mater.* **2013**, *2*, 1304-1308.
117. Aoyama, K.; Kuroda, S.; Morihiro, T.; Kanaya, N.; Kubota, T.; Kakiuchi, Y.; Kikuchi, S.; Nishizaki, M.; Kagawa, S.; Tazawa, H.; Fujiwara, T. Liposome-encapsulated plasmid DNA of telomerase-specific oncolytic adenovirus with stealth effect on the immune system. *Sci Rep.* **2017**, *7*, 14177.
118. Record, M.; Silvente-Poirot, S.; Poirot, M.; Wakelam, M. J. O. Extracellular vesicles: lipids as key components of their biogenesis and functions. *J Lipid Res.* **2018**, *59*, 1316-1324.
119. Huang, H.; Sun, M.; Liu, M.; Pan, S.; Liu, P.; Cheng, Z.; Li, J.; Xu, H.; Liu, F.; Pang, Z. Full encapsulation of oncolytic virus using hybrid erythroctye-liposome membranes for augmented anti-refractory tumor effectiveness. *Nano Today.* **2022**, *47*, 101671.
120. Wang, Y.; Huang, H.; Zou, H.; Tian, X.; Hu, J.; Qiu, P.; Hu, H.; Yan, G. Liposome encapsulation of oncolytic virus M1 to reduce immunogenicity and immune clearance in vivo. *Mol Pharm.* **2019**, *16*, 779-785.
121. Lin, Y.; Zhang, H.; Liang, J.; Li, K.; Zhu, W.; Fu, L.; Wang, F.; Zheng, X.; Shi, H.; Wu, S.; Xiao, X.; Chen, L.; Tang, L.; Yan, M.; Yang, X.; Tan, Y.; Qiu, P.; Huang, Y.; Yin, W.; Su, X.; Hu, H.; Hu, J.; Yan, G. Identification and characterization of alphavirus M1 as a selective oncolytic virus targeting ZAP-defective human cancers. *Proc Natl Acad Sci U S A.* **2014**, *111*, E4504-4512.
122. Huang, C. H.; Dong, T.; Phung, A. T.; Shah, J. R.; Larson, C.; Sanchez, A. B.; Blair, S. L.; Oronsky, B.; Trogler, W. C.; Reid, T.; Kummel, A. C. Full remission of CAR-deficient tumors by DOTAP-folate liposome encapsulation of adenovirus. *ACS Biomater Sci Eng.* **2022**, *8*, 5199-5209.
123. Garofalo, M.; Saari, H.; Somersalo, P.; Crescenti, D.; Kuryk, L.; Aksela, L.; Capasso, C.; Madetoja, M.; Koskinen, K.; Oksanen, T.; Mäkitie, A.; Jalasvuori, M.; Cerullo, V.; Ciana, P.; Yliperttula, M. Antitumor effect of oncolytic virus and paclitaxel encapsulated in extracellular vesicles for lung cancer treatment. *J Control Release.* **2018**, *283*, 223-234.
124. Garofalo, M.; Villa, A.; Rizzi, N.; Kuryk, L.; Rinner, B.; Cerullo, V.; Yliperttula, M.; Mazzaferro, V.; Ciana, P. Extracellular vesicles enhance the targeted delivery of immunogenic oncolytic adenovirus

and paclitaxel in immunocompetent mice. *J Control Release.* **2019**, *294*, 165-175.

125. Chyzy, A.; Tomczykowa, M.; Plonska-Brzezinska, M. E. Hydrogels as potential nano-, micro- and macro-scale systems for controlled drug delivery. *Materials (Basel).* **2020**, *13*, 188.
126. Le, T. M. D.; Jung, B. K.; Li, Y.; Duong, H. T. T.; Nguyen, T. L.; Hong, J. W.; Yun, C. O.; Lee, D. S. Physically crosslinked injectable hydrogels for long-term delivery of oncolytic adenoviruses for cancer treatment. *Biomater Sci.* **2019**, *7*, 4195-4207.
127. Deng, S.; Iscaro, A.; Zambito, G.; Mijiti, Y.; Minicucci, M.; Essand, M.; Lowik, C.; Muthana, M.; Censi, R.; Mezzanotte, L.; Di Martino, P. Development of a new hyaluronic acid based redox-responsive nanohydrogel for the encapsulation of oncolytic viruses for cancer immunotherapy. *Nanomaterials (Basel).* **2021**, *11*, 144.
128. Hadryś, A.; Sochanik, A.; McFadden, G.; Jazowiecka-Rakus, J. Mesenchymal stem cells as carriers for systemic delivery of oncolytic viruses. *Eur J Pharmacol.* **2020**, *874*, 172991.
129. Jazowiecka-Rakus, J.; Sochanik, A.; Rusin, A.; Hadryś, A.; Fidyk, W.; Villa, N.; Rahman, M. M.; Chmielik, E.; Franco, L. S.; McFadden, G. Myxoma virus-loaded mesenchymal stem cells in experimental oncolytic therapy of murine pulmonary melanoma. *Mol Ther Oncolytics.* **2020**, *18*, 335-350.
130. Fares, J.; Ahmed, A. U.; Ulasov, I. V.; Sonabend, A. M.; Miska, J.; Lee-Chang, C.; Balyasnikova, I. V.; Chandler, J. P.; Portnow, J.; Tate, M. C.; Kumthekar, P.; Lukas, R. V.; Grimm, S. A.; Adams, A. K.; Hébert, C. D.; Strong, T. V.; Amidei, C.; Arrieta, V. A.; Zannikou, M.; Horbinski, C.; Zhang, H.; Burdett, K. B.; Curiel, D. T.; Sachdev, S.; Aboody, K. S.; Stupp, R.; Lesniak, M. S. Neural stem cell delivery of an oncolytic adenovirus in newly diagnosed malignant glioma: a first-in-human, phase 1, dose-escalation trial. *Lancet Oncol.* **2021**, *22*, 1103-1114.
131. Mooney, R.; Majid, A. A.; Batalla-Covello, J.; Machado, D.; Liu, X.; Gonzaga, J.; Tirughana, R.; Hammad, M.; Lesniak, M. S.; Curiel, D. T.; Aboody, K. S. Enhanced delivery of oncolytic adenovirus by neural stem cells for treatment of metastatic ovarian cancer. *Mol Ther Oncolytics.* **2019**, *12*, 79-92.
132. Hammad, M.; Cornejo, Y. R.; Batalla-Covello, J.; Majid, A. A.; Burke, C.; Liu, Z.; Yuan, Y. C.; Li, M.; Dellinger, T. H.; Lu, J.; Chen, N. G.; Fong, Y.; Aboody, K. S.; Mooney, R. Neural stem cells improve the delivery of oncolytic chimeric orthopoxvirus in a metastatic ovarian cancer model. *Mol Ther Oncolytics.* **2020**, *18*, 326-334.
133. Guo, Y.; Zhang, Z.; Xu, X.; Xu, Z.; Wang, S.; Huang, D.; Li, Y.; Mou, X.; Liu, F.; Xiang, C. Menstrual blood-derived stem cells as delivery vehicles for oncolytic adenovirus virotherapy for colorectal cancer. *Stem Cells Dev.* **2019**, *28*, 882-896.
134. Santos, J.; Heiniö, C.; Quixabeira, D.; Zafar, S.; Clubb, J.; Pakola, S.; Cervera-Carrascon, V.; Havunen, R.; Kanerva, A.; Hemminki, A. Systemic delivery of oncolytic adenovirus to tumors using tumor-infiltrating lymphocytes as carriers. *Cells.* **2021**, *10*, 978.
135. Liu, X.; Xu, J.; Yao, T.; Ding, J.; Li, S.; Su, R.; Zhang, H.; Li, H.; Yue, Q.; Gao, X. Cryo-shocked cancer cells as an oncolytic adenovirus reservoir for glioblastoma immunotherapy. *ACS Appl Mater Interfaces.* **2023**, *15*, 67-76.
136. Breitbach, C. J.; Arulanandam, R.; De Silva, N.; Thorne, S. H.; Patt, R.; Daneshmand, M.; Moon, A.; Ilkow, C.; Burke, J.; Hwang, T. H.; Heo, J.; Cho, M.; Chen, H.; Angarita, F. A.; Addison, C.; McCart, J. A.; Bell, J. C.; Kirn, D. H. Oncolytic vaccinia virus disrupts tumor-associated vasculature in humans. *Cancer Res.* **2013**, *73*, 1265-1275.

Received: April 25, 2023
Revised: May 26, 2023
Accepted: June 13, 2023
Available online: June 28, 2023

Biomaterials Translational

Biological approaches to the repair and regeneration of the rotator cuff tendon-bone enthesis: a literature review

Ahlam A. Abdalla[1,*,†], *Catherine J. Pendegrass*[2,*]

Key Words:
enthesis; rotator cuff; stem cells; tissue engineering; tendon-bone enthesis

From the Contents

ABSTRACT

Entheses are highly specialised organs connecting ligaments and tendons to bones, facilitating force transmission, and providing mechanical strengths to absorb forces encountered. Two types of entheses, fibrocartilaginous and fibrous, exist in interfaces. The gradual fibrocartilaginous type is in rotator cuff tendons and is more frequently injured due to the poor healing capacity that leads to loss of the original structural and biomechanical properties and is attributed to the high prevalence of retears. Fluctuating methodologies and outcomes of biological approaches are challenges to overcome for them to be routinely used in clinics. Therefore, stratifying the existing literature according to different categories (chronicity, extent of tear, and studied population) would effectively guide repair approaches. This literature review supports tissue engineering approaches to promote rotator cuff enthesis healing employing cells, growth factors, and scaffolds period. Outcomes suggest its promising role in animal studies as well as some clinical trials and that combination therapies are more beneficial than individualized ones. It then highlights the importance of tailoring interventions according to the tear extent, chronicity, and the population being treated. Contributing factors such as loading, deficiencies, and lifestyle habits should also be taken into consideration. Optimum results can be achieved if biological, mechanical, and environmental factors are approached. It is challenging to determine whether variations are due to the interventions themselves, the animal models, loading regimen, materials, or tear mechanisms. Future research should focus on tailoring interventions for different categories to formulate protocols, which would best guide regenerative medicine decision making.

http://doi.org/10.12336/biomatertransl.2023.02.004

How to cite this article:
Abdalla, A.; Pendegrass, C. Biological approaches to the repair and regeneration of the rotator cuff tendon-bone enthesis: a literature review. *Biomater Transl.* **2023**, *4*(2), 85-103.

Introduction

Entheses are highly specialised interfaces between fibrous isotropic tendons and ligaments (elastic modulus = 450 MPa axially) that provide tensile strength, and rigid inelastic isotropic bones (elastic modulus = 20 GPa) that optimise compressive loads, facilitating joint motion.[1] Entheses evolved highly specialised structures that effectively dampen the forces encountered in the region of peak strain, to facilitate seamless stress transfer and prevent tendon avulsion; whilst maintaining effective communication between tendons and bones to preserve homeostasis.[2-4] This heterogenous interface is unique and owing to its complexity and propensity to heal with biomechanically inferior scar tissue, presents significant challenges to repair and regeneration.

Rotator cuff (RC) tears are common with an increasing prevalence of partial and full thickness tears after the age of 50, and a 90% surgical repair failure.[5-7] The capacity to repair the damaged enthesis is insufficient, because of the tissue's lack of regeneration, leading to scar formation with inferior mechanical properties at the repair site.[8] Trials to enhance the healing progress of the RC enthesis have been directed towards

regenerative methods.[7] To date, there are no records of a single successful clinical biological approach achieving an enhanced healing of the injured enthesis. This review investigates the potential use of tailored biological therapies in different RC tear mechanisms, chronicity, and populations treated.

Entheses types

Histologically, there are two types of entheses classified according to the presence or absence of fibrocartilage, Fibrocartilaginous and Fibrous. Fibrous entheses insert via collagen fibres at the metaphysis or diaphysis to dissipate load over a large area, such as the deltoid and the medial collateral ligament, while fibrocartilaginous are at the epiphyses of long bones, such as the RC and Achilles tendons.[9, 10] The fibrocartilage of fibrocartilaginous entheses is not distributed evenly throughout the interface; appearing thickest in the deepest layers and absent superficially, consistent with the highest stress distribution.[11, 12] Fibrocartilaginous entheses, such as the RC, are more commonly injured and will therefore be the focus of this review.[13]

Entheses microstructure

Fibrocartilaginous entheses comprise four layers: dense fibrous tendon, fibrocartilage, mineralised fibrocartilage, and bone. The layers gradually increase in stiffness from tendon to bone to distribute forces over wider surface areas. The first level is composed of organised parallel appearance of collagen I and low levels of Proteoglycans within interspaced elongated tendon fibroblasts. The non-mineralised layer is populated with rows of round fibrochondrocytes embedded in a collagen II- and III-rich extracellular matrix (ECM), and low levels of collagen X, proteoglycans, and glycosaminoglycans. The fibrocartilage and mineralised fibrocartilage regions are separated by a tide mark. The mineralised fibrocartilage merges into bone, which consists of osteoblasts, osteocytes, and osteoclasts, alongside collagen I and a 69% elevated mineral content of which 99% is hydroxyapatite.[14]

The progressive structure and composition of entheses allow minimisation of the mechanical vulnerability that would arise due to the large elastic modulus mismatch. The structural and mechanical properties of entheses are a result of mechanical loading that have an essential role in enthesis maturation, allowing load transmission and stress reduction.[14] This highlights the importance of developing repair solutions that mimic the native biological and mechanical integration of entheses.

Entheses mechanical properties

Force transmission via the enthesis dynamically involves fibre realignment, crimp deformation, and sliding, which are essential for remodelling and turnover. Fibrocartilage enthesis acts like a stretch break that limits tendon narrowing at the insertion, which is a region of stress concentration, hence tendons cross-sectional area increases as they insert into the bone.[15, 16] The unmineralised region resists compression, while the mineralised resists shearing, creating a two-layered protective component.[17] Levels of unmineralised fibrocartilage are higher at entheses with more varied ranges of insertion angles, highlighting its functional role. The mineralised fibrocartilage attachment into bone is rather atypical, providing entheses with varied mechanical integrity.[14] Owing to the complex structure of the enthesis; when damaged, it is extremely challenging to repair surgically. The functionally gradual layers are not restored after repairs and the subsequent healing process.[2, 18, 19]

Entheses embryological development

Embryologically, it has been hypothesised that initially hyaline cartilage at the enthesis exists alone, and tendons attach to it. The cartilage erodes from the bone and is replaced by the fibrocartilaginous enthesis akin to a growth plate. This emphasises the fibrocartilaginous enthesis development within the tendon.[20,21] *In utero*, the enthesis is originally organised as an unmineralised cartilaginous unit that is mineralised postnatally by endochondral ossification.[22-24] Transcription factors, such as SRY-box 9, have been found essential for chondrogenesis, and others for tenogenesis such as mohawk and scleraxis.[25-27] Scleraxis knockout mice demonstrated a lower bone mineral density, decreased attachment strength, and disorganised collagen fibres.[23,28] Growth factors (GFs), such as transforming growth factor-beta (TGF-β) and bone morphogenetic protein (BMP) are regulators in early enthesis formation, and molecules such as Indian hedgehog (Ihh) and parathyroid hormone-related protein regulate late mineralisation.[22, 23, 29-31] During early development, enthesis progenitor cells proliferate and lengthen it, and express collagen I. Stimulated by BMP-4 and Ihh, at the base of the developing enthesis, the cells differentiate into unmineralised fibrochondrocytes, and express collagen I and II. By stimulation of Ihh at the postnatal stage, fibrochondrocytes undergo hypertrophic differentiation at the base of the enthesis. As the mineralised fibrochondrocytes form, collagen X and alkaline phosphate are expressed.[32]

Since tissue distortion and decreased mineralisation are seen in paralysed mice models, muscle loading is essential for the developing enthesis maturation alongside molecular components.[33-35] Disordered cell patterns and lack of enthesis regional transition are effects of reduced muscular stress during development.[36, 37] A balance between GFs and mechanical stimulation gives rise to the mature complex enthesis structure and composition.

***Corresponding authors:** Ahlam A. Abdalla, ahlam.abdalla.21@ucl.ac.uk; Catherine J. Pendegrass, c.pendegrass@ucl.ac.uk.

†**Present Addresses:** Department of Orthopaedics & Musculoskeletal Science, Division of Surgery & Interventional Sciences, University College London, Brockley Hill, Stanmore, UK

1 Institute of Sport, Exercise and Health (ISEH), Division of Surgery & Interventional Sciences, University College London, London, UK; 2 Department of Orthopaedics & Musculoskeletal Science, Division of Surgery & Interventional Sciences, University College London, Brockley Hill, Stanmore, UK

Rotator cuff enthesis and scar tissue

High rates of RC retears are well documented, where various improved suture techniques have been ineffective in reducing them.[38] Surgical repairs for RC tears are often performed via a single or double row suture technique with the aim of approximating the ruptured soft tissue segment from bone. However, due to factors such as age, tear chronicity, and poor vascularity, high retear rates persist with scar-mediated tissue of disorganised matrix and inferior mechanical properties forms.[7, 19, 39-42] Scar formation is thought to be a result of TGF-β1 production by macrophages during the inflammatory phase, leading to fibroblast recruitment.[43] Since expression of TGF-β is elevated at injured entheses, it increases collagen I and III deposition and inhibits chondrogenic differentiation.[19]

Factors influencing healing

Despite better outcomes being linked to intact repairs, it does not guarantee patient satisfaction with functional outcomes.[44,45] Variables affecting outcomes of RC repairs include (I) Age: decrease in turnover, fatty infiltration and tear retraction are thought to be the cause for altering the enthesis healing in older populations regardless of the surgical procedure used.[46-51] (II) Muscle atrophy: severe pre-operative atrophy and fatty infiltration were linked to lower post-operative repair integrity.[45, 52, 53] (III) Smoking: nicotine has been linked to impairments in biomechanical properties and delayed healing.[54] (IV) Diabetes and hypercholesterolemia: they have shown to reduce RC enthesis mechanical properties.[55] Additionally, diabetes increased post-operative complications, such as infections and failures after RC repairs, while hypercholesterolemia increased tendon-related pathologies.[56,57] (V) Obesity demonstrated inferior mechanical properties and poorer histological outcomes with high fat diet.[58] This suggests that long-term maintenance of dietary intake to manage lipid levels and blood glucose prior to injury might have a positive influence on the healing process. (VI) Contrasting evidence exists regarding the effect of vitamin D levels on RC enthesis healing. Animal studies suggest a negative influence of low vitamin D on RC repair, while clinical trials found no correlation between vitamin D levels and retear rates.[59, 60] However, a large clinical study of arthroscopic RC repair found bone mineral density to be a reliable indicator of RC recovery.[61] (VII) Non-steroidal anti-inflammatory drugs: they negatively affect healing in the acute post-operative stage for up to 6 weeks, while positively on remodelling of collagen matrix in chronic stages.[62, 63]

Methodology

An electronic database search was performed using UCL's Online Library Service and PubMed. Keywords used were "enthesis AND rotator cuff", "rotator cuff AND tear", "rotator cuff OR enthesis", "tissue engineering AND rotator cuff", "stem cells AND rotator cuff enthesis", and "growth factors AND rotator cuff enthesis". Outcomes of *in-vivo*, *in-vitro*, and clinical studies on RC enthesis repair involving various tear extent, mechanism, chronicity, and population studies were also included. Exclusion criteria included other types of entheses, and surgical and rehabilitative interventions.

A total of 59 relevant studies were found after exclusion criteria were applied. Of these, 45 presented positive, 10 negative, and 4 mixed findings.

Literature was then summarised based on three main interventions: stem cells, GFs, and scaffolds. Findings were then categorised into groups according to their findings and methodologies (acute-full, chronic-full, acute-partial, chronic-partial, in aging and younger populations, and *in-vitro* studies). **Figure 1** summarises the methodology process.

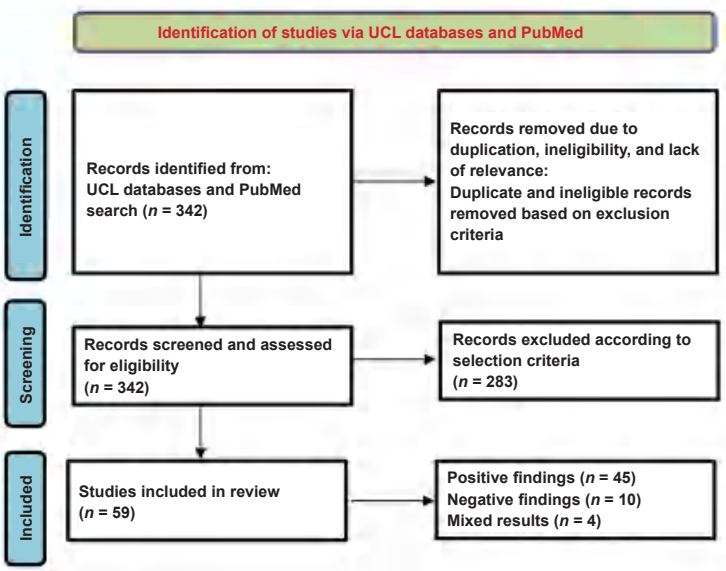

Figure 1. A flowchart representing selection stages of the studies for their inclusion in the literature review.

Literature Review Findings

Cells and rotator cuff enthesis healing

Various stem cells such as mesenchymal stem cells (MSCs), adipose-derived stem cells (ADSCs), and bone marrow MSCs (BMSCs) are under investigation for potential use in enthesis regeneration.[64]

Mesenchymal stem cells

RC enthesis repairs could benefit from MSCs' capacity for self-renewal and multipotency, their availability, accessibility, and low immunogenicity.[65] Moreover, MSCs' local synthesis of GFs may improve the environment for healing.[66] Animal model studies have proven MSCs' potential for increasing ultimate load failure and resistance to mechanical deformation, enhancing bone quality, and attracting new fibrocartilage formation at the repaired site.[67] Additionally, exogenous hyaluronic acid and MSCs have been showing promising potential to reduce retears.[68]

Bone marrow mesenchymal stem cells

BMSCs enhanced structural integrity of the repair and decreased the risk of retears in a chronic full tear cohort that underwent arthroscopic RC surgery with repeated channelling.[69] Moreover, partial tear BMSC-enhanced repairs and prevented retears in 10-year follow-ups.[70] Additionally, arthroscopy surface holding with BMSC stimulation increased RC repair integrity in large chronic tears.[71] BMSCs stimulated by bioactive factors were more effective in promoting tissue regeneration. Platelet-rich plasma (PRP)-infused BMSCs improved GF production, osteogenic differentiation capacity, cell death resistance *in-vitro*, and biomechanical properties of newly formed bone *in-vivo*.[72] Conversely, structure, composition, and strength of the repaired enthesis remained unchanged, despite BMSCs being present and active metabolically.[73] However, this may be due to the short time taken to conduct the study, since stem cells require a longer time to be effective.[74] Moreover, adenoviral MT1-matrix metalloproteinase (MMP)-augmented MSCs resulted in better fibrocartilage formation, and higher ultimate load and stress to failure after 4-week repair of acute full tears, while long-term effects require further research.[75]

Adipose-derived stem cells

ADSCs have a comparable shape and expression of the cluster differentiation surface marker protein to BMSCs with greater colony-forming and adipogenic capacity. They demonstrated multipotency *in-vitro*; developing into adipose, osteogenic, chondrogenic, and myogenic cells.[76] Four groups were compared in a chronic full rabbit repair model: saline + suture, suture + ADSCs, saline, and ADSCs. ADSC and saline groups failed to heal, while suture + ADSCs group had a larger load to failure and less fatty infiltration than saline + suture group.[77] Moreover, ADSCs imbedded in a fibrin sealant resulted in superior histological and biomechanical outcomes, in acute full murine RC repairs.[78] As for the ideal location to deliver cells, regeneration was found most effective when stem cell sheets were interposed at the enthesis, in chronic full tears.[79]

In contrast, ADSCs in acute and chronic rat RC reconstruction models did not enhance biomechanical characteristics. However, inflammation was reduced, which could potentially lead to a more elastic repair and less scar formation after the healing process.[80] Furthermore, TGF-β3 supplementation did not enhance ADSCs' effect on healing, despite its known role in the development of the enthesis.[81] The absence of other mediators that are present during development and the presence of inflammatory mediators may have affected the bioactivity of TGF-β3 at the repair time. However, this study did not measure healing at different time points and ADSCs were not labeled to permit analysis of cell retention.

Due to contradictory evidence, it is unclear whether ADSCs constitute a good option to speed RC tendon-bone healing. To demonstrate its value in RC healing, more animal and clinical research is required. Additionally, challenges of availability, seeding, survival, and specificity of such therapies and the ethical regulatory barriers are yet to be overcome for this to reach a clinical trial. **Table 1** summarises the findings.

Cell pathways and rotator cuff enthesis healing

Ihh signaling molecule

Ihh signaling is active during the initial phases of RC enthesis healing.[29, 82, 83] Fibrocartilage production in an acute full rat RC repair model had higher numbers of Ihh chondrocyte-like cells with MSC augmentation. Increased GLI family zinc finger 1 (Gli1) and Patched1 expression suggests that Ihh signaling pathway controls fibrocartilage production process brought on by stem cells. While both are expressed in fibroblasts of the tendon mid-substance, Ihh is primarily expressed in chondrocytes of the fibrocartilage region, which may indicate a coordinated interaction between chondrocytes and fibroblasts during healing.[82] Additionally, immature mice with acute partial tears had a better recovery than adult mice due to the increased density of $Gli1^+$ cells near the injured enthesis, mimicking its natural developmental process.[83]

Parathyroid hormone related protein

Parathyroid hormone (PTH) has been demonstrated to enhance tissue repair via a chondrogenic pathway.[84, 85] Osteoblasts speed up tendon-bone healing when PTH binds to its receptor in BMSCs during the tendon-bone healing process. Chen et al.[86] showed that PTH may influence the tendon-bone healing process by maintaining the proliferation of BMSCs.

Daily systemic PTH injections boosted fibrocartilage development, type-I procollagen-producing cells, and vascularity, which improved collagen fibre structure and mineralised fibrocartilage production in acute full RC tears.[87] Biomechanically, Duchman et al reported higher load to failure in recombinant human PTH-treated acute full RC tear rat model, and expression of intracellular and extracellular vascular endothelial growth factor (VEGF) with controlled recombinant human PTH systemic injections.[88] Clinical investigations of advanced cases with chronic large tears achieved similar outcomes, and reduced retear rates.[89] **Table 2** summarises the findings.

Table 1. Summary of cell-based therapies literature findings

Author	Study	Model	Tear	Intervention	Outcome measure	Results
Honda et al.[68]	*In-vivo*	Rabbit	Chronic full	MSC + HA	Biomechanical, histological, and immunohistochemical analyses	Positive: Improved ultimate load and faster healing
Jo et al.[69]	Clinical	Human	Chronic full	BMSC + arthroscopic repeated channeling	Pain scale, ROM, muscle strength, patient satisfaction questionnaire, and functional scores. Structural integrity by MRI and CT	Positive: Enhanced structural integrity of the repair and decreased retears
Hernigou et al.[70]	Clinical	Human	Chronic partial	BMSC + arthroscopy	MRI	Positive: Faster complete healing/retear prevention
Taniguchi et al.[71]	Clinical	Human	Chronic partial	ASH + BMSC	MRI	Positive: Reduced retear rates/better integrity
Han et al.[72]	*In-vitro*, *in-vivo*	Rat	Acute full	PRP-infused BMSC	Expression of genes that related to tissue repair, bone formation, and tendon regeneration;	Positive: Stronger signals to angiogenesis, bone formation, and tendon generation *in-situ*
					Biomechanical assessment	Promoted healing *in-vivo*
Gulotta et al.[73]	*In-vivo*	Rat	Acute full	BMSC	Biomechanical & histological analyses	Negative: No change in structure, composition, or strength
Gulotta et al.[75]	*In-vivo*	Rat	Acute full	MT1-MMP-transduced MSCs	Biomechanical & histological analyses	Positive: Better fibrocartilage formation, higher ultimate load and stress to failure, and higher stiffness
Oh et al.[77]	*In-vivo*	Rabbit	Chronic full	ADSC + suture	Electromyographic, biomechanical & histological analyses	Positive: Larger load to failure and less fat infiltration
Chen et al.[78]	*In-vivo*	Murine	Acute full	ADSC imbedded in fibrin sealant scaffold	Biomechanical & histological analyses	Positive: Better biomechanical strength and histological score
Choi et al.[79]	*In-vivo*	Rat	Chronic full	ADSC sheets interposed at the enthesis	Biomechanical & histological analyses	Positive: Successful complete regeneration and biomechanical strength
Valencia Mora et al.[80]	*In-vivo*	Rat	Chronic full	ADSC, ADSC + TGF-β3	Biomechanical & histological analyses	Positive: Reduced inflammation
						Negative: Unchanged maximum load, elastic energy, mechanical deformation, and stiffness

Note: ADSC: adipose-derived stem cell; ASH: arthroscopy surface holding; BMSC: bone marrow mesenchymal stem cell; CT: computed tomography; HA: hyaluronic acid; MMP: matrix metalloproteinase; MRI: magnetic resonance imaging; MSC: mesenchymal stem cell; PRP: platelet-rich plasma; ROM: range of motion; TGF: transforming growth factor.

Growth factors

GFs have been investigated to modulate stem cells in RC enthesis of small and large animal models.[90-96] Fibroblast growth factor 2 (FGF-2), growth differentiation factor, TGF-β3, and platelet-derived growth factor are commonly used examples.[97-104] GFs such as BMP-12, -13, -14, basic fibroblast growth factor, cartilage oligomeric matrix protein, connective tissue growth factor, platelet-derived growth factor-B, and TGF-β1 have been found to be involved in enthesis healing process, one week after acute full rat supraspinatus repair. By 16 weeks, GF upregulation was back to pre-injury levels, indicating exogenous supplementation of these substances may encourage successful healing in acute stages.[105] Angiogenesis and fibroblast proliferation are both powerfully stimulated by basic fibroblast growth factor. It continues to be strongly exhibited throughout the healing process, peaking at 7 and 9 days.[106] Similar outcomes were attained in acute full sheep model RC tear, where BMP and VEGF induced angiogenesis and vasculogenesis, causing faster and better recovery.[43, 107]

Studies investigated TGF-β3's potential to push scar-mediated healing to a regenerative one.[108-111] Sustained delivery of TGF-β3 via a heparin/fibrin-based system in a rat model improved RC enthesis healing, while still inferior to an uninjured enthesis and disorganised scarring.[110] Conversely, studies reported no improvement in biomechanical properties

Table 2. Summary of signaling molecules therapies literature findings

Author	Study	Model	Tear	Intervention	Outcome measure	Study results
Zong et al.[82]	*In-vivo*	Rat	Acute full	Ihh + MSC	Immunohistochemical staining and proliferating cell nuclear antigen staining	Positive: Increased Gli1 and Patched1 expression. More organised and stronger staining for collagen II
Schwartz et al.[29]	*In-vivo*	Murine	Acute partial	Ihh	Lineage tracing	Positive: Gli1 lineage cells that originate in utero eventually populate the entire mature enthesis. Ablation of the Hh-responsive cells during the first week of postnatal development resulted in a loss of mineralised fibrocartilage
Schwartz et al.[83]	*In-vivo*	Mouse	Acute partial	Ihh	Lineage tracing	Positive: High levels of Gli1 expression in immature mice and mature entheses had fewer $Gli1^{+}$ cells
Hettrich et al.[87]	*In-vivo*	Rat	Acute full	Systemic PTH	Histologic, immunohistochemical, biomechanical analyses	Positive: Higher stiffness, bone volume and mineral content; More fibrocartilage, osteoblasts, and blood vessels formation; Better collagen orientation
Duchman et al.[88]	*In-vivo*	Rat	Acute full	Systemic rhPTH	Biomechanical and histologic analysis	Positive: Higher load to failure. Expression of intracellular and extracellular VEGF
Oh et al.[89]	Clinical	Human	Chronic full	Systemic rhPTH	MRI, ROM, American Shoulder and Elbow Surgeons and Constant scores, and simple shoulder test	Positive: Lower retear rate

Note: Gli1: GLI family zinc finger 1; Hh: hedgehog; Ihh: Indian hedgehog; MRI: magnetic resonance imaging; MSC: mesenchymal stem cell; PTH: parathyroid hormone; rhPTH: recombinant human parathyroid hormone; ROM: range of motion; VEGF: vascular endothelial growth factor.

or scar reduction, with TGF-β3 and neutralising bodies for TGF-β1 and -β2 delivered via osmotic pumps, while inhibiting TGF-β1 improved RC enthesis quality by reducing fibrosis, fatty infiltration, and muscle atrophy.[108, 112] This however may be due to the delivery method used in the study, as antibodies were not delivered directly to the interface, rather to the bursal surface. Additionally, TGF-β1 release could compete for receptors with TGF-β3, which leads to reduced effectiveness of TGF-β3 treatment. A suggested solution is to combine TGF-β3 with a cytokine antagonist and TGF-β-neutralising antibodies or MMP inhibitors for acute full tears.[32]

Recombinant human FGF-18 was investigated for chondrogenic differentiation of BMSCs in a rat acute full tear model and enhanced regeneration in acute full RC tears.[113] Furthermore, tumour necrosis factor (TNF) cytokine has been found to suppress chondrogenic stimulation via nuclear factor-kappa B by downregulating SRY-box 9 expression, whilst TGF-β3 solely was not ideal.[114] While TNF inhibitor pegylated soluble TNF-R1 increased fibrocartilage and enhanced load to failure and stiffness, no improvement was seen past 8 weeks.[115]

Since loading after RC repairs is essential to prevent bone loss at the enthesis attachment, to achieve a mechanically resilient enthesis, collagen fibres within the tendon must attach to bone via mineralised fibrocartilage and remodel the underlying bone.[30, 116] Hence, osteoinductive factors (BMP-2–7) are used to induce chondrogenic differentiation and stimulate ECM component synthesis such as proteoglycans and collagen-II. Additionally, BMP-7 improved enthesis matrix maturation in gelatin hydrogel sheets of acute full RC tears.[117, 118] Conversely, Rodeo et al.[107] implanted TGF-β1–3, BMP-2–7, and FGF in a collagen I matrix sponge and compared it to collagen sponge alone, in a sheep acute RC repair. While the study reported greater bone, fibrocartilage, and soft tissue formation, stiffness was less than collagen sponge only group.[107] Although frequently having superior mechanical properties compared to controls, GF-enhanced repairs lack identical biomechanical qualities as native entheses.

GF temporal expression

Despite being present in all stages of healing, GF signal different pathways with different cell types during each stage. BMP-12, -13, -14, bFGF, connective tissue growth factor, platelet-derived growth factor, TGF-β1, and cartilage oligomeric matrix protein-1 are upregulated at the initial inflammatory stage, and subside by 16 weeks.[105] The delay of TGF-β1 upregulation at 8 weeks is correlated with scar formation process.[119] However, BMP-12 is expressed during all three phases, with a marked increase at eight weeks of remodelling stage. This highlights

GF temporal expression involved in various stages of healing, which is essential in developing GFs delivery devices that can be introduced to spatiotemporally target RC repairs. Since healing process is regulated by multiple GFs, targeting one is not ideal functionally or mechanically.[105] **Table 3** summarises the findings.

Table 3. Summary of growth factor-based therapies literature findings

Author	Study	Model	Tear	Intervention	Outcome measure	Study results
Würgler-Hauri et al.[105]	*In-vivo*	Rat	Acute full	BMP-12–14, bFGF, COMP, CTGF, PDGFB, TGF-β1	Immunohistochemical staining	Positive: Increase in the expression of all GFs at 1 week, and followed by a return to control or undetectable levels by 16 weeks
Kobayashi et al.[106]	*In-vivo*	Rabbit	Acute full	BMP-12–14, bFGF, COMP, CTGF, PDGFB, TGF-β1	Light microscopy after staining with hematoxylin-eosin and Elastica-Masson; Immunohistochemical staining	Positive: GFs are involved in early phases of healing promotion
Rodeo et al.[107]	*In-vivo*	Sheep	Acute full	BMP and VEGF	MRI, plain radiographs, histologic analysis, and biomechanical testing	Positive: Greater formation of new bone, fibrocartilage, and soft tissue, with an increase in tendon attachment strength
Angeline and Rodeo[43]	*In-vivo*	Sheep	Acute full	BMP and VEGF	Histologic analysis	Positive: Induced angiogenesis and vasculogenesis. Faster and better recovery
Manning et al.[110]	*In-vivo*	Rat	Acute full	TGF-β3	Histologic and biomechanical analyses	Negative: Disorganised scar and inferior mechanical properties
Kim et al.[108]	*In-vivo*	Rat	Acute full	TGF-β3	Histologic and biomechanical analyses	Negative: Disorganised scar and inferior mechanical properties
Davies et al.[112]	*In-vivo*	Mouse	Acute full	Inhibiting TGF-β1	Histologic analysis	Positive: Reduced fibrosis, fatty infiltration, and muscle atrophy
Jensen et al.[32]	*In-vivo*	Mouse	Acute full and partial	TGF-β3 + cytokine + MMP inhibitors	Reviewing the literature	Positive: Enhanced healing
Zhou et al.[113]	*In-vivo*	Rat	Acute full	rhFGF-18	Histologic analysis	Positive: Promoted chondrogenesis and promoted healing and regeneration
Sitcheran et al.[114]	*In-vivo*	Mouse	Acute full	TGF-β3	Histologic analysis	Negative: No improvement in healing
Gulotta et al.[115]	*In-vivo*	Rat	Acute and chronic full	TNF inhibitor	Histologic and biomechanical analyses	Positive: Elevated fibrocartilage, and enhanced load to failure and stiffness
Dorman et al.[117]	*In-vivo*	Mouse	Acute full	BMP-2–7	Histologic analysis	Positive: Fully healed enthesis without toxicity
Kabuto et al.[118]	*In-vivo*	Rat	Acute full	BMP-2–7	Histologic and biomechanical analyses	Positive: Improved biomechanical properties

Note: bFGF: basic fibroblast growth factor; BMP: bone morphogenetic protein; COMP: cartilage oligomeric matrix protein; CTGF: connective tissue growth factor; GF: growth factor; MMP: matrix metalloproteinase; MRI: magnetic resonance imaging; PDGF: platelet derived growth factor; rhFGF: recombinant human fibroblast growth factor; TGF: transforming growth factor; TNF: tumour necrosis factor; VEGF: vascular endothelial growth factor.

Scaffolds and augments

Augmentations via ECM or synthetic materials could potentially optimise RC enthesis healing.[120] Allografts, synthetic polymers, autografts, and xenografts have been used for RC repairs.[121] Despite improvements in xenografts and allografts decellularisation procedures, they still carry the risk of infection and inflammatory responses from residual donor DNA, high degradation rates, inferior mechanical qualities, and non-specific induction abilities.[43] These concerns have sparked an interest to create grafts and scaffolds for enhanced repairs. Engineered scaffolds with a mix of natural and synthetic biomaterials offer an alternative solution to combat adverse effects caused by synthetic materials. Natural biomaterials including fibrin, collagen, elastin, and hyaluronic acid offer extracellular signals that facilitate cell infiltration and tissue regeneration, where positive results with good host tissue integration, remodelling, and improvement in biomechanical qualities are reported in animal trials employing them.[122, 123]

Known to selectively differentiate BMSCs to chondrocytes, and gelatin methacrylol, a novel biomaterial with promising results in drug carrying, enhanced healing. kartogenin-loaded gelatin methacrylol hydrogel scaffold with bone marrow stimulation promoted fibrocartilage formation and resulted in superior mechanical properties in acute full RC repairs.[124] Compared to traditional double row suture repairs, engineered tissue grafts with 6 months follow-up showed 11% increased elastic modulus, the repaired enthesis was formed similarly to the native tissue, suggesting potential long-term retear prevention.[93]

Exosome-delivered BMP-2 and polyaspartic acid in an acute full RC tear rabbit model resulted in increased tissue mineral density and ultimate load strength, via Smad/RUNX2 signaling pathway. Additionally, tendon regeneration- and cartilage differentiation-related expressions were upregulated, suggesting the positive potential of using bioactive scaffolds in enthesis healing.[125] Since stem cells contribute to healing by autocrine/paracrine signaling through GFs and cytokines, delivering GFs via scaffolds is a simpler and more direct approach to improve RC healing. While interleukin-1 beta inhibited chondrogenesis and maturation of MSCs, the mechanical functionality of the tissue was preserved with three-dimensional (3D) woven polycaprolactone scaffolds.[126] Highlighting the importance of developing strategies to protect against the deleterious effects of cytokines.

A novel strategy combined a 3D printed polylactide-co-glycolide acid scaffold with a cell-laden collagen hydrogel to fabricate layered structures. Mechanical properties improved supporting growth, proliferation, tenogenic differentiation of human ADSCs, and excellent biocompatibility.[127]

As for clinical studies, long-term effect of a polypropylene patch was assessed on large chronic RC repairs and compared with collagen patches, in a patient cohort of 66-year-old. Results showed superior outcomes in muscle strength, pain score, and tendon integrity via ultrasound after a 3-year follow-up.[128] Repairs augmented with 3D biological collagen-I mesh in moderate and large RC tears of patients over 50 years, followed-up for 24-month resulted in better arranged collagen fibres, inflammatory cells less infiltrated, and lower RC retears at 17%.[129]

Although revealed to lower re-ruptures and tissue oedema in animals, porcine small intestine submucosa has been shown ineffective in humans.[130, 131] Due to poor functional results and significant complications, trials cautioned against using small intestine submucosa for RC repairs.[131, 132]

In general, scaffolds provide a growth microenvironment for cells and can be used as carriers for seeded cells and GFs, creating optimal conditions for RC enthesis healing. However, those technologies are still tackling the formation of fibrous cartilage, inflammatory reactions, elevated degeneration rates of the grafted scaffolds, and long-term follow-up.

Demineralised bone matrix

Demineralised bone matrix (DBM) is cancellous bone with osteoinductive and osteoconductive characteristics, known to elicit good adhesion, proliferation, and differentiation of MSCs.[133] DBM-based repairs have not been consistent in improving collagen organisation and fibrocartilage formation, nor result in higher bone mineral density.[134] However, supplementing them with BMSCs resulted in superior outcomes in chronic full tears.[135] Additionally, the use of DBM-based sponge hydrated with PRP resulted improved strength and histological structure in chronic full tears.[136] Despite this, when evaluating the clinical outcomes of patients undergoing biologically enhanced DBM-augmented RC repairs, 50% of patients' magnetic resonance imaging (MRI) confirmed supraspinatus failure.[137]

A more recent study fabricated a gradient multi-tissue construct that mimics structural, compositional, and cellular heterogeneity of the native enthesis designed by 3D cell-printing and tissue-specific decellularised ECM bioinks, where findings suggested improvement in restoring shoulder function.[138] The first human pilot study was performed to assess the safety and efficacy of autologous dermal fibroblast (ADF) injections on full chronic RC repairs of patients aged 20–80 years. Fibroblast samples were obtained from the patients' gluteal region and cultured for four weeks. Patients from both, the control group who did not have an ADF injection, and experimental group, underwent standardised post-operative rehabilitation program involving ice application for 5 days and tramadol for a week, alongside abduction brace immobilisation for five weeks. Exercises such as shoulder shrug and active elbow and forearm range of motion were encouraged immediately after surgery. 10–12 weeks after surgery active-assisted, active range of motion, and strengthening exercises were performed, with return to sport allowed after 6 months. Successful healing without adverse effects was reported in 1-year follow-up.[139] However, this study was limited by the small number of participants and the optimal dosage of ADF was not established. It is difficult to conclude the effectiveness of DBM-based augments on the overall healing process. Larger studies are necessary to examine its true effectiveness and long-term effect.

Platelet-rich plasma

PRP provides a rich source of GFs and cytokines such as PDGF, TGF-β, FGF, VEGF, and IGF.[140] In a study comparing the clinical and structural outcomes between arthroscopic repair of full thickness RC tears with and without PRP supplementation, retear rates were lower with PRP in tears greater than 3 cm, with improved Constant score.[141] Conversely, platelet-rich fibrin clot matrix, a variant of PRP with a fibrin matrix showed no difference in tendon thickness and greater tuberosity coverage in chronic full tears, and positive outcomes in partial tears.[142] However, this could be due to variable PRP preparation used, the nature of PRP used, and level of platelet activation not being accounted.[143] Thus, future research should focus on controlled PRP formulations to judge the benefits of this intervention more accurately.

Systematic reviews revealed PRP injections intraoperatively to produce better long-term pain and shoulder function outcomes following repairs in chronic full tears. While for

short-term follow-ups, PRP was superior in improving function only, in partial RC tears.[144-147] Post-operative subacromial PRP injections on patients with partial RC tears revealed improvement in functional outcomes up to 6 months, despite magnetic resonance imaging structural outcomes being insignificant, and long-term follow-up not being recorded.[148] Moreover, PRP combined with sodium hyaluronate yielded better outcomes in partial RC tears in younger population after 12 months of follow-up.[149] Recent meta-analyses showed PRP augments with double-row constructs have the best outcomes for chronic full tears, according to visual analogue scale (VAS), Constant, Simple Shoulder Test and retears.[150, 151]

Ilhanli et al.[152] debated that PRP may be as effective as physiotherapy interventions in patients with chronic partial tears followed up for 12 months. Despite a study showing an increase in PRP concentration after exercise, it remains unknown whether physiotherapy could enhance the effect of PRP.[153] Moreover, the literature varies in terms of exercise type, intensity, and duration for RC tears.[154] Standard rehabilitation protocols and ideal platelet concentrations for PRP augmented repairs are essential to preserve outcomes and create tailored care for patients with different backgrounds and abilities.

PRP is considered a suitable alternative to corticosteroid injections, which are commonly used clinically to manage RC tears. Achieving pain relief and good clinical outcomes add to the benefit of avoiding the adverse effects of corticosteroids on the body, which makes it an alternative approach to managing symptomatic RC tears, in both; young and athletic, and older populations with comorbidities. **Table 4** summarises the findings.

Table 4. Summary of scaffold-based therapies literature findings

Author	Study	Model	Tear	Intervention	Outcome measure	Study results
Huang et al.[124]	*In-vivo*	Rabbit	Acute full	KGN-loaded GelMA hydrogel + BMSC scaffold	Macroscopy, microcomputed tomography, histology, and biomechanical tests	Positive: Promoted fibrocartilage formation and superior mechanical properties
Novakova et al.[93]	*In-vivo*	Sheep	Acute full	Engineered tendon construct with BMSCs	X-ray and biomechanical tests	Positive: Native-like enthesis with higher modulus
Han et al.[125]	*In-vivo*	Rabbit	Acute full	BMP-2 + polyaspartic acid + Smad/RUNX2 signaling	Transmission electron microscopy staining; Biomechanics and histological assessment	Positive: Increased bone and tissue mineral density and ultimate load strength
Ousema et al.[126]	*In-vitro*	RC tear		3D woven PCL scaffold + IL-1 inhibition on MSCs	Histological, biomechanical, and immunohistochemistry analyses	Positive: Mechanical functionality preserved with the use of a 3D woven PCL scaffold
Jiang et al.[127]	*In-vitro*	RC tear		3D PLGA scaffold + a cell-laden collagen hydrogel + ADSCs	Histological and biomechanics analyses	Positive: Improvement in mechanical properties and biocompatibility
Iannotti et al.[131]	Clinical	Human	Chronic full	SIS	Penn shoulder-score questionnaire and MRI	Negative: No improvement in healing and clinical results
Malcarney et al.[132]	Clinical	Human	Chronic full	SIS	Study discontinued due to adverse effects	Negative: Inflammatory reaction
Sclamberg et al.[130]	Clinical	Human	Chronic full	SIS	Patient questionnaire, MRI, and ASES	Negative: No improvement and worse pot-operative outcomes
Ciampi et al.[128]	Clinical	Aging human	Chronic full	Polypropylene augmentation patch	Ultrasound, muscle strength, and VAS	Positive: Improved muscle strength, pain score, and tendon integrity
Cai et al.[129]	Clinical	Aging human	Chronic full	3D biological collagen-I mesh	MRI, VAS, UCLA SST, and Constant score	Positive: Less retear rates
Hoberman et al.[133]	*In-vitro*	RC tear		DBM + BMSCs + PRP	Adhesion, proliferation, and differentiation assays	Positive: Better adhesion, proliferation, and differentiation
Thangarajah et al.[134]	*In-vivo*	Rat	Chronic full	DBM	Histological analysis	Negative: No improvement in collagen organisation and fibrocartilage formation
Thangarajah et al.[135]	*In-vivo*	Rat	Chronic full	DBM + MSCs	Histological analysis	Positive: Enhanced healing

Table 4. Continued

Author	Study	Model	Tear	Intervention	Outcome measure	Study results
Smith et al.[136]	*In-vivo*	Canine	Chronic full	PRP + DBM	Histological and biomechanical analysis	Positive: Improvement in strength and histological structure
Wellington et al.[137]	Clinical	Human	Chronic full	DBM + MSCs	MRI	Negative: Supraspinatus failure
Chae et al.[138]	*In-vivo*	Mouse	Chronic full	3D cell-printed tendon-bone interface construct	Gait analysis, histological and biomechanical analysis	Positive: Fully formed enthesis, improved shoulder outcome and biomechanical properties
Yoon et al.[139]	Clinical	Aging and young human	Chronic full	ADF	ROM, VAS, and MRI	Positive: No adverse effects, improved VAS, and functional scores
Warth et al.[141]	Clinical	Human	Chronic full	PRP	MRI and Constant score	Positive: Lower retear and improved constant score
Castricini et al.[142]	Clinical	Human	Chronic partial	Autologous PRFM	MRI	Positive: Improved tendon integrity
			Chronic full	Autologous PRFM	MRI	Negative: No difference in constant score and tendon integrity
Giovannetti de Sanctis et al.[144]	Systematic review	Human	Chronic partial	PRP	Shoulder function and VAS	Positive: Improved pain and shoulder function
Von Wehren et al.[145]	Clinical	Human	Chronic partial	PRP	MRI, Constant score, ASES, shoulder ROM, and VAS	Positive: Improved pain and function
Xu and Xue[146]	Systematic review	Human	Chronic full	PRP	Retear rate, Constant, UCLA, ASES, VAS, and adverse effects	Positive: Improved shoulder outcome and reduced retear rate
Rha et al.[147]	Clinical	Human	Chronic partial	PRP	Shoulder Pain and Disability Index, ROM, and ultrasound	Positive: No adverse effects, and improved shoulder pain and function
Shams et al.[148]	Clinical	Human	Chronic partial	PRP	MRI, ASES, Constant Score, SST, and VAS	Positive: Improved shoulder function and minor MRI improvement
Cai et al.[149]	Clinical	Young human	Acute partial	SH + PRP	VAS, Constant score, and MRI	Positive: Better VAS, constant score, and MRI findings
Ryan et al.[150]	Systematic review	Human	Chronic full	PRP	Constant, ASES, UCLA, SST, VAS, and retear rate	Positive: Reduced retear rates and improved clinical outcomes
Lavoie-Gagne et al.[151]	Systematic review and meta-analysis	Human	Chronic full	PRP	Clinical characteristics, retear rates, ROM, and patient reported outcomes	Positive: Reduced retear rates and improved clinical outcomes
Ilhanli et al.[152]	Clinical	Human	Chronic partial	PRP	ROM, VAS, Disabilities of Arm, Shoulder and Hand questionnaire, Neer's, Hawkins' and drop arm tests and Beck Depression Inventory questionnaire	Negative: Results were not superior to physiotherapy

Note: 3D: three-dimensional; ADF: autologous dermal fibroblast; ADSC: adipose-derived stem cell; ASES: American Shoulder and Elbow Surgeons; BMP-2: bone morphogenetic protein-2; BMSC: bone marrow mesenchymal stem cell; DBM: demineralised bone matrix; GelMA: gelatin methacrylol; IL-1: interleukin-1; KGN: kartogenin; MRI: magnetic resonance imaging; PCL: polycaprolactone; PLGA: polylactide-co-glycolide acid; PRFM: platelet-rich fibrin clot matrix; PRP: platelet-rich plasma; RC: rotator cuff; ROM: range of motion; SH: sodium hyaluronate; SIS: small intestine submucosa; SST: Simple Shoulder Test; UCLA: University of California Los Angeles; VAS: visual analogue scale.

Biomechanical Loading Response

Loading tendons is critical for the maintenance of developing entheses, and tissue deformity, delayed mineralisation, and porous non-mineralised tissues are observed when unloaded. Mechanical stimulation increases TGF-β1 and Prrx1$^+$ cells to stimulate enthesis repair.[155] Unloading affects chondrocyte hypertrophy, leading to fibrocartilage absence at the insertion by eight weeks of immobilisation.[36] Reduced humeral volume with flatter surface and morphological changes comparable to those with cerebral palsy were noted, which is attributed to an increase in osteoclasts activity. Hence, blocking osteoclasts activity by bisphosphonate drugs partially recovers bone mineralisation and volume.[36, 37] This imbalance, therefore, contributes to developing an overall mechanically inferior tissue.

While prolonged and immediate mechanical loading induced adverse effects, low-intensity loading was beneficial as opposed to complete removal.[156-158] Since immediate excessive and prolonged loading produce adverse effects, and removal causes malformation, a requirement for balance between loading and healing is essential. When compared to various rehabilitative regimens, simple progressive loading is ideal.[159]

Discussion

RC tears are one of the most common causes of pain and dysfunctions in the shoulders, occurring in 9% under the age of 20 years to 62% until 80 years old.[160] Overhead-sport athletes are at higher risk of chronic RC injuries, due to repetitive loads leading to microtraumas, while contact-sport athletes have a higher risk of traumatic acute tears.[161] As for the aging population, degenerative pathologies are the most prevalent mechanism of injury.[162] Older patients with chronic tears would benefit from non-operative approaches, and younger athletes presenting acute tears require surgery, due to expectations of returning to competition. However, competitive athletes record lower return rates compared to recreational ones.[163] The reason for this remains multifactorial and may not be directly related to the repair, but rather a result of psychological factors such as fear of injury reoccurrence.[164, 165]

RC repairs present good short-term pain and function improvement, and high retears in the long-term.[166] Failure of complete healing urges the shift to alternative strategies aiming at restoring the native tissue's structure and biomechanical properties. Since the RC enthesis is made of a variety of cellular components organised in a gradient complex ECM structure, its regeneration requires the co-regulation of multiple factors.[167]

Stem cell role

The effectiveness of using stem cells to promote RC enthesis healing lies in regulating the differentiation of stem cells into target cells. This regulation is affected by certain factors: (1) the interaction between cells, (2) GFs and signaling molecules in promoting their expression, and (3) local microenvironment and mechanical stimulation. Obtaining stem cells and their survival rate are issues faced when used for RC enthesis healing, hence, improving this can broaden their use in hypoxic conditions. Additionally, methods in which stem cells are taken from patients can reduce patient inconvenience.[167]

Growth factor role

GFs regulate RC enthesis healing in several ways: (1) different GFs are expressed in stages of healing, with GFs promoting angiogenesis present in the inflammatory stage, and those endorsing cell differentiation for collagen synthesis at the repair and remodelling stages.[168] (2) As a signaling molecule, by promoting the expression of genes and proteins related to regulate the biological behavior of cells. (3) By interacting with other GFs. It is essential to consider that: (1) GFs have a short half-life, thus carriers to delay their local release rate and maintain their effect are essential. (2) GFs have different effects based on the tear type. (3) The role of some GFs and their signaling pathways remains unclear. Considerable variations persist between studies in the preparation of GFs (recombinant, synthetic), delivery methods (local injections, systemic, within scaffold, coated sutures), and timing (pre-, peri-, post-operative, and repeated dosages).

Scaffold's role

The choice of scaffold material should meet the growing needs of specific cells, simulate its ECM, mechanically support, and provide a suitable growth environment. Since the main component at the RC insertion is collagen, the application of biomaterials with collagen matrix as the main component is the most effective.[92, 129] Patches designs are essential to assure its proper interaction with the microenvironment for proliferation, adhesion, differentiation, and morphology.[169-172]

Summarised outcomes

Findings suggested a lack of single optimal strategy for restoring RC enthesis. Mechanical stimulation is necessary; its absence cause detrimental effects, and long-term progressive loading rehabilitation aids in achieving a comprehensive RC repair.[16, 36, 37, 155, 157, 159]

Augmenting MSCs with adenoviral MT1-MMP had positive biomechanical outcomes in acute full tears[75] (**Figure 2**). ADSCs present contradicting outcomes in acute and chronic full tears, and BMSCs were recorded as negative in acute.[73, 77, 80, 81] However infusing BMSCs with PRP and imbedding ADSCs in fibrin sealant scaffold enhance repairs.[72, 78] Conversely, TGF-β3-supplemented ADSCs did not enhance acute full tear healing.[80] For chronic full ones, MSCs combined with hyaluronic acid, BMSCs with repeated channeling, and ADSC sheets interposed improved outcomes.[68, 69, 79] Clinical trials in chronic partial tears with BMSC-enhanced augmentation improved healing and prevented retears.[70, 71]

For signaling molecules, systemic PTH produced positive outcomes in full acute and chronic tears.[87-89] Ihh with MSCs had positive outcomes in acute partial and full tears.[29, 82, 83] BMP-12–14, basic fibroblast growth factor, COMP, connective tissue growth factor, PDGFB, BMP-2–7, recombinant human FGF-18, TGF-β1, and the combination of BMP and VEGF resulted positively, while TGF-β3 remained ineffective in acute full tears.[43, 105-107, 110, 113, 114, 117, 118] Inhibiting TGF-β1 was effective in acute full tears, and TNF inhibition was better in full acute and chronic tears.[112, 115] Most promising outcomes were attained by combining TGF-β3 with a cytokine and MMP inhibitor in acute partial and full tears.[32]

Figure 2. Categorised literature findings: stem cells, GFs, and scaffolds vary in effect depending on the extent of the tear, chronicity level, population, and their combinations. Majority of studies investigated acute full tears, while less studies were investigating partial and full chronic tears. Very few studies considered the age of the studied population. 3D: three-dimensional; ADF: autologous dermal fibroblast; ADSC: adipose-derived stem cell; bFGF: basic fibroblast growth factor; BMP: bone morphogenetic protein; BMSC: bone marrow mesenchymal stem cell; COMP: cartilage oligomeric matrix protein; CTGF: connective tissue growth factor; DBM: demineralised bone matrix; GelMA: gelatin methacrylol; GF: growth factor; HA: hyaluronic acid; Ihh: Indian hedgehog; KGN: kartogenin; MMP: matrix metalloproteinase; MSC: mesenchymal stem cell; PCL: polycaprolactone; PDGFB: platelet-derived growth factor-B; PLGA: polylactide-co-glycolide acid; PRFM: platelet-rich fibrin clot matrix; PRP: platelet-rich plasma; PTH: parathyroid hormone; SH: sodium hyaluronate; SIS: small intestine submucosa; TGF: transforming growth factor; TNF: tumour necrosis factor.

Outcomes from scaffold-based studies are promising and reached clinical trials. Polypropylene augmentation patch resulted in good outcomes in aging models with chronic full tears.[128] 3D cell-printed tendon-bone interface construct revealed positive outcomes in chronic full tears contrasting small intestine submucosa.[130-132,138] Kartogenin-loaded gelatin methacrylol with BMSCs, engineered constructs with BMSCs, and BMP-2 with polyaspartic acid and Smad/RUNX2 improved acute full tears.[93, 124, 125] DBM-based scaffold was not beneficial, however, augmenting it with MSCs and PRP in separate animal models was effective.[134-136] Clinical trials on DBM and MSCs combination did not replicate similar outcomes.[137] This could be attributed to the varied forms of scaffold materials, since animal models have shown promising results with strips of cancellous DBM, while clinical studies used sponges. Sponges can be displaced from the interface site, whereas strips and patches can be more securely sutured into the interface.

Autologous platelet-rich fibrin clot matrix clinical studies were more beneficial in chronic partial than full tears.[142] ADF was safe and effective in younger and older populations with chronic full tears.[139] While PRP is proven beneficial in chronic partial and full tears, it wasn't superior to physiotherapy.[126, 141, 144-148, 150-152] Sodium hyaluronate combined PRP was effective in acute and partial tears of younger populations.[149] 3D collagen I mesh augmentation in older populations with chronic full tears resulted in positive long-term outcomes.[129] Novel multifactorial lab-based tissue engineering strategies such as 3D-woven polycaprolactone scaffold with IL-1 inhibition on MSCs, 3D polylactide-co-glycolide acid scaffold in cell-laden collagen hydrogel and ADSCs, BMSCs and PRP enhanced DBM-based scaffold had promising outcomes.[126, 127, 133]

Potential reasons for variations

Outcomes vary since there is no standardised controlled environment prior and after repairs. They differ in methodologies, animal models, and mechanical follow-ups; some allow free mobilisation after repairs, while others impose treadmill walking regimens or restrict movement.

It is difficult to determine if variations are due to the interventions, animal models, mechanical environment, or extent and mechanism of tears. Some studies created acute dissection or detachment, immediately injecting it with the examined substances prior to repairs. However, that does not represent the clinical acute and chronic mechanism of tear, as it does not allow time for the inflammatory process to take place; no blood supply restriction, enthesis degeneration, and fatty infiltration. Other studies subject animals to a treadmill regimen prior to the intervention to exhaust tendons and replicate overuse. Findings should be similar in both scenarios, to indicate that the intervention has a definitive outcome.[173] Treadmill regimen does not ideally replicate injury process in athletes performing sports since childhood. Professionally trained athletes have a lower risk of RC injury compared to amateurs that lack proper loading techniques, healthy balanced diet, sleep routine, and psychological well-being. This might fit amateur athletes scenario who are exposed to improper unconditioned loading. Additionally, small animal models such as rats and rodents have a far better healing capacity than larger animals and humans. Their measures of success should not be solely determined based on morphology, but also the timeframe and long-term effects. Surgical techniques used also affect the outcome of biological therapies. Introducing stem cells via tunnels produced superior outcomes to surface repairs. Additionally, biomaterial patch that covered the repair addressed MSCs long-term survival.[174-176]

Clinical outcomes are affected by patients' occupation, demographics, age, gender, comorbidities, and tear mechanism and extent. Moreover, patient outcome measures have a degree of subjectivity, affected by expectations and psychosocial well-being.

Conclusion

To take research of tendon-bone enthesis for RC tears forward, there are critical factors involved in the healing of the enthesis, which is supported by what has been presented and rationale for, where without them there wouldn't be a successful healing. Tissue engineering has promising outcomes in achieving the complex RC enthesis structure and function. Different cells and GFs at specific times and environmental control can maximise the restoration of the native enthesis. Despite the positive outcomes of tissue engineering strategies, progressive loading environment is essential for optimum healing. Although the effects of the discussed interventions have mostly been confirmed in animal experiments, the intrinsic connections between cells at the interface and the molecular signaling pathways involved in tissue repair and regeneration still need to be further explored in humans. Nevertheless, the limitations mentioned are important to be considered for future studies to be applied in clinical practice.

This paper described the microscopic anatomy of the healthy RC enthesis, its role in facilitating force transmission, and the biomechanical adaptations. It then discussed the structural changes that accompany injured RC enthesis and the factors influencing its healing potential. Positive outcomes in the field of stem cells, GFs, and scaffolds along with their challenges, limitations, and variety of implementation are explained. The results support the proposed hypothesis that interventions should be tailored according to the tear extent, chronicity, and population studied.

Study limitations

Inconsistencies in reported outcomes derive from variations in patients' occupation, demographics, age, gender, comorbidities, and tear mechanism and extent. Moreover, patient reported outcome measures are subjective, and influenced by expectations and psychosocial well-being. Perspective studies would benefit from addressing the following:

1. The difficulties in advancing *in vivo* studies to clinical trials and the regulatory constraints associated with utilising biological interventions which have proven successful in the former, to the latter.
2. Biological materials availability and manufacturing in forms that can be utilised clinically in RC repair.
3. The potential for personalised biological intervention materials.
4. Solutions for aging patients and professional athletes requiring 100% recovery to return to competition.
5. Influential medical, environmental, social, and psychological factors.

Author contributions

Both authors contributed to the design, literature research, analysis, and preparation of the manuscript. Both authors revised the manuscript and approved the final version of the manuscript.

Financial support

None.

Acknowledgement

Ahlam A. Abdalla would like to extend my gratitude to Dr. Catherine Pendegrass for encouraging and supporting me throughout. We appreciate UCL for providing the resources and easy access to the literature, as it was essential to obtain the requirements and complete this paper. This review was supported by the United Arab Emirates Ministry of Education, and University College London.

Conflicts of interest statement

Both authors declare that they have no competing interests.

Open access statement

This is an open access journal, and articles are distributed under the terms of the Creative Commons Attribution-NonCommercial-ShareAlike 4.0 License, which allows others to remix, tweak, and build upon the work non-commercially, as long as appropriate credit is given and the new creations are licensed under the identical terms.

1. Liu, Y. X.; Thomopoulos, S.; Birman, V.; Li, J. S.; Genin, G. M. Bi-material attachment through a compliant interfacial system at the tendon-to-bone insertion site. *Mech Mater.* **2012**, *44*, 10.1016/j.mechmat.2011.1008.1005.
2. Thomopoulos, S.; Williams, G. R.; Gimbel, J. A.; Favata, M.; Soslowsky, L. J. Variation of biomechanical, structural, and compositional properties along the tendon to bone insertion site. *J Orthop Res.* **2003**, *21*, 413-419.
3. Shaw, H. M.; Benjamin, M. Structure-function relationships of entheses in relation to mechanical load and exercise. *Scand J Med Sci Sports.* **2007**, *17*, 303-315.
4. Lu, H. H.; Thomopoulos, S. Functional attachment of soft tissues to bone: development, healing, and tissue engineering. *Annu Rev Biomed Eng.* **2013**, *15*, 201-226.

5. Milgrom, C.; Schaffler, M.; Gilbert, S.; van Holsbeeck, M. Rotator-cuff changes in asymptomatic adults. The effect of age, hand dominance and gender. *J Bone Joint Surg Br.* **1995**, *77*, 296-298.
6. Yamaguchi, K.; Ditsios, K.; Middleton, W. D.; Hildebolt, C. F.; Galatz, L. M.; Teefey, S. A. The demographic and morphological features of rotator cuff disease. A comparison of asymptomatic and symptomatic shoulders. *J Bone Joint Surg Am.* **2006**, *88*, 1699-1704.
7. Galatz, L. M.; Ball, C. M.; Teefey, S. A.; Middleton, W. D.; Yamaguchi, K. The outcome and repair integrity of completely arthroscopically repaired large and massive rotator cuff tears. *J Bone Joint Surg Am.* **2004**, *86*, 219-224.
8. Shindle, M. K.; Chen, C. C.; Robertson, C.; DiTullio, A. E.; Paulus, M. C.; Clinton, C. M.; Cordasco, F. A.; Rodeo, S. A.; Warren, R. F. Full-thickness supraspinatus tears are associated with more synovial inflammation and tissue degeneration than partial-thickness tears. *J Shoulder Elbow Surg.* **2011**, *20*, 917-927.
9. Benjamin, M.; Qin, S.; Ralphs, J. R. Fibrocartilage associated with human tendons and their pulleys. *J Anat.* 1995, *187* (Pt 3), 625-633.
10. Benjamin, M.; Kumai, T.; Milz, S.; Boszczyk, B. M.; Boszczyk, A. A.; Ralphs, J. R. The skeletal attachment of tendons--tendon "entheses". *Comp Biochem Physiol A Mol Integr Physiol.* **2002**, *133*, 931-945.
11. Frowen, P.; Benjamin, M. Variations in the quality of uncalcified fibrocartilage at the insertions of the extrinsic calf muscles in the foot. *J Anat.* **1995**, *186* (Pt 2), 417-421.
12. Matyas, J. R.; Anton, M. G.; Shrive, N. G.; Frank, C. B. Stress governs tissue phenotype at the femoral insertion of the rabbit MCL. *J Biomech.* **1995**, *28*, 147-157.
13. Yang, P. J.; Temenoff, J. S. Engineering orthopedic tissue interfaces. *Tissue Eng Part B Rev.* **2009**, *15*, 127-141.
14. Benjamin, M.; Ralphs, J. R. Fibrocartilage in tendons and ligaments--an adaptation to compressive load. *J Anat.* **1998**, *193 (Pt 4)*, 481-494.
15. Connizzo, B. K.; Adams, S. M.; Adams, T. H.; Jawad, A. F.; Birk, D. E.; Soslowsky, L. J. Multiscale regression modeling in mouse supraspinatus tendons reveals that dynamic processes act as mediators in structure-function relationships. *J Biomech.* **2016**, *49*, 1649-1657.
16. Schwartz, A. G.; Lipner, J. H.; Pasteris, J. D.; Genin, G. M.; Thomopoulos, S. Muscle loading is necessary for the formation of a functional tendon enthesis. *Bone.* **2013**, *55*, 44-51.
17. Knese, K. H.; Biermann, H. Osteogenesis in tendon and ligament insertions in the area of the original chondral apophyses. *Z Zellforsch Mikrosk Anat.* **1958**, *49*, 142-187.
18. Thomopoulos, S.; Hattersley, G.; Rosen, V.; Mertens, M.; Galatz, L.; Williams, G. R.; Soslowsky, L. J. The localized expression of extracellular matrix components in healing tendon insertion sites: an in situ hybridization study. *J Orthop Res.* **2002**, *20*, 454-463.
19. Galatz, L. M.; Sandell, L. J.; Rothermich, S. Y.; Das, R.; Mastny, A.; Havlioglu, N.; Silva, M. J.; Thomopoulos, S. Characteristics of the rat supraspinatus tendon during tendon-to-bone healing after acute injury. *J Orthop Res.* **2006**, *24*, 541-550.
20. Ralphs, J. R.; Tyers, R. N.; Benjamin, M. Development of functionally distinct fibrocartilages at two sites in the quadriceps tendon of the rat: the suprapatella and the attachment to the patella. *Anat Embryol (Berl).* **1992**, *185*, 181-187.
21. Rufai, A.; Benjamin, M.; Ralphs, J. R. Development and ageing of phenotypically distinct fibrocartilages associated with the rat Achilles tendon. *Anat Embryol (Berl).* **1992**, *186*, 611-618.
22. Blitz, E.; Viukov, S.; Sharir, A.; Shwartz, Y.; Galloway, J. L.; Pryce, B. A.; Johnson, R. L.; Tabin, C. J.; Schweitzer, R.; Zelzer, E. Bone ridge patterning during musculoskeletal assembly is mediated through SCX regulation of Bmp4 at the tendon-skeleton junction. *Dev Cell.* **2009**, *17*, 861-873.
23. Blitz, E.; Sharir, A.; Akiyama, H.; Zelzer, E. Tendon-bone attachment unit is formed modularly by a distinct pool of Scx- and Sox9-positive progenitors. *Development.* **2013**, *140*, 2680-2690.
24. Galatz, L.; Rothermich, S.; VanderPloeg, K.; Petersen, B.; Sandell, L.; Thomopoulos, S. Development of the supraspinatus tendon-to-bone insertion: localized expression of extracellular matrix and growth factor genes. *J Orthop Res.* **2007**, *25*, 1621-1628.
25. Ito, Y.; Toriuchi, N.; Yoshitaka, T.; Ueno-Kudoh, H.; Sato, T.; Yokoyama, S.; Nishida, K.; Akimoto, T.; Takahashi, M.; Miyaki, S.; Asahara, H. The Mohawk homeobox gene is a critical regulator of tendon differentiation. *Proc Natl Acad Sci U S A.* **2010**, *107*, 10538-10542.
26. Schweitzer, R.; Chyung, J. H.; Murtaugh, L. C.; Brent, A. E.; Rosen, V.; Olson, E. N.; Lassar, A.; Tabin, C. J. Analysis of the tendon cell fate using Scleraxis, a specific marker for tendons and ligaments. *Development.* **2001**, *128*, 3855-3866.
27. Sugimoto, Y.; Takimoto, A.; Akiyama, H.; Kist, R.; Scherer, G.; Nakamura, T.; Hiraki, Y.; Shukunami, C. Scx+/Sox9+ progenitors contribute to the establishment of the junction between cartilage and tendon/ligament. *Development.* **2013**, *140*, 2280-2288.
28. Killian, M. L.; Thomopoulos, S. Scleraxis is required for the development of a functional tendon enthesis. *FASEB J.* **2016**, *30*, 301-311.
29. Schwartz, A. G.; Long, F.; Thomopoulos, S. Enthesis fibrocartilage cells originate from a population of Hedgehog-responsive cells modulated by the loading environment. *Development.* **2015**, *142*, 196-206.
30. Dyment, N. A.; Breidenbach, A. P.; Schwartz, A. G.; Russell, R. P.; Aschbacher-Smith, L.; Liu, H.; Hagiwara, Y.; Jiang, R.; Thomopoulos, S.; Butler, D. L.; Rowe, D. W. Gdf5 progenitors give rise to fibrocartilage cells that mineralize via hedgehog signaling to form the zonal enthesis. *Dev Biol.* **2015**, *405*, 96-107.
31. Dyment, N. A.; Hagiwara, Y.; Matthews, B. G.; Li, Y.; Kalajzic, I.; Rowe, D. W. Lineage tracing of resident tendon progenitor cells during growth and natural healing. *PLoS One.* **2014**, *9*, e96113.
32. Jensen, P. T.; Lambertsen, K. L.; Frich, L. H. Assembly, maturation, and degradation of the supraspinatus enthesis. *J Shoulder Elbow Surg.* **2018**, *27*, 739-750.
33. Santoni, B. G.; McGilvray, K. C.; Lyons, A. S.; Bansal, M.; Turner, A. S.; Macgillivray, J. D.; Coleman, S. H.; Puttlitz, C. M. Biomechanical analysis of an ovine rotator cuff repair via porous patch augmentation in a chronic rupture model. *Am J Sports Med.* **2010**, *38*, 679-686.
34. Mori, D.; Funakoshi, N.; Yamashita, F.; Wakabayashi, T. Effect of fatty degeneration of the infraspinatus on the efficacy of arthroscopic patch autograft procedure for large to massive rotator cuff tears. *Am J Sports Med.* **2015**, *43*, 1108-1117.
35. Hakimi, O.; Mouthuy, P. A.; Zargar, N.; Lostis, E.; Morrey, M.; Carr, A. A layered electrospun and woven surgical scaffold to enhance endogenous tendon repair. *Acta Biomater.* **2015**, *26*, 124-135.
36. Thomopoulos, S.; Kim, H. M.; Rothermich, S. Y.; Biederstadt, C.; Das, R.; Galatz, L. M. Decreased muscle loading delays maturation of the tendon enthesis during postnatal development. *J Orthop Res.* **2007**, *25*, 1154-1163.
37. Tatara, A. M.; Lipner, J. H.; Das, R.; Kim, H. M.; Patel, N.; Ntouvali, E.; Silva, M. J.; Thomopoulos, S. The role of muscle loading on bone (Re) modeling at the developing enthesis. *PLoS One.* **2014**, *9*, e97375.
38. Rhee, Y. G.; Cho, N. S.; Yoo, J. H. Clinical outcome and repair integrity

after rotator cuff repair in patients older than 70 years versus patients younger than 70 years. *Arthroscopy.* **2014**, *30*, 546-554.
39. Melis, B.; Nemoz, C.; Walch, G. Muscle fatty infiltration in rotator cuff tears: descriptive analysis of 1688 cases. *Orthop Traumatol Surg Res.* **2009**, *95*, 319-324.
40. Meyer, D. C.; Farshad, M.; Amacker, N. A.; Gerber, C.; Wieser, K. Quantitative analysis of muscle and tendon retraction in chronic rotator cuff tears. *Am J Sports Med.* **2012**, *40*, 606-610.
41. Saadat, F.; Deymier, A. C.; Birman, V.; Thomopoulos, S.; Genin, G. M. The concentration of stress at the rotator cuff tendon-to-bone attachment site is conserved across species. *J Mech Behav Biomed Mater.* **2016**, *62*, 24-32.
42. Kanazawa, T.; Gotoh, M.; Ohta, K.; Honda, H.; Ohzono, H.; Shimokobe, H.; Shiba, N.; Nakamura, K. Histomorphometric and ultrastructural analysis of the tendon-bone interface after rotator cuff repair in a rat model. *Sci Rep.* **2016**, *6*, 33800.
43. Angeline, M. E.; Rodeo, S. A. Biologics in the management of rotator cuff surgery. *Clin Sports Med.* **2012**, *31*, 645-663.
44. Harryman, D. T., 2nd; Mack, L. A.; Wang, K. Y.; Jackins, S. E.; Richardson, M. L.; Matsen, F. A., 3rd. Repairs of the rotator cuff. Correlation of functional results with integrity of the cuff. *J Bone Joint Surg Am.* 1991, *73*, 982-989.
45. Liem, D.; Lichtenberg, S.; Magosch, P.; Habermeyer, P. Magnetic resonance imaging of arthroscopic supraspinatus tendon repair. *J Bone Joint Surg Am.* **2007**, *89*, 1770-1776.
46. Charousset, C.; Bellaïche, L.; Kalra, K.; Petrover, D. Arthroscopic repair of full-thickness rotator cuff tears: is there tendon healing in patients aged 65 years or older? *Arthroscopy.* **2010**, *26*, 302-309.
47. Cho, N. S.; Rhee, Y. G. The factors affecting the clinical outcome and integrity of arthroscopically repaired rotator cuff tears of the shoulder. *Clin Orthop Surg.* **2009**, *1*, 96-104.
48. Nho, S. J.; Shindle, M. K.; Adler, R. S.; Warren, R. F.; Altchek, D. W.; MacGillivray, J. D. Prospective analysis of arthroscopic rotator cuff repair: subgroup analysis. *J Shoulder Elbow Surg.* **2009**, *18*, 697-704.
49. Oh, J. H.; Kim, S. H.; Kang, J. Y.; Oh, C. H.; Gong, H. S. Effect of age on functional and structural outcome after rotator cuff repair. *Am J Sports Med.* **2010**, *38*, 672-678.
50. Tashjian, R. Z.; Hollins, A. M.; Kim, H. M.; Teefey, S. A.; Middleton, W. D.; Steger-May, K.; Galatz, L. M.; Yamaguchi, K. Factors affecting healing rates after arthroscopic double-row rotator cuff repair. *Am J Sports Med.* **2010**, *38*, 2435-2442.
51. Boileau, P.; Brassart, N.; Watkinson, D. J.; Carles, M.; Hatzidakis, A. M.; Krishnan, S. G. Arthroscopic repair of full-thickness tears of the supraspinatus: does the tendon really heal? *J Bone Joint Surg Am.* **2005**, *87*, 1229-1240.
52. Thomazeau, H.; Boukobza, E.; Morcet, N.; Chaperon, J.; Langlais, F. Prediction of rotator cuff repair results by magnetic resonance imaging. *Clin Orthop Relat Res.* **1997**, 275-283.
53. Goutallier, D.; Postel, J. M.; Gleyze, P.; Leguilloux, P.; Van Driessche, S. Influence of cuff muscle fatty degeneration on anatomic and functional outcomes after simple suture of full-thickness tears. *J Shoulder Elbow Surg.* **2003**, *12*, 550-554.
54. Galatz, L. M.; Silva, M. J.; Rothermich, S. Y.; Zaegel, M. A.; Havlioglu, N.; Thomopoulos, S. Nicotine delays tendon-to-bone healing in a rat shoulder model. *J Bone Joint Surg Am.* **2006**, *88*, 2027-2034.
55. Bedi, A.; Fox, A. J.; Harris, P. E.; Deng, X. H.; Ying, L.; Warren, R. F.; Rodeo, S. A. Diabetes mellitus impairs tendon-bone healing after rotator cuff repair. *J Shoulder Elbow Surg.* **2010**, *19*, 978-988.
56. Chen, A. L.; Shapiro, J. A.; Ahn, A. K.; Zuckerman, J. D.; Cuomo, F. Rotator cuff repair in patients with type I diabetes mellitus. *J Shoulder Elbow Surg.* **2003**, *12*, 416-421.
57. Tilley, B. J.; Cook, J. L.; Docking, S. I.; Gaida, J. E. Is higher serum cholesterol associated with altered tendon structure or tendon pain? A systematic review. *Br J Sports Med.* **2015**, *49*, 1504-1509.
58. Bolam, S. M.; Park, Y. E.; Konar, S.; Callon, K. E.; Workman, J.; Monk, A. P.; Coleman, B.; Cornish, J.; Vickers, M. H.; Munro, J. T.; Musson, D. S. Obesity impairs enthesis healing after rotator cuff repair in a rat model. *Am J Sports Med.* **2021**, *49*, 3959-3969.
59. Angeline, M. E.; Ma, R.; Pascual-Garrido, C.; Voigt, C.; Deng, X. H.; Warren, R. F.; Rodeo, S. A. Effect of diet-induced vitamin D deficiency on rotator cuff healing in a rat model. *Am J Sports Med.* **2014**, *42*, 27-34.
60. Ryu, K. J.; Kim, B. H.; Lee, Y.; Dan, J.; Kim, J. H. Low serum vitamin d is not correlated with the severity of a rotator cuff tear or retear after arthroscopic repair. *Am J Sports Med.* **2015**, *43*, 1743-1750.
61. Chung, S. W.; Oh, J. H.; Gong, H. S.; Kim, J. Y.; Kim, S. H. Factors affecting rotator cuff healing after arthroscopic repair: osteoporosis as one of the independent risk factors. *Am J Sports Med.* **2011**, *39*, 2099-2107.
62. Cohen, D. B.; Kawamura, S.; Ehteshami, J. R.; Rodeo, S. A. Indomethacin and celecoxib impair rotator cuff tendon-to-bone healing. *Am J Sports Med.* **2006**, *34*, 362-369.
63. Chan, K. M.; Fu, S. C. Anti-inflammatory management for tendon injuries - friends or foes? *Sports Med Arthrosc Rehabil Ther Technol.* **2009**, *1*, 23.
64. Rak Kwon, D.; Jung, S.; Jang, J.; Park, G. Y.; Suk Moon, Y.; Lee, S. C. A 3-Dimensional bioprinted scaffold with human umbilical cord blood-mesenchymal stem cells improves regeneration of chronic full-thickness rotator cuff tear in a rabbit model. *Am J Sports Med.* **2020**, *48*, 947-958.
65. García-Gómez, I.; Elvira, G.; Zapata, A. G.; Lamana, M. L.; Ramírez, M.; Castro, J. G.; Arranz, M. G.; Vicente, A.; Bueren, J.; García-Olmo, D. Mesenchymal stem cells: biological properties and clinical applications. *Expert Opin Biol Ther.* **2010**, *10*, 1453-1468.
66. Lee, E. H.; Hui, J. H. The potential of stem cells in orthopaedic surgery. *J Bone Joint Surg Br.* **2006**, *88*, 841-851.
67. Morton-Gonzaba, N.; Carlisle, D.; Emukah, C.; Chorath, K.; Moreira, A. Mesenchymal stem cells and their application to rotator cuff pathology: A meta-analysis of pre-clinical studies. *Osteoarthr Cartil Open.* **2020**, *2*, 100047.
68. Honda, H.; Gotoh, M.; Kanazawa, T.; Ohzono, H.; Nakamura, H.; Ohta, K.; Nakamura, K. I.; Fukuda, K.; Teramura, T.; Hashimoto, T.; Shichijo, S.; Shiba, N. Hyaluronic acid accelerates tendon-to-bone healing after rotator cuff repair. *Am J Sports Med.* **2017**, *45*, 3322-3330.
69. Jo, C. H.; Shin, J. S.; Park, I. W.; Kim, H.; Lee, S. Y. Multiple channeling improves the structural integrity of rotator cuff repair. *Am J Sports Med.* **2013**, *41*, 2650-2657.
70. Hernigou, P.; Flouzat Lachaniette, C. H.; Delambre, J.; Zilber, S.; Duffiet, P.; Chevallier, N.; Rouard, H. Biologic augmentation of rotator cuff repair with mesenchymal stem cells during arthroscopy improves healing and prevents further tears: a case-controlled study. *Int Orthop.* **2014**, *38*, 1811-1818.
71. Taniguchi, N.; Suenaga, N.; Oizumi, N.; Miyoshi, N.; Yamaguchi, H.; Inoue, K.; Chosa, E. Bone marrow stimulation at the footprint of arthroscopic surface-holding repair advances cuff repair integrity. *J Shoulder Elbow Surg.* **2015**, *24*, 860-866.
72. Han, L.; Fang, W. L.; Jin, B.; Xu, S. C.; Zheng, X.; Hu, Y. G.

Enhancement of tendon-bone healing after rotator cuff injuries using combined therapy with mesenchymal stem cells and platelet rich plasma. *Eur Rev Med Pharmacol Sci.* **2019**, *23*, 9075-9084.

73. Gulotta, L. V.; Kovacevic, D.; Ehteshami, J. R.; Dagher, E.; Packer, J. D.; Rodeo, S. A. Application of bone marrow-derived mesenchymal stem cells in a rotator cuff repair model. *Am J Sports Med.* **2009**, *37*, 2126-2133.
74. Nourissat, G.; Diop, A.; Maurel, N.; Salvat, C.; Dumont, S.; Pigenet, A.; Gosset, M.; Houard, X.; Berenbaum, F. Mesenchymal stem cell therapy regenerates the native bone-tendon junction after surgical repair in a degenerative rat model. *PLoS One.* **2010**, *5*, e12248.
75. Gulotta, L. V.; Kovacevic, D.; Montgomery, S.; Ehteshami, J. R.; Packer, J. D.; Rodeo, S. A. Stem cells genetically modified with the developmental gene MT1-MMP improve regeneration of the supraspinatus tendon-to-bone insertion site. *Am J Sports Med.* **2010**, *38*, 1429-1437.
76. Vishnubalaji, R.; Al-Nbaheen, M.; Kadalmani, B.; Aldahmash, A.; Ramesh, T. Comparative investigation of the differentiation capability of bone-marrow- and adipose-derived mesenchymal stem cells by qualitative and quantitative analysis. *Cell Tissue Res.* **2012**, *347*, 419-427.
77. Oh, J. H.; Chung, S. W.; Kim, S. H.; Chung, J. Y.; Kim, J. Y. 2013 Neer Award: Effect of the adipose-derived stem cell for the improvement of fatty degeneration and rotator cuff healing in rabbit model. *J Shoulder Elbow Surg.* **2014**, *23*, 445-455.
78. Chen, Y.; Xu, Y.; Dai, G.; Shi, Q.; Duan, C. Enhanced Repaired Enthesis Using Tenogenically Differentiated Adipose-Derived Stem Cells in a Murine Rotator Cuff Injury Model. *Stem Cells Int.* **2022**, *2022*, 1309684.
79. Choi, J. H.; Shim, I. K.; Shin, M. J.; Lee, Y. N.; Koh, K. H. Stem cell sheet interpositioned between the tendon and bone would be better for healing than stem cell sheet overlaid above the tendon-to-bone junction in rotator cuff repair of rats. *PLoS One.* **2022**, *17*, e0266030.
80. Valencia Mora, M.; Antuña Antuña, S.; García Arranz, M.; Carrascal, M. T.; Barco, R. Application of adipose tissue-derived stem cells in a rat rotator cuff repair model. *Injury.* **2014**, *45 Suppl 4*, S22-27.
81. Rothrauff, B. B.; Smith, C. A.; Ferrer, G. A.; Novaretti, J. V.; Pauyo, T.; Chao, T.; Hirsch, D.; Beaudry, M. F.; Herbst, E.; Tuan, R. S.; Debski, R. E.; Musahl, V. The effect of adipose-derived stem cells on enthesis healing after repair of acute and chronic massive rotator cuff tears in rats. *J Shoulder Elbow Surg.* **2019**, *28*, 654-664.
82. Zong, J. C.; Mosca, M. J.; Degen, R. M.; Lebaschi, A.; Carballo, C.; Carbone, A.; Cong, G. T.; Ying, L.; Deng, X. H.; Rodeo, S. A. Involvement of Indian hedgehog signaling in mesenchymal stem cell-augmented rotator cuff tendon repair in an athymic rat model. *J Shoulder Elbow Surg.* **2017**, *26*, 580-588.
83. Schwartz, A. G.; Galatz, L. M.; Thomopoulos, S. Enthesis regeneration: a role for Gli1+ progenitor cells. *Development.* **2017**, *144*, 1159-1164.
84. Nakazawa, T.; Nakajima, A.; Shiomi, K.; Moriya, H.; Einhorn, T. A.; Yamazaki, M. Effects of low-dose, intermittent treatment with recombinant human parathyroid hormone (1-34) on chondrogenesis in a model of experimental fracture healing. *Bone.* **2005**, *37*, 711-719.
85. Kakar, S.; Einhorn, T. A.; Vora, S.; Miara, L. J.; Hon, G.; Wigner, N. A.; Toben, D.; Jacobsen, K. A.; Al-Sebaei, M. O.; Song, M.; Trackman, P. C.; Morgan, E. F.; Gerstenfeld, L. C.; Barnes, G. L. Enhanced chondrogenesis and Wnt signaling in PTH-treated fractures. *J Bone Miner Res.* **2007**, *22*, 1903-1912.
86. Chen, Y.; Bai, B.; Zhang, S.; Ye, J.; Chen, Y.; Zeng, Y. Effects of parathyroid hormone on calcium ions in rat bone marrow mesenchymal stem cells. *Biomed Res Int.* **2014**, *2014*, 258409.
87. Hettrich, C. M.; Beamer, B. S.; Bedi, A.; Deland, K.; Deng, X. H.; Ying, L.; Lane, J.; Rodeo, S. A. The effect of rhPTH on the healing of tendon to bone in a rat model. *J Orthop Res.* **2012**, *30*, 769-774.
88. Duchman, K. R.; Goetz, J. E.; Uribe, B. U.; Amendola, A. M.; Barber, J. A.; Malandra, A. E.; Fredericks, D. C.; Hettrich, C. M. Delayed administration of recombinant human parathyroid hormone improves early biomechanical strength in a rat rotator cuff repair model. *J Shoulder Elbow Surg.* **2016**, *25*, 1280-1287.
89. Oh, J. H.; Kim, D. H.; Jeong, H. J.; Park, J. H.; Rhee, S. M. Effect of recombinant human parathyroid hormone on rotator cuff healing after arthroscopic repair. *Arthroscopy.* **2019**, *35*, 1064-1071.
90. Gross, G.; Hoffmann, A. Therapeutic strategies for tendon healing based on novel biomaterials, factors and cells. *Pathobiology.* **2013**, *80*, 203-210.
91. Caliari, S. R.; Harley, B. A. Composite growth factor supplementation strategies to enhance tenocyte bioactivity in aligned collagen-GAG scaffolds. *Tissue Eng Part A.* **2013**, *19*, 1100-1112.
92. Hee, C. K.; Dines, J. S.; Dines, D. M.; Roden, C. M.; Wisner-Lynch, L. A.; Turner, A. S.; McGilvray, K. C.; Lyons, A. S.; Puttlitz, C. M.; Santoni, B. G. Augmentation of a rotator cuff suture repair using rhPDGF-BB and a type I bovine collagen matrix in an ovine model. *Am J Sports Med.* **2011**, *39*, 1630-1639.
93. Novakova, S. S.; Mahalingam, V. D.; Florida, S. E.; Mendias, C. L.; Allen, A.; Arruda, E. M.; Bedi, A.; Larkin, L. M. Tissue-engineered tendon constructs for rotator cuff repair in sheep. *J Orthop Res.* **2018**, *36*, 289-299.
94. Tokunaga, T.; Shukunami, C.; Okamoto, N.; Taniwaki, T.; Oka, K.; Sakamoto, H.; Ide, J.; Mizuta, H.; Hiraki, Y. FGF-2 stimulates the growth of tenogenic progenitor cells to facilitate the generation of tenomodulin-positive tenocytes in a rat rotator cuff healing model. *Am J Sports Med.* **2015**, *43*, 2411-2422.
95. Uggen, C.; Dines, J.; McGarry, M.; Grande, D.; Lee, T.; Limpisvasti, O. The effect of recombinant human platelet-derived growth factor BB-coated sutures on rotator cuff healing in a sheep model. *Arthroscopy.* **2010**, *26*, 1456-1462.
96. Zhao, S.; Zhao, J.; Dong, S.; Huangfu, X.; Li, B.; Yang, H.; Zhao, J.; Cui, W. Biological augmentation of rotator cuff repair using bFGF-loaded electrospun poly(lactide-co-glycolide) fibrous membranes. *Int J Nanomedicine.* **2014**, *9*, 2373-2385.
97. Sahoo, S.; Toh, S. L.; Goh, J. C. A bFGF-releasing silk/PLGA-based biohybrid scaffold for ligament/tendon tissue engineering using mesenchymal progenitor cells. *Biomaterials.* **2010**, *31*, 2990-2998.
98. Ker, E. D.; Nain, A. S.; Weiss, L. E.; Wang, J.; Suhan, J.; Amon, C. H.; Campbell, P. G. Bioprinting of growth factors onto aligned sub-micron fibrous scaffolds for simultaneous control of cell differentiation and alignment. *Biomaterials.* **2011**, *32*, 8097-8107.
99. James, R.; Kumbar, S. G.; Laurencin, C. T.; Balian, G.; Chhabra, A. B. Tendon tissue engineering: adipose-derived stem cell and GDF-5 mediated regeneration using electrospun matrix systems. *Biomed Mater.* **2011**, *6*, 025011.
100. Raabe, O.; Shell, K.; Fietz, D.; Freitag, C.; Ohrndorf, A.; Christ, H. J.; Wenisch, S.; Arnhold, S. Tenogenic differentiation of equine adipose-tissue-derived stem cells under the influence of tensile strain, growth differentiation factors and various oxygen tensions. *Cell Tissue Res.* **2013**, *352*, 509-521.
101. Holladay, C.; Abbah, S. A.; O'Dowd, C.; Pandit, A.; Zeugolis, D. I. Preferential tendon stem cell response to growth factor supplementation. *J Tissue Eng Regen Med.* **2016**, *10*, 783-798.
102. Durant, T. J.; Dyment, N.; McCarthy, M. B.; Cote, M. P.; Arciero, R. A.;

Mazzocca, A. D.; Rowe, D. Mesenchymal stem cell response to growth factor treatment and low oxygen tension in 3-dimensional construct environment. *Muscles Ligaments Tendons J.* **2014**, *4*, 46-51.
103. Cheng, X.; Tsao, C.; Sylvia, V. L.; Cornet, D.; Nicolella, D. P.; Bredbenner, T. L.; Christy, R. J. Platelet-derived growth-factor-releasing aligned collagen-nanoparticle fibers promote the proliferation and tenogenic differentiation of adipose-derived stem cells. *Acta Biomater.* **2014**, *10*, 1360-1369.
104. Manning, C. N.; Schwartz, A. G.; Liu, W.; Xie, J.; Havlioglu, N.; Sakiyama-Elbert, S. E.; Silva, M. J.; Xia, Y.; Gelberman, R. H.; Thomopoulos, S. Controlled delivery of mesenchymal stem cells and growth factors using a nanofiber scaffold for tendon repair. *Acta Biomater.* **2013**, *9*, 6905-6914.
105. Würgler-Hauri, C. C.; Dourte, L. M.; Baradet, T. C.; Williams, G. R.; Soslowsky, L. J. Temporal expression of 8 growth factors in tendon-to-bone healing in a rat supraspinatus model. *J Shoulder Elbow Surg.* **2007**, *16*, S198-203.
106. Kobayashi, M.; Itoi, E.; Minagawa, H.; Miyakoshi, N.; Takahashi, S.; Tuoheti, Y.; Okada, K.; Shimada, Y. Expression of growth factors in the early phase of supraspinatus tendon healing in rabbits. *J Shoulder Elbow Surg.* **2006**, *15*, 371-377.
107. Rodeo, S. A.; Potter, H. G.; Kawamura, S.; Turner, A. S.; Kim, H. J.; Atkinson, B. L. Biologic augmentation of rotator cuff tendon-healing with use of a mixture of osteoinductive growth factors. *J Bone Joint Surg Am.* **2007**, *89*, 2485-2497.
108. Kim, H. M.; Galatz, L. M.; Das, R.; Havlioglu, N.; Rothermich, S. Y.; Thomopoulos, S. The role of transforming growth factor beta isoforms in tendon-to-bone healing. *Connect Tissue Res.* **2011**, *52*, 87-98.
109. Kovacevic, D.; Fox, A. J.; Bedi, A.; Ying, L.; Deng, X. H.; Warren, R. F.; Rodeo, S. A. Calcium-phosphate matrix with or without TGF-β3 improves tendon-bone healing after rotator cuff repair. *Am J Sports Med.* **2011**, *39*, 811-819.
110. Manning, C. N.; Kim, H. M.; Sakiyama-Elbert, S.; Galatz, L. M.; Havlioglu, N.; Thomopoulos, S. Sustained delivery of transforming growth factor beta three enhances tendon-to-bone healing in a rat model. *J Orthop Res.* **2011**, *29*, 1099-1105.
111. Nagura, I.; Kokubu, T.; Mifune, Y.; Inui, A.; Takase, F.; Ueda, Y.; Kataoka, T.; Kurosaka, M. Characterization of progenitor cells derived from torn human rotator cuff tendons by gene expression patterns of chondrogenesis, osteogenesis, and adipogenesis. *J Orthop Surg Res.* **2016**, *11*, 40.
112. Davies, M. R.; Liu, X.; Lee, L.; Laron, D.; Ning, A. Y.; Kim, H. T.; Feeley, B. T. TGF-β small molecule inhibitor SB431542 reduces rotator cuff muscle fibrosis and fatty infiltration by promoting fibro/adipogenic progenitor apoptosis. *PLoS One.* **2016**, *11*, e0155486.
113. Zhou, Z.; Song, W.; Zhang, G.; Zhan, S.; Cai, Z.; Yu, W.; He, Y. The recombinant human fibroblast growth factor-18 (sprifermin) improves tendon-to-bone healing by promoting chondrogenesis in a rat rotator cuff repair model. *J Shoulder Elbow Surg.* **2022**, *31*, 1617-1627.
114. Sitcheran, R.; Cogswell, P. C.; Baldwin, A. S., Jr. NF-kappaB mediates inhibition of mesenchymal cell differentiation through a posttranscriptional gene silencing mechanism. *Genes Dev.* **2003**, *17*, 2368-2373.
115. Gulotta, L. V.; Kovacevic, D.; Cordasco, F.; Rodeo, S. A. Evaluation of tumor necrosis factor α blockade on early tendon-to-bone healing in a rat rotator cuff repair model. *Arthroscopy.* **2011**, *27*, 1351-1357.
116. Waldorff, E. I.; Lindner, J.; Kijek, T. G.; Downie, B. K.; Hughes, R. E.; Carpenter, J. E.; Miller, B. S. Bone density of the greater tuberosity is decreased in rotator cuff disease with and without full-thickness tears. *J Shoulder Elbow Surg.* **2011**, *20*, 904-908.
117. Dorman, L. J.; Tucci, M.; Benghuzzi, H. In vitro effects of bmp-2, bmp-7, and bmp-13 on proliferation and differentation of mouse mesenchymal stem cells. *Biomed Sci Instrum.* **2012**, *48*, 81-87.
118. Kabuto, Y.; Morihara, T.; Sukenari, T.; Kida, Y.; Oda, R.; Arai, Y.; Sawada, K.; Matsuda, K.; Kawata, M.; Tabata, Y.; Fujiwara, H.; Kubo, T. Stimulation of rotator cuff repair by sustained release of bone morphogenetic protein-7 using a gelatin hydrogel sheet. *Tissue Eng Part A.* **2015**, *21*, 2025-2033.
119. Dahlgren, L. A.; Mohammed, H. O.; Nixon, A. J. Temporal expression of growth factors and matrix molecules in healing tendon lesions. *J Orthop Res.* **2005**, *23*, 84-92.
120. Carr, J. B., 2nd; Rodeo, S. A. The role of biologic agents in the management of common shoulder pathologies: current state and future directions. *J Shoulder Elbow Surg.* **2019**, *28*, 2041-2052.
121. Neviaser, J. S.; Neviaser, R. J.; Neviaser, T. J. The repair of chronic massive ruptures of the rotator cuff of the shoulder by use of a freeze-dried rotator cuff. *J Bone Joint Surg Am.* **1978**, *60*, 681-684.
122. Dejardin, L. M.; Arnoczky, S. P.; Ewers, B. J.; Haut, R. C.; Clarke, R. B. Tissue-engineered rotator cuff tendon using porcine small intestine submucosa. Histologic and mechanical evaluation in dogs. *Am J Sports Med.* **2001**, *29*, 175-184.
123. Zheng, M. H.; Chen, J.; Kirilak, Y.; Willers, C.; Xu, J.; Wood, D. Porcine small intestine submucosa (SIS) is not an acellular collagenous matrix and contains porcine DNA: possible implications in human implantation. *J Biomed Mater Res B Appl Biomater.* **2005**, *73*, 61-67.
124. Huang, C.; Zhang, X.; Luo, H.; Pan, J.; Cui, W.; Cheng, B.; Zhao, S.; Chen, G. Effect of kartogenin-loaded gelatin methacryloyl hydrogel scaffold with bone marrow stimulation for enthesis healing in rotator cuff repair. *J Shoulder Elbow Surg.* **2021**, *30*, 544-553.
125. Han, L.; Liu, H.; Fu, H.; Hu, Y.; Fang, W.; Liu, J. Exosome-delivered BMP-2 and polyaspartic acid promotes tendon bone healing in rotator cuff tear via Smad/RUNX2 signaling pathway. *Bioengineered.* **2022**, *13*, 1459-1475.
126. Ousema, P. H.; Moutos, F. T.; Estes, B. T.; Caplan, A. I.; Lennon, D. P.; Guilak, F.; Weinberg, J. B. The inhibition by interleukin 1 of MSC chondrogenesis and the development of biomechanical properties in biomimetic 3D woven PCL scaffolds. *Biomaterials.* **2012**, *33*, 8967-8974.
127. Jiang, X.; Wu, S.; Kuss, M.; Kong, Y.; Shi, W.; Streubel, P. N.; Li, T.; Duan, B. 3D printing of multilayered scaffolds for rotator cuff tendon regeneration. *Bioact Mater.* **2020**, *5*, 636-643.
128. Ciampi, P.; Scotti, C.; Nonis, A.; Vitali, M.; Di Serio, C.; Peretti, G. M.; Fraschini, G. The benefit of synthetic versus biological patch augmentation in the repair of posterosuperior massive rotator cuff tears: a 3-year follow-up study. *Am J Sports Med.* **2014**, *42*, 1169-1175.
129. Cai, Y. Z.; Zhang, C.; Jin, R. L.; Shen, T.; Gu, P. C.; Lin, X. J.; Chen, J. D. Arthroscopic rotator cuff repair with graft augmentation of 3-dimensional biological collagen for moderate to large tears: a randomized controlled study. *Am J Sports Med.* **2018**, *46*, 1424-1431.
130. Sclamberg, S. G.; Tibone, J. E.; Itamura, J. M.; Kasraeian, S. Six-month magnetic resonance imaging follow-up of large and massive rotator cuff repairs reinforced with porcine small intestinal submucosa. *J Shoulder Elbow Surg.* **2004**, *13*, 538-541.
131. Iannotti, J. P.; Codsi, M. J.; Kwon, Y. W.; Derwin, K.; Ciccone, J.; Brems, J. J. Porcine small intestine submucosa augmentation of surgical repair of chronic two-tendon rotator cuff tears. A randomized, controlled trial. *J Bone Joint Surg Am.* **2006**, *88*, 1238-1244.

132. Malcarney, H. L.; Bonar, F.; Murrell, G. A. Early inflammatory reaction after rotator cuff repair with a porcine small intestine submucosal implant: a report of 4 cases. *Am J Sports Med.* **2005**, *33*, 907-911.
133. Hoberman, A. R.; Cirino, C.; McCarthy, M. B.; Cote, M. P.; Pauzenberger, L.; Beitzel, K.; Mazzocca, A. D.; Dyrna, F. Bone marrow-derived mesenchymal stromal cells enhanced by platelet-rich plasma maintain adhesion to scaffolds in arthroscopic simulation. *Arthroscopy.* **2018**, *34*, 872-881.
134. Thangarajah, T.; Henshaw, F.; Sanghani-Kerai, A.; Lambert, S. M.; Blunn, G. W.; Pendegrass, C. J. The effectiveness of demineralized cortical bone matrix in a chronic rotator cuff tear model. *J Shoulder Elbow Surg.* **2017**, *26*, 619-626.
135. Thangarajah, T.; Sanghani-Kerai, A.; Henshaw, F.; Lambert, S. M.; Pendegrass, C. J.; Blunn, G. W. Application of a demineralized cortical bone matrix and bone marrow-derived mesenchymal stem cells in a model of chronic rotator cuff degeneration. *Am J Sports Med.* **2018**, *46*, 98-108.
136. Smith, M. J.; Pfeiffer, F. M.; Cook, C. R.; Kuroki, K.; Cook, J. L. Rotator cuff healing using demineralized cancellous bone matrix sponge interposition compared to standard repair in a preclinical canine model. *J Orthop Res.* **2018**, *36*, 906-912.
137. Wellington, I. J.; Muench, L. N.; Hawthorne, B. C.; Uyeki, C. L.; Antonacci, C. L.; McCarthy, M. B.; Connors, J. P.; Kia, C.; Mazzocca, A. D.; Berthold, D. P. Clinical outcomes following biologically enhanced demineralized bone matrix augmentation of complex rotator cuff repair. *J Clin Med.* **2022**, *11*, 2956.
138. Chae, S.; Yong, U.; Park, W.; Choi, Y. M.; Jeon, I. H.; Kang, H.; Jang, J.; Choi, H. S.; Cho, D. W. 3D cell-printing of gradient multi-tissue interfaces for rotator cuff regeneration. *Bioact Mater.* **2023**, *19*, 611-625.
139. Yoon, J. Y.; Park, J. H.; Rhee, S. M.; Jeong, H. J.; Han, J.; Lee, J. H.; Jeon, S.; Oh, J. H. Safety and efficacy of autologous dermal fibroblast injection to enhance healing after full-thickness rotator cuff repair: first-in-human pilot study. *Orthop J Sports Med.* **2021**, *9*, 23259671211052996.
140. Randelli, P.; Randelli, F.; Ragone, V.; Menon, A.; D'Ambrosi, R.; Cucchi, D.; Cabitza, P.; Banfi, G. Regenerative medicine in rotator cuff injuries. *Biomed Res Int.* **2014**, *2014*, 129515.
141. Warth, R. J.; Dornan, G. J.; James, E. W.; Horan, M. P.; Millett, P. J. Clinical and structural outcomes after arthroscopic repair of full-thickness rotator cuff tears with and without platelet-rich product supplementation: a meta-analysis and meta-regression. *Arthroscopy.* **2015**, *31*, 306-320.
142. Castricini, R.; Longo, U. G.; De Benedetto, M.; Panfoli, N.; Pirani, P.; Zini, R.; Maffulli, N.; Denaro, V. Platelet-rich plasma augmentation for arthroscopic rotator cuff repair: a randomized controlled trial. *Am J Sports Med.* **2011**, *39*, 258-265.
143. Mazzocca, A. D.; McCarthy, M. B.; Chowaniec, D. M.; Cote, M. P.; Romeo, A. A.; Bradley, J. P.; Arciero, R. A.; Beitzel, K. Platelet-rich plasma differs according to preparation method and human variability. *J Bone Joint Surg Am.* **2012**, *94*, 308-316.
144. Giovannetti de Sanctis, E.; Franceschetti, E.; De Dona, F.; Palumbo, A.; Paciotti, M.; Franceschi, F. The efficacy of injections for partial rotator cuff tears: a systematic review. *J Clin Med.* **2020**, *10*, 51.
145. von Wehren, L.; Blanke, F.; Todorov, A.; Heisterbach, P.; Sailer, J.; Majewski, M. The effect of subacromial injections of autologous conditioned plasma versus cortisone for the treatment of symptomatic partial rotator cuff tears. *Knee Surg Sports Traumatol Arthrosc.* **2016**, *24*, 3787-3792.
146. Xu, W.; Xue, Q. Application of platelet-rich plasma in arthroscopic rotator cuff repair: a systematic review and meta-analysis. *Orthop J Sports Med.* **2021**, *9*, 23259671211016847.
147. Rha, D. W.; Park, G. Y.; Kim, Y. K.; Kim, M. T.; Lee, S. C. Comparison of the therapeutic effects of ultrasound-guided platelet-rich plasma injection and dry needling in rotator cuff disease: a randomized controlled trial. *Clin Rehabil.* **2013**, *27*, 113-122.
148. Shams, A.; El-Sayed, M.; Gamal, O.; Ewes, W. Subacromial injection of autologous platelet-rich plasma versus corticosteroid for the treatment of symptomatic partial rotator cuff tears. *Eur J Orthop Surg Traumatol.* **2016**, *26*, 837-842.
149. Cai, Y. U.; Sun, Z.; Liao, B.; Song, Z.; Xiao, T.; Zhu, P. Sodium hyaluronate and platelet-rich plasma for partial-thickness rotator cuff tears. *Med Sci Sports Exerc.* **2019**, *51*, 227-233.
150. Ryan, J.; Imbergamo, C.; Sudah, S.; Kirchner, G.; Greenberg, P.; Monica, J.; Gatt, C. Platelet-rich product supplementation in rotator cuff repair reduces retear rates and improves clinical outcomes: a meta-analysis of randomized controlled trials. *Arthroscopy.* **2021**, *37*, 2608-2624.
151. Lavoie-Gagne, O.; Fury, M. S.; Mehta, N.; Harkin, W. E.; Bernstein, D. N.; Berlinberg, E. J.; Parvaresh, K.; O'Donnell, E.; Forsythe, B. Double-row repair with platelet-rich plasma optimizes retear rates after small to medium full-thickness rotator cuff repair: a systematic review and network meta-analysis of randomized controlled trials. *Arthroscopy.* **2022**, *38*, 2714-2729.
152. Ilhanli, I.; Guder, N.; Gul, M. Platelet-rich plasma treatment with physical therapy in chronic partial supraspinatus tears. *Iran Red Crescent Med J.* **2015**, *17*, e23732.
153. Anz, A. W.; Parsa, R. S.; Romero-Creel, M. F.; Nabors, A.; Tucker, M. S.; Harrison, R. M.; Matuska, A. M. Exercise-mobilized platelet-rich plasma: short-term exercise increases stem cell and platelet concentrations in platelet-rich plasma. *Arthroscopy.* **2019**, *35*, 192-200.
154. Osborne, J. D.; Gowda, A. L.; Wiater, B.; Wiater, J. M. Rotator cuff rehabilitation: current theories and practice. *Phys Sportsmed.* **2016**, *44*, 85-92.
155. Xiao, H.; Zhang, T.; Li, C.; Cao, Y.; Wang, L.; Chen, H.; Li, S.; Guan, C.; Hu, J.; Chen, D.; Chen, C.; Lu, H. Mechanical stimulation promotes enthesis injury repair by mobilizing Prrx1(+) cells via ciliary TGF-β signaling. *Elife.* **2022**, *11*, e73614.
156. Galatz, L. M.; Charlton, N.; Das, R.; Kim, H. M.; Havlioglu, N.; Thomopoulos, S. Complete removal of load is detrimental to rotator cuff healing. *J Shoulder Elbow Surg.* **2009**, *18*, 669-675.
157. Gimbel, J. A.; Van Kleunen, J. P.; Williams, G. R.; Thomopoulos, S.; Soslowsky, L. J. Long durations of immobilization in the rat result in enhanced mechanical properties of the healing supraspinatus tendon insertion site. *J Biomech Eng.* **2007**, *129*, 400-404.
158. Hettrich, C. M.; Gasinu, S.; Beamer, B. S.; Stasiak, M.; Fox, A.; Birmingham, P.; Ying, O.; Deng, X. H.; Rodeo, S. A. The effect of mechanical load on tendon-to-bone healing in a rat model. *Am J Sports Med.* **2014**, *42*, 1233-1241.
159. Chen, H.; Li, S.; Xiao, H.; Wu, B.; Zhou, L.; Hu, J.; Lu, H. Effect of exercise intensity on the healing of the bone-tendon interface: a mouse rotator cuff injury model study. *Am J Sports Med.* **2021**, *49*, 2064-2073.
160. Teunis, T.; Lubberts, B.; Reilly, B. T.; Ring, D. A systematic review and pooled analysis of the prevalence of rotator cuff disease with increasing age. *J Shoulder Elbow Surg.* **2014**, *23*, 1913-1921.
161. Kaplan, L. D.; Flanigan, D. C.; Norwig, J.; Jost, P.; Bradley, J. Prevalence and variance of shoulder injuries in elite collegiate football players. *Am J Sports Med.* **2005**, *33*, 1142-1146.

162. Mall, N. A.; Lee, A. S.; Chahal, J.; Sherman, S. L.; Romeo, A. A.; Verma, N. N.; Cole, B. J. An evidenced-based examination of the epidemiology and outcomes of traumatic rotator cuff tears. *Arthroscopy.* **2013**, *29*, 366-376.
163. Altintas, B.; Anderson, N.; Dornan, G. J.; Boykin, R. E.; Logan, C.; Millett, P. J. Return to sport after arthroscopic rotator cuff repair: is there a difference between the recreational and the competitive athlete? *Am J Sports Med.* **2020**, *48*, 252-261.
164. Burns, J. P.; Snyder, S. J. Arthroscopic rotator cuff repair in patients younger than fifty years of age. *J Shoulder Elbow Surg.* **2008**, *17*, 90-96.
165. Antoni, M.; Klouche, S.; Mas, V.; Ferrand, M.; Bauer, T.; Hardy, P. Return to recreational sport and clinical outcomes with at least 2years follow-up after arthroscopic repair of rotator cuff tears. *Orthop Traumatol Surg Res.* **2016**, *102*, 563-567.
166. Cao, Y. S.; Wan, Y. F. Progress on tendon-to-bone healing after rotator cuff repair. *Zhongguo Gu Shang.* **2018**, *31*, 1172-1179.
167. Font Tellado, S.; Balmayor, E. R.; Van Griensven, M. Strategies to engineer tendon/ligament-to-bone interface: Biomaterials, cells and growth factors. *Adv Drug Deliv Rev.* **2015**, *94*, 126-140.
168. Prabhath, A.; Vernekar, V. N.; Sanchez, E.; Laurencin, C. T. Growth factor delivery strategies for rotator cuff repair and regeneration. *Int J Pharm.* **2018**, *544*, 358-371.
169. Chowdhury, F.; Na, S.; Li, D.; Poh, Y. C.; Tanaka, T. S.; Wang, F.; Wang, N. Material properties of the cell dictate stress-induced spreading and differentiation in embryonic stem cells. *Nat Mater.* **2010**, *9*, 82-88.
170. McMurray, R. J.; Gadegaard, N.; Tsimbouri, P. M.; Burgess, K. V.; McNamara, L. E.; Tare, R.; Murawski, K.; Kingham, E.; Oreffo, R. O.; Dalby, M. J. Nanoscale surfaces for the long-term maintenance of mesenchymal stem cell phenotype and multipotency. *Nat Mater.* **2011**, *10*, 637-644.
171. Dalby, M. J.; Gadegaard, N.; Tare, R.; Andar, A.; Riehle, M. O.; Herzyk, P.; Wilkinson, C. D.; Oreffo, R. O. The control of human mesenchymal cell differentiation using nanoscale symmetry and disorder. *Nat Mater.* **2007**, *6*, 997-1003.
172. Gentleman, E.; Swain, R. J.; Evans, N. D.; Boonrungsiman, S.; Jell, G.; Ball, M. D.; Shean, T. A.; Oyen, M. L.; Porter, A.; Stevens, M. M. Comparative materials differences revealed in engineered bone as a function of cell-specific differentiation. *Nat Mater.* **2009**, *8*, 763-770.
173. Derwin, K. A.; Baker, A. R.; Iannotti, J. P.; McCarron, J. A. Preclinical models for translating regenerative medicine therapies for rotator cuff repair. *Tissue Eng Part B Rev.* **2010**, *16*, 21-30.
174. Ficklscherer, A.; Serr, M.; Loitsch, T.; Niethammer, T. R.; Lahner, M.; Pietschmann, M. F.; Müller, P. E. The influence of different footprint preparation techniques on tissue regeneration in rotator cuff repair in an animal model. *Arch Med Sci.* **2017**, *13*, 481-488.
175. Li, X.; Shen, P.; Su, W.; Zhao, S.; Zhao, J. Into-tunnel repair versus onto-surface repair for rotator cuff tears in a rabbit model. *Am J Sports Med.* **2018**, *46*, 1711-1719.
176. Bilsel, K.; Yildiz, F.; Kapicioglu, M.; Uzer, G.; Elmadag, M.; Pulatkan, A.; Esrefoglu, M.; Bozdag, E.; Milano, G. Efficacy of bone marrow-stimulating technique in rotator cuff repair. *J Shoulder Elbow Surg.* **2017**, *26*, 1360-1366.

Received: February 4, 2023
Revised: March 15, 2023
Accepted: May 5, 2023
Available online: June 28, 2023

Three-dimensional biofabrication of nanosecond laser micromachined nanofibre meshes for tissue engineered scaffolds

Ross H. McWilliam[1], Wenlong Chang[2], Zhao Liu[3], Jiayuan Wang[3], Fengxuan Han[3], Richard A. Black[1], Junxi Wu[1], Xichun Luo[2], Bin Li[3], Wenmiao Shu[1,]*

Key Words:
3D biofabrication; electrospinning; hierarchical scaffold; micromachining; tissue engineering

From the Contents

ABSTRACT

There is a high demand for bespoke grafts to replace damaged or malformed bone and cartilage tissue. Three-dimensional (3D) printing offers a method of fabricating complex anatomical features of clinically relevant sizes. However, the construction of a scaffold to replicate the complex hierarchical structure of natural tissues remains challenging. This paper reports a novel biofabrication method that is capable of creating intricately designed structures of anatomically relevant dimensions. The beneficial properties of the electrospun fibre meshes can finally be realised in 3D rather than the current promising breakthroughs in two-dimensional (2D). The 3D model was created from commercially available computer-aided design software packages in order to slice the model down into many layers of slices, which were arrayed. These 2D slices with each layer of a defined pattern were laser cut, and then successfully assembled with varying thicknesses of 100 μm or 200 μm. It is demonstrated in this study that this new biofabrication technique can be used to reproduce very complex computer-aided design models into hierarchical constructs with micro and nano resolutions, where the clinically relevant sizes ranging from a simple cube of 20 mm dimension, to a more complex, 50 mm-tall human ears were created. In-vitro cell-contact studies were also carried out to investigate the biocompatibility of this hierarchal structure. The cell viability on a micromachined electrospun polylactic-co-glycolic acid fibre mesh slice, where a range of hole diameters from 200 μm to 500 μm were laser cut in an array where cell confluence values of at least 85% were found at three weeks. Cells were also seeded onto a simpler stacked construct, albeit made with micromachined poly fibre mesh, where cells can be found to migrate through the stack better with collagen as bioadhesives. This new method for biofabricating hierarchical constructs can be further developed for tissue repair applications such as maxillofacial bone injury or nose/ear cartilage replacement in the future.

http://doi.org/10.12336/biomatertransl.2023.02.005

How to cite this article:
McWilliam, R. H.; Chang, W.; Liu, Z.; Wang, J.; Han, F.; Black, R. A.; Wu. J.; Luo, X.; Li, B.; Shu, W. Three-dimensional biofabrication of nanosecond laser micromachined nanofibre meshes for tissue engineered scaffolds. *Biomater Transl.* **2023**, *4*(2), 104-114.

Introduction

Bone and cartilage are examples of tissue that are both capable of being distinctly and prominently shaped whilst being prone to injury and damage. Injuries and abnormalities to the bone and cartilage such as microtia and anotia of the ear and tumour removal are a prevalent problem facing health services.[1-8] Taking anotia and microtia (where the ear cartilage either does not or only partly develops *in utero*) as an example, a global study covering the years 1988 to 2007, the prevalence stands at approximately 2.06 cases per 10,000 neonatal patients,[9] and the current treatment of autografting a shaped costal cartilage graft requires several invasive surgeries and a risk of donor site morbidity.[10] Additionally, over 500,000 bone graft surgeries were performed annually in the USA.[11] Current treatments for

maxillofacial bone repair require either autografting pelvic bone, an invasive surgery with the risk of donor site morbidity, or metal plate implants, which are uncomfortable, prone to wear or based on more costly titanium alloys.[12, 13]

These current treatments can be improved upon greatly using biomaterials and processes that are more compatible with native tissue and development.[5, 14-16] Electrospinning, where fibre meshes are created by using a potential difference to draw a polymer from a source – such as in a solvent solution – to a collector, is one such technique regarded as producing a fine nanofiber mesh.[17, 18] Both natural and synthetic polymer fibre meshes can be fabricated, and studies have shown that they have advantageous properties with regards to cell viability, response and differentiation due to their resemblance to tissue extracellular membrane (ECM).[19] However, the main difficulty of electrospinning and bone and cartilage repair is to scale up the process in three-dimensional (3D) and fabricate a precise 3D structure with clinically relevant dimensions.[20] To this end, melt electrowriting is one technique that combines electrospinning with additive manufacturing and is capable of producing 3D structures of fibre meshes with unprecedented micro and nanoscale precision. The polymer filaments are drawn from the molten polymer instead of a solvent dispersion, and directly deposited on the substrate under the action of electrostatic forces. Fabrication thickness is still limited to achieve any clinically relevant sizes due to the deteriorated electrical field for thicker constructs.[21-24]

The technique of 3D bioprinting, on the other hand, offers a means of fabricating bespoke, clinically relevant sized, hierarchal structures.[25-30] This technique involves the use of cells and a specifically designed biomaterial scaffold to fabricate a 3D hierarchal graft, which can be scaled to clinically relevant sizes according to a patient's specific anatomical structure.[31, 32] However, the main challenge of 3D bioprinting is the ability to print the scalable sizes that can be self-supportive whilst using materials that resemble the ECM. Currently, it is difficult to achieve a 3D bioprinted structure having both adequate biological and mechanical function.[33]

In an attempt to overcome these problems, electrospun fibre meshes have been proposed.[34-36] One recent approach involves stacking two-dimensional (2D) layers of electrospun mesh and 3D printed discs on top of each other to make a 3D shape.[37] While the methodology implemented in these studies has shown promising results *in vitro*, there is scope for improvements to be made in order to biofabricate patient specific constructs at scale and having clinically relevant dimensions.

To date, there it has been challenging to mimic faithfully the 3D hierarchical structures that make up complex human tissue.[38] Any novel fabrication method must take into account the macro scale to match the clinically relevant size of the tissue being replaced, the microscale precision for the anatomic shape and to allow cell migration and accurate ECM formation, and nanoscale precision for the morphological resemblance to ECM to maximise native cell viability and performance.[39, 40]

In this paper, we report a novel method for 3D biofabricate tissue scaffolds with microscale precision from nanofibrous materials. The method involves stacking 2D nanofibre meshes that have been laser cut into distinct cross-sectional shapes in a prescribed sequence, the position and orientation of each slice being specified to achieve an accurate representation of the anatomical feature. The stacked nanofibrous meshes alone would not allow cell migration through each slice, something that would be an issue for the potential success of any graft where cells are required to be uniformly dispersed, due to the lack of microporosity within the nanofiber meshes; this also hinders nutrient diffusion to cells within the construct and the potential for vascularisation, vital for ensuring cell survival and thus the success of the graft. Using a nanosecond laser cutter to micromachine arrays of circular voids of different diameters into fibre meshes have already been shown to support cell growth and proliferation.[41, 42] Equally important is the length scale and interconnectivity of the voids, to ensure that cells are uniformly dispersed through the structure at the time of seeding, and that once attached those cells are able to proliferate throughout the structure and deposit ECM, thereby consolidating the tissue scaffold and ensuring effective engraftment to the surrounding host tissue.[43] Using this novel method various designs were successfully fabricated with good accuracy and with application relevant sizes and cosmetics, ranging from some simple shapes up to realistic, anatomically relevant body parts such as a human ear.

The aim of the present study is to explore further the potential of micromachining techniques to optimise the microporosity and performance of such 3D constructs *in vitro*.

Methods

Scaffold fabrication

The polycaprolactone (PCL) nanofiber mesh from which the cell scaffolds were fabricated was produced in sheet form using a bespoke electrospinning apparatus at the University of Strathclyde.[44] PCL pellets (molecular weight = 80,000; Sigma-Aldrich, Gillingham, UK) were dissolved in a 9:1 mixture of acetone and dimethyl formamide (DMF; both from Sigma-Aldrich) to a final concentration of 17 wt%. The polymer dispersion was delivered from a 5 mL syringe (Sigma-Aldrich) fitted with a 20G gauge needle (Vicson, UK) at a flow rate of 2 mL/h. The electrostatic potential was set at –15 kV. The polylactic-co-glycolic acid (PLGA) nanofibre mesh was kindly donated by The Electrospinning Company Ltd. (Oxfordshire, UK).

*Corresponding author: Wenmiao Shu, will.shu@strath.ac.uk.

1 Department of Biomedical Engineering, University of Strathclyde, Glasgow, UK; 2 Centre for Precision Manufacturing, Design, Manufacturing & Engineering Management, University of Strathclyde, Glasgow, UK; 3 Orthopaedic Institute, Department of Orthopaedic Surgery, The First Affiliated Hospital, Soochow University, Suzhou, Jiangsu Province, China

Design and three-dimensional construction of scaffold

In order to ensure an accurate 3D reconstruction, stacking method was devised to facilitate the layer-by-layer assembly of each slice in the correct sequence. This method can be described as using a square, acrylic base with four tall steel pins in each corner, each 3 mm in diameter, to guide the alignment of each slice (a sheet that has been cut using a CO_2 laser, a square that is the same dimensions as the base, and with a 3 mm hole in each corner orientated exactly in line with the pins). In this way, having successfully positioned the individual sections, one on top of the other, the full 3D reconstruction may be realised.

A computer model of the desired shape (for the purpose of proving the concept of a cube, a hemisphere, a pyramid and an ear, all of varying sizes) was constructed in computer aided design (CAD) software (Inventor® Version 2018, Autodesk, Dublin, Ireland), to which four 3 mm cylinders (corresponding to the pins) and an enclosure (corresponding to the base) were added. A 1-mm thick support structure was added to locate the shape of the surrounding enclosure. A rendered view of the final 3D model is shown in **Figure 1A**. This model was saved as a stereolithography (stl) file and opened in Slicer (Version 1.3.0 GNU Affero), a slicing software often utilised for 3D printing (additive manufacturing). Thereafter, the file was exported in the open standard scalable vector graphic (svg) file format, in which the layer thickness is specified by the user and the model is sliced horizontally into layers, each having this well-defined thickness. The model was then imported into Inkscape (version 0.92 GNU General Public Licence), in which the model was further processed to yield an array of slices having the appropriate dimensions (a sample of an 'ungrouped' and arrayed svg is shown in **Figure 1B**). Each slice was then numbered (to help with the construction process later) and saved as a drawing exchange format (dxf) file for laser cutting by a TMX65 50 W CO_2 laser (CTR Lasers, Northampton, UK). **Figure 1C** shows an example of the electrospun polymer sheet after processing by the laser, complete with 3-mm diameter alignment holes at each corner, while **Figure 1D** shows an example of the layers from which the part is to be constructed.

In order to ensure an accurate 3D reconstruction of the laser cut-outs, a stacking method was devised to facilitate the layer-by-layer assembly of each slice in the correct sequence on a custom-made jig. The jig was fabricated in acrylic from a block 55 mm × 55 mm in size and fitted with four stainless steel pins, each 3 mm in diameter (**Figure 1E**). In this way, having successfully positioned the individual sections, one on top of the other, the full, 3D reconstruction of the desired shape could be realised.

For the purpose of demonstrating the technique, two grades of filter paper (Cat 50 and Cat 40, respectively; GE Whatman, Buckinghamshire, UK) were used. The former had a nominal thickness of 100 μm and the latter 200 μm.

Once the shapes had been cut out of the material by the laser, they were assembled as described above and bound together with a 4% aqueous solution of sodium alginate (Sigma-Aldrich). In **Figure 1E**, step 1, the correctly numbered laser cut slice is slotted onto the alignment base. Step 2 shows the application of the alginate via a needle and syringe (alternatively, the solution was dispensed from a bioprinting nozzle). In step 3 the corresponding construct slice is adhered to the preceding construct slice in the correct position and orientation as dictated by the alignment slice. Steps 4 and 5 show how the process repeats itself until all the slices have been laid onto the structure. Thereafter, the 3D construct was immersed in a calcium chloride solution (100 mM) to cross-link the alginate and strengthen the structure. Finally, the alignment slices were removed carefully from the alignment base, leaving only the desired structure standing on the base. In a further experiment, above steps were repeated with collagen instead of alginate in step 2 of **Figure 1E** and thermally cross-linking in a 37°C incubator for 1 hour.

Morphological analysis of the polycaprolactone nanofibre mesh

A scanning electron microscope (SEM) image was taken of a typical PCL electrospun fibre mesh using a Hitachi TM-1000 Desktop SEM Machine (Chiyoda, Japan). From this image, the diameters of ten random fibres were measured using ImageJ (version 1.53e; National Institutes of Health, Bethesda, MD, USA), and an average was taken. Ten randomly selected pores were then measured (also with ImageJ) for their area and the length at their narrowest point. This is to determine if there is a possibility for cell mobility through the nanofiber mesh.

***In vitro* studies**

Cell-contact studies: cell viability

Murine adipose derived stem cells (ADSCs) were kindly donated by researchers at the University of Glasgow, UK. Cells were cultured using minimal essential media (MEM; Gibco, Thermofisher Scientific, Inchinnan, UK) containing 10% fetal bovine serum (Gibco, Thermofisher Scientific) and and 1% penicillin/streptomycin (Corning, Thermofisher Scientific), in an incubator set at 37°C and 5% CO_2 atmosphere.

Micromachined two-dimensional slice

An *in-vitro* cell-contact study was performed on individual micromachined PLGA sheets in order to understand whether the application of an appropriate cell type, in this case, ADSCs, which have the potential to differentiate into osteoblasts after they have become attached to and proliferated on such a 2D construct. Here, a V2-1-100-20-20 nanosecond laser (IPG Photonics, Coventry, UK) was used to cut an array of holes of varying sizes in the range 200, 300, 400, and 500 μm. The diameter of the holes that were made in the PLGA sheets was verified by direct measurement using a Brunel SP50 light microscope (Chippenham, UK). ImageJ was used to measure the average diameter of each hole sampled by taking three measurements for each hole and taking an average. Three holes for each sample were then measured and the average hole diameter for that array was calculated.

The samples were sterilised in a 70% ethanol solution for 1 hour, and washed three times with phosphate buffered saline (Gibco, Thermofisher Scientific), after which 200,000 ADSCs were seeded onto each array. For live/dead staining, the samples were stained with fluorescein and propidium iodide at day 21 to assess cell growth and viability, and then viewed under an inverted epifluorescent microscope (Nikon Eclipse TE300 Epifluorescent inverted microscope, Minato city, Tokyo, Japan).

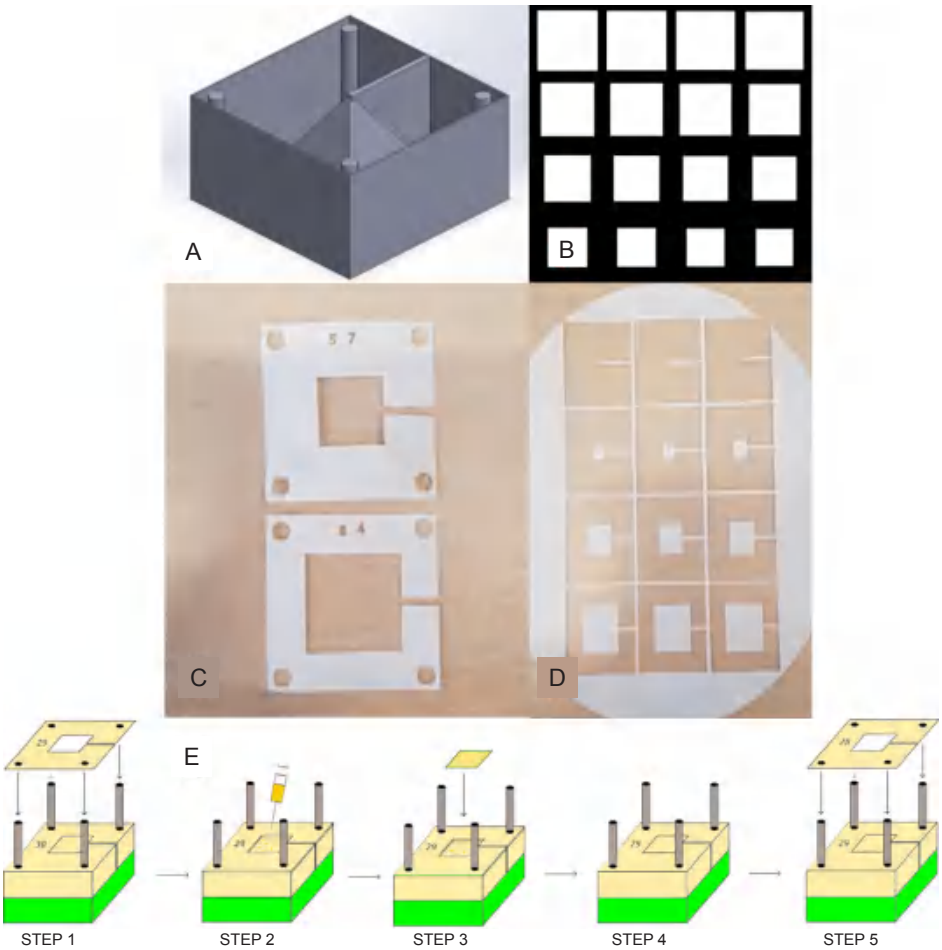

Figure 1. Design and assembly process for fabricating a 3D construct. (A) CAD model with 3D construction and surrounding box and cylinders. (B) Section of the array in InkScape showing different 2D slice shapes used to construct the pyramid. (C) Laser cut alignment slices with an appropriate number designating order. (D) Shape slices on the bulk material to be cross-referenced with alignment slice and placed accordingly on the construct. (E) Schematic of the steps involved in the assembly process, where accurate 3D reconstructions can be created from the 2D slices: Step 1 – placement of alignment slice 29 on the rig using the four holes; Step 2 – Deposition of a couple of drops of alginate solution using a syringe; Steps 3 and 4 – placement of the appropriate shape slice corresponding with alignment slice 29; Step 5 – starting the process again with alignment slice 28. This process continues until all slices are placed. 2D: two-dimensional; 3D: three-dimensional; CAD: computer-aided design. Created with Inventor® Vension 2018.

Prior to this, a 7-day cytotoxicity study was performed using the same number of ADSCs on a 500 μm micromachined PLGA mesh. This sample was stained with fluorescein and propidium iodide and imaged using a Zoe Microscope (Bio-Rad, Hertfordshire, UK).

Micromachined three-dimensional construct

A direct cell-contact study was also conducted in order to determine the cell viability, migration and proliferation throughout a structure according to the methods detailed as above. The cells used in this experiment were ADSCs. The structures in this case are to be far simpler than those made with the paper, with a micromachined electrospun PCL fibre mesh to be used instead and will be a short cylinder using three stacked 14 mm diameter discs. This is so that they can fit neatly into a 24-well plate well. Before assembly the discs were micromachined using the nanosecond laser, to produce circular voids 500 μm in diameter, with a 1 mm pitch. This void size, which is comparable to that of cancellous bone, has been found previously in this study (Section 'Morphological assessment of micromachined fibre meshes') to promote good cell viability. The average pore diameter was calculated by taking three diameter measurements and calculating the average, to be compared with the intended diameter of 500 μm.

The discs were sterilised using a solution of 70% ethanol, dried sufficiently and washed three times with PBS. Each structure was made using three discs, adhered together using 4% sodium alginate crosslinked by calcium chloride, then placed in a 24-well plate well. They were stacked (and this is consistent with all experimentation in the same manner) randomly on top of each other. ADSCs were then seeded onto the structure at a density of 1×10^6, then submerged in culture media.

The discs were stained with fluorescein and propidium iodide at two time points (1 and 7 days; $n = 2$) to assess cell growth and viability. In order to test the perfusion of the cells each of the layers were delaminated and viewed under an inverted epifluorescent microscope.

The above methodology was repeated using collagen as the binding agent instead of alginate. Type 1 collagen (rat tail, , 3 mg/mL, Sigma-Aldrich) was prepared of which 0.5 mL was used to prepare each stack, comprising three layers, which were left for 1 hour in an incubator to gel (cross link). The cells were seeded at a density of 3×10^6 cells per sample stack. Cell viability was assessed at days 1 and 4 ($n = 2$).

Results

Construction of three-dimensional demonstrators

Using the method, 3D constructs of the following shapes were created: a simple cube, with dimensions 20 mm in each direction (**Figure 2A**); a pyramid made from 77 slices with a 20 mm square base and 21.6 mm tall (**Figure 2B**); and a hemisphere 15 mm in diameter (**Figure 2C**). The latter shape was fabricated in different sizes to verify the dimensional accuracy of the construction process and with a view to producing more complex anatomic structures, in this case, a life size model of the human ear (**Figure 2D**).

Finally, a life-sized model of the human ear was fabricated (approximately 50 mm in height) but the paper used was 100 μm, half the thickness of the layer height of the previous ears and shapes constructed. The intention of using thinner layers of paper was to produce a smoother structure, where smaller features can be more pronounced and accurately represented. The result reflected the intention behind this move, where the ear looks better and is shown in **Figure 2E**.

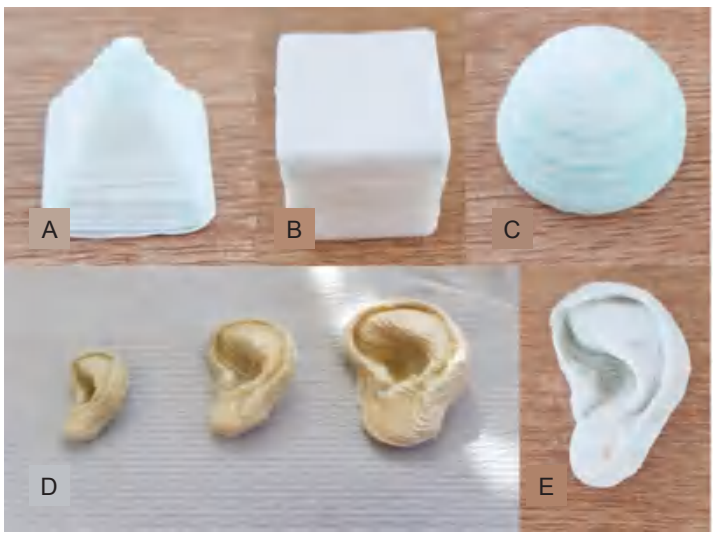

Figure 2. Examples of 3D demonstrators assembled according to the novel fabrication method. (A) Camera image of a pyramid. (B) Camera image of a successfully printed cube. (C) Camera image of a successfully printed hemisphere. (D) Three scale models of a human ear (200 μm slices) of three different sizes. (E) The corresponding ear with greater resolution (100 μm slices), which has excellent fidelity for anatomical size and accurately replicates the complex features of the human ear. Scale bars: 10 mm (A–C, E), 50 mm (D).

Morphological assessment of micromachined fibre meshes

Figure 3 shows the SEM image of a PCL electrospun nanofibre mesh that would be used in coming studies. The clear nanofibre formation shows the effectiveness of the electrospinning process. The average fibre diameter was measured to be 1.801 ± 0.411 μm. The average pore area was found to be 28.612 ± 10.07 μm^2, where their corresponding 'narrowest pore diameter' is 4.542 ± 1.159 μm.

The first micromachining test and the cytotoxicity test showed excellent results. The micromachined hole is close to a circle in shape and the hole is cut completely through the mesh, thus showing the necessity of using the nanosecond laser (**Figure 4A**). The live/dead stain shows excellent cell viability on this micromachined mesh (**Figure 4B**).

Figure 4C–F shows the light microscope images of the PLGA nanofibre meshes post-micromachining, in order from 200 to 500 μm hole diameters respectively. The holes imaged have good circularity and the difference in diameter can be seen visually when comparing these images. **Figure 4G–J** shows the live/dead staining images of the micromachined mesh with the varying hole sizes at the time-point week 3, with alive ADSCs shown as green. All samples have good cell viability, with plenty of green cells and almost no dead cells to be seen.

Viability of cells seeded in polycaprolactone and polylactic-co-glycolic acid three-dimensional scaffolds

Figure 4K–M shows the light microscope images of an array of perforations on three different samples of PCL electrospun mesh material, while **Figure 5** details the diameter of each hole. The stack samples for the *in vitro* experiment were created successfully as per the methodology, and the cells were seeded on the top of each stack.

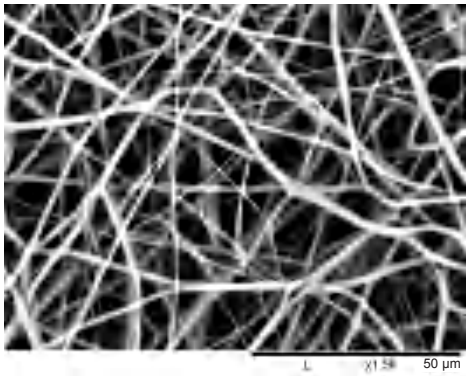

Figure 3. Desktop scanning electron microscope image of an electrospun polycaprolactone nanofibre mesh to be micromachined and used in *in vitro* testing. An average nanofibre diameter was 1.801 µm (n = 10) was found. Scale bars: 50 µm.

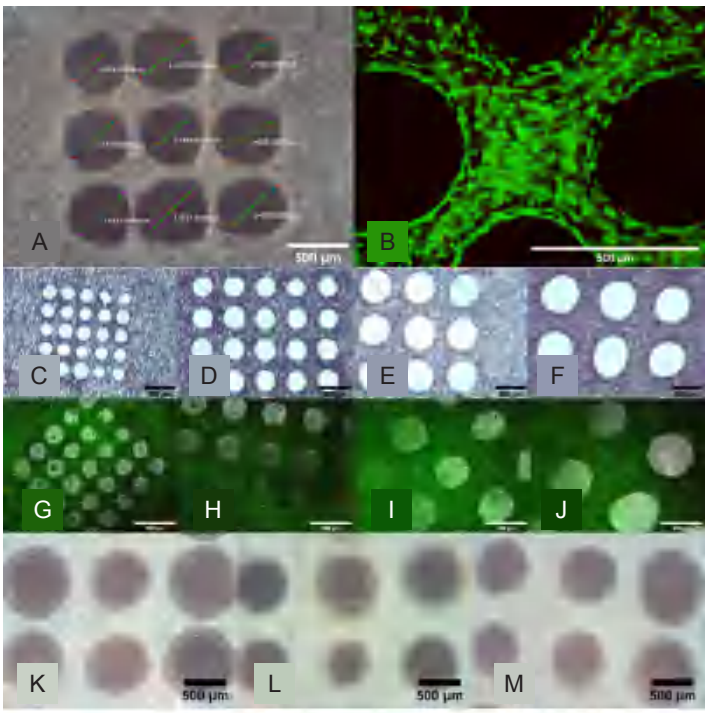

Figure 4. Morphological assessment of the perforated micromachined fibre mesh. (A, B) First cytotoxicity test of the 500 µm micromachined PLGA mesh. (A) Light Microscopy image of the micromachined array showing good circularity. (B) Live/dead image showing excellent cell viability and the holes clearly defined. (C–F) Light microscopy images of the 200 (C), 300 (D), 400 (E), and 500 (F) µm hole arrays, which show good circularity and even distribution. (G–J) Epifluorescent microscope images of live ADSCs on the micromachined fibre mesh with 200 (G), 300 (H), 400 (I), and 500 (J) µm hole arrays, with excellent cell viability seen across all samples, and 'bridging' of cells across. (K–M) Light microscope images of three selected micromachined electrospun PCL fibre mesh samples, all micromachined with the same setting but with minor variances as a result of the non-uniform thickness of the PCL nanofibre mesh. Scale bars: 500 µm. PCL: polycaprolactone; PLGA: polylactic-co-glycolic acid.

Figure 6 shows the live/dead images obtained on the slices from the alginate and the collagen stacks constructed. At two time points (days 1 and 7) slices 1, 2 and 3 on the alginate stacks are being compared with slices 1, 2 and 3 from the collagen stacks. It can be seen from the alginate stacks (**Figure 6A–F**) that there are surviving cells on the top slices at each time point (**Figure 6A** for day 1 and **Figure 6D** for day 7), but that there are no live cells on slices 2 and 3 even after 14 days. The opposite however can be said of the collagen stacks of which the live/dead images are shown in **Figure 6G–L**), where even after 1 day live cells can be seen on the lower stacks (**Figure 6I**).

This confirms the hypothesis that the alginate does not aid in cell migration whereas the collagen does. Therefore, it can be said that the collagen provides a better biological response to the alginate as an adhesive. Cell counting analysis, which quantifies the data from **Figure 6** by showing the live number of cells on each slice by using ImageJ software, also reinforces this data. It can be seen that the number of cells on the lower slices on the alginate stacks (blue columns) is far fewer than those on the collagen stacks (red columns), regardless of the time point.

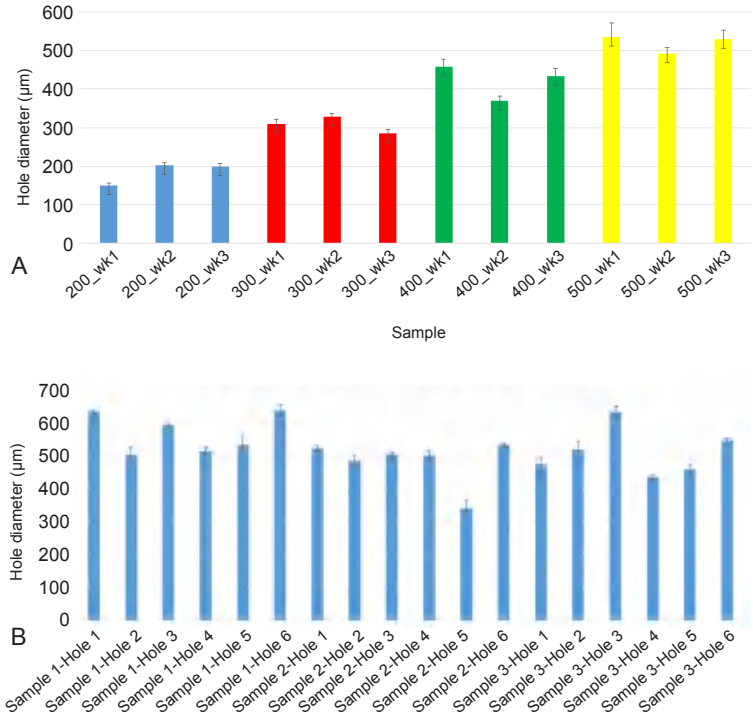

Figure 5. The average diameter of the micromachined perforations in the electrospun fibre mesh samples. (A) The actual average hole diameter of each array (n = 3 holes) compared to the intended hole diameter of the PLGA samples, where the average diameter can be seen to be close to the intended diameter and a clear difference between each sample type seen. (B) The average diameter of each hole (n = 3 holes) in three representative micromachined electrospun PCL fibre mesh samples, with a wider variance of values around the intended 500 μm hole diameter due to using the same laser settings on the non-uniform thickness of the PCL nanofibre mesh. 3D: three-dimensional; PCL: polycaprolactone; PLGA: polylactic-co-glycolic acid.

Discussion

Construction of three-dimensional demonstrators

One of the first issues was that (apart from the cube which has the same cross section throughout the structure) it is difficult to ensure that the construct slice is placed with the correct alignment slice. The way this issue was resolved by adding a thin connection on the CAD model between the intended construct and the outside alignment (**Figure 1A**). This is then seen as a thin connection between the construct slice to the extraneous parts of the paper sheet (as shown in **Figure 1D**). This can be identified as associating with the correct numbered alignment slice which has been completely cut away (**Figure 1C**). The removal of the alignment slices from the construct upon completion of the stacking process[45] was performed carefully in order to prevent delamination and construct deterioration.

It was expected that the process of using crosslinked alginate would swell the construct in the z direction, so that the actual height of the construct would be different from that of the expected height (the number of slices multiplied by the height of each slice).[46] **Table 1** shows the ratio between the expected height and the actual height for the cube, the pyramid and the hemisphere. If an average of the three ratios are taken (found to be 1.38) then the number of slices of future slices can be adjusted to ensure that the height is accurate to that of the CAD model and not swelled due to the alginate. This adjustment was implemented when using a slicer (sliced to svg using 276 μm layer height instead of 200 μm for example).

Table 1. Actual versus the predicted height of the cube, pyramid and hemisphere, along with the ratio of the discrepancy

Shape	Expected height (mm)	Actual height (mm)	Ratio
Cube	18.00	24.77	1.376
Hemisphere	12.60	16.87	1.350
Pyramid	15.40	21.62	1.404

Note: These values are fairly close together, and so can be used to determine that a swelling coefficient of 1.38 should be used for future prints to ensure accurate z-axis fidelity.

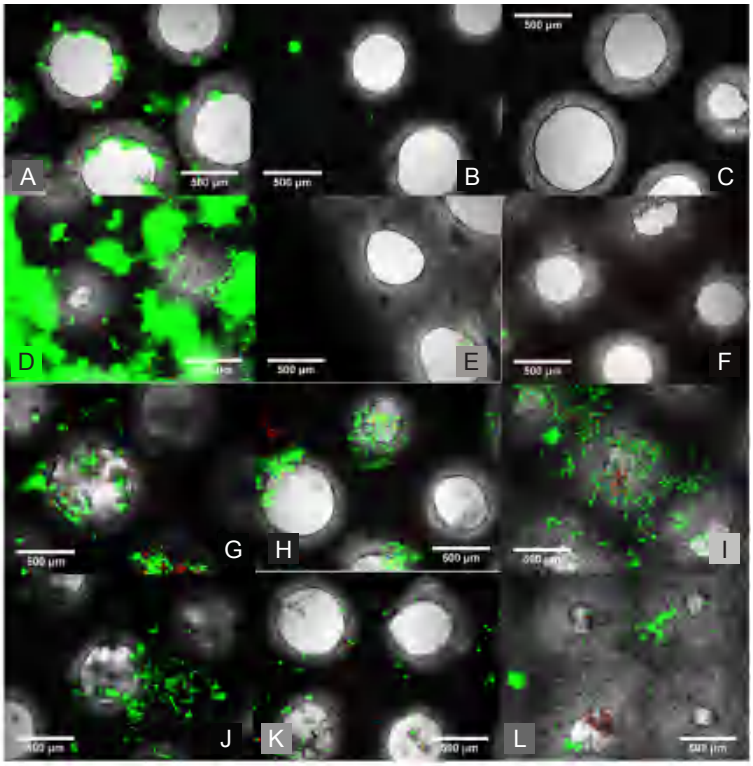

Figure 6. Live/dead staining of ADSCs on the alginate and collagen stacks. (A–F) Inverted epifluorescent microscope images after live/dead staining of ADSCs on the alginate stacks. (A) Slice 1 (top slice) showing some good cell viability on day 1. (B) Slice 2 (middle slice) showing very limited cell presence indicating no cell mobility through the construct on day 1. (C) Slice 3 (bottom slice) showing no cells and thus no mobility through the cross-linked alginate on day 3. (D) Slice 1 (top slice) showing good cell viability with some stain intake by the alginate on day 7. (E) Slice 2 (middle slice) showing limited cell viability and thus mobility on day 7. (F) Slice 3 (bottom slice) showing no cell viability and thus no mobility through the alginate even on day 7. (G–L) inverted epifluorescent microscope images after live/dead staining of ADSCs on the collagen stacks. (G) Slice 1 (top slice) showing good cell viability on day 1. (H) Slice 2 (middle slice) showing good cell viability and therefore cells must be able to travel through on day 1. (I) Slice 3 (bottom slice) showing good cell viability and thus demonstrating the mobility of cells through the collagen and the micromachined fibre mesh even after 1 day. (J) Slice 1 (top slice) showing good cell viability on day 4. (K) Slice 2 (middle slice) showing good cell viability and therefore cells must be able to travel through on day 4. (L) Slice 3 (bottom slice) showing good cell viability and thus demonstrating the mobility of cells through the collagen and the micromachined fibre mesh on day 4. Scale bars: 500 μm. ADSC: adipose derived stem cell.

The next stage was to create a structure that is geometrically more complex, and to demonstrate the applicability of manufacturing technique for the purpose of creating scaffolds for use in maxillofacial and other surgical cosmesis procedures. At first, an ear with a height of approximately 50 mm was created successfully, with the different complex features of the ear prominent and clear. The next ear to be made was smaller at 28 mm tall, more akin to the size of a neonatal ear, and a third ear with a height of 38 mm was also constructed, both made using 0.2 mm thick paper slice. These demonstrators are shown in **Figure 2D**. One of the new challenges that came with fabricating the ear shape was that of the introduction of 2 different construct slices within one alignment slice, and the potential for loose sections that would be lost during the cutting process or wrongly attached to the structure. This was solved by adding more webs during the CAD process. The other new challenge comes from the fact that the cross-sectional area of ascending pieces increases in some parts of the construct. This increases the likelihood of unwanted adherence between the construct and the alignment slices, and also increases the likelihood of delamination when removing the alignment slices. This challenge can only be overcome by careful removal and, like before, better targeting of the application of alginate.

Using the thinner filter paper had the effect of reducing the layer height, a common method of increasing the resolution of a printed model. The ear in **Figure 2E** utilises filter paper that is half the thickness of the previous models. This has the effect of smoothing out the complex features of the ear. This has the drawback of doubling the length of time taken to fabricate the construct, which would have to be considered when this method is used to biomanufacture cell-laden scaffold constructs.

Morphological assessment of micromachined fibre meshes

From the SEM image of the electrospun nanofibre mesh, the average nanofibre diameter was found to be 1.801 μm. One study found that undifferentiated murine ADSCs have a diameter of 14.9 μm.47 Firstly, this is three times larger than

the average 'narrowest pore diameter' within the nanofibre mesh, indicating a need for micromachining to fulfill the desire for cell mobility through the mesh (and thus the construct). Secondly, it has been shown in literature that a mesh of nanofibres with a diameter smaller than the size of the cell has beneficial properties with respect to cell attachment and thus viability.[48] The diameter of the nanofibres is considerably smaller than the cells used, and such cell viability should be preserved.

It can be found in the literature that the process of micromachining holes into a fibre mesh can enhance the cell viability of the mesh.[41, 42] It is important in tissue engineering to have the construct mimic certain properties that are found in natural tissue ECM. Nanofiber meshes have good nanoporosity but further alterations are required in order to make it a more suitable mimic to that of bone ECM, for example. Micromachining is one such method used to achieve a better microporous representation, and as such improve the cell response within the scaffold.

Figure 4A–D clearly shows that the morphology of the micromachined holes created is uniformly rounded in shape, indicating a clean cut through from the nanosecond laser. This justifies the use of a nanosecond laser which ablates the polymer mesh through evaporation.[49] Analysis of the hole diameter also shows that the settings of the laser can be controlled in such a way as to accurately achieve the intended hole diameter. **Figure 5A** plots the actual average hole diameter against the intended diameter. It can be seen that the standard deviation (i.e. how round the hole is) increases as the hole diameter increases, suggesting that the round morphology is harder to control with the higher energies required to machine such a hole size.

It can be seen that the cells are surviving well on the array even well into the three-week time frame, and when left long enough the cells will attempt to 'bridge' even very large holes; by week 3 most 500 μm holes have been closed by the cells. Even with the large area of the holes which would account for dead space the confluence values are all calculated to be above 85%. This effect has promise for potential cell growth within these holes and vascularisation within the scaffold, a process that is vital for its success in the application of tissue engineering.

Viability of cells seeded in polycaprolactone and polylactic-co-glycolic acid three-dimensional scaffolds

It can be seen from **Figures 4I–K** and **5B** that the hole size is more difficult to control in the PCL electrospun fibre meshes used compared to the PLGA fibre meshes. This could be a result of the PCL fibre mesh having a more non-uniform thickness than the PLGA fibre mesh, meaning that the same parameters used for the micromachining process would produce inconsistent holes.

Comparing the two different adhesive types (alginate and collagen) showed that the stacks with cross linked alginate were less prone to delamination, especially surviving over longer cell culture conditions. The collagen samples, even though left for a sufficient time to thermally cross-link, were far more likely to break up and delaminate if not treated carefully. All samples maintained their shape by the end of the test.

As such, it can be said that the alginate adhesive provides better mechanical properties than the collagen adhesive, something to consider when potentially extrapolating this technique into the application of a bone graft.

It was initially hypothesised that the alginate would provide a barrier to any cell migration from the top of the stack through to the bottom due to its bioinert and dense properties (one reason why alginate is favoured in encapsulation applications for example[50]). Collagen however, with its bioactive properties was hypothesised to aid in cell migration through the stack. It was also hoped that the micromachined mesh would also aid cell migration.

The biofabricated construct is designed to be biomimetic whereby the 3D hierarchal structure found in natural human tissue such as bone and cartilage can be fabricated using this new approach. At a macro level, the biofabrication method is capable of creating anatomically accurate ear constructs of clinically relevant size. At the micro level, micromachining is implemented to enhance the microporosity properties to both aid cell migration through the construct and also help to replicate the natural porosity of bone ECM. At the nano level, the electrospun fibre mesh has already been shown to aid cell viability and proliferation due to its natural resemblance to natural tissue ECM.

Any cartilage or bone graft that would be utilised would have to be both mechanically and biologically sound, and biofabrication has a key role to play in the final implementation of such a successful, bespoke tissue engineered graft. The innovative biofabricated construct that is created utilises a wide range of techniques including electrospun nanofiber mesh, which is micromachined prior to assembly in a novel 3D fabrication method. This hierarchal construct can be described as having the potential to be both cosmetically accurate and induce a positive biological response. Different adhesives and cross-linking methods can be investigated to try to marry these two concepts. It is also important to broaden the cell types used and properly characterise the structures, something that will be achieved in future work.

Conclusion

This study has brought forth a novel and innovative way of fabricating a 3D hierarchical scaffold graft with good macro, micro and nanoscale precision, whilst also being able to utilise materials that have already shown promise within this application at the 2D level. At the macro level, the method of stacking 2D sheets of fibre mesh allows for bespoke grafts of clinically relevant sizes to be made, which would be of biocompatible and aesthetical benefit to any individual patient. At the micro level, it was found that the implementation of micromachined laser cut holes into each 2D slice provided an additional benefit to the graft by allowing for cell migration through the structure, by improving the microporosity of the fibre meshes. A replication of the nano level of the hierarchical structure was achieved by utilising nanofibre polymer meshes which have a similar morphology to the ECM of natural tissue. This study has also provided an insight into the role

of the adhesive used. Unsurprisingly, collagen proved to have better cell attachment, viability and migration however the stacks for which alginate was used as the binder provided better mechanical properties where delamination and adhesive degradation were less likely.

Further investigation is required into optimising the adhesive used so that it can be both mechanically and biologically suitable. The current adhesives used in this study both require optimisation in this regard. The capacity to involve better techniques of cell distribution using 3D bioprinting, the potential for the introduction of automation, as well as the wide range of model designs that can be achieved using such a fabrication method (to expand on the range of applications such as maxillofacial bone injury or nose/ear cartilage replacement) only adds to the promise.

Author contributions

WS and RHM conceived the idea and wrote the manuscript. RHM and WC designed and performed the experiments, with WC using the nanosecond laser. WS, BL, XL and RAB supervised the study. ZL, JW, FH, JW, XL and BL helped analyse the data and provided valuable advice. WS, RHM and RAB revised the manuscript. All authors approved the final version of the manuscript.

Financial support

The authors acknowledge the funding support from the EPSRC (Funding Reference Number EP/L015995/1 & EP/W004860/1), the Royal Society (IEC\NSFC\201166), the National Natural Science Foundation of China (No. 82111530157) and the Priority Academic Program Development (PAPD) of Jiangsu Higher Education Institutions.

Acknowledgement

We would like to thank Dr. Mathis Riehle University of Glasgow for the donation of ADSCs, Katie Henderson and Graeme MacKenzie in the SIPBS Department in the University of Strathclyde for Technical Assistance. We would like to thank the Electrospinning Company for donating the PLGA fibre meshes.

Conflicts of interest statement

None.

Editor note: Wenmiao Shu is an Editorial Board member of *Biomaterials Translational*. He was blinded from reviewing or making decisions on the manuscript. The article was subject to the journal's standard procedures, with peer review handled independently of this Editorial Board member and his research group.

Open access statement

This is an open access journal, and articles are distributed under the terms of the Creative Commons Attribution-NonCommercial-ShareAlike 4.0 License, which allows others to remix, tweak, and build upon the work non-commercially, as long as appropriate credit is given and the new creations are licensed under the identical terms.

1. Templer, J.; Renner, G. J. Injuries of the external ear. *Otolaryngol Clin North Am.* **1990**, *23*, 1003-1018.
2. Harris, J.; Källén, B.; Robert, E. The epidemiology of anotia and microtia. *J Med Genet.* **1996**, *33*, 809-813.
3. Gassner, R.; Tuli, T.; Hächl, O.; Rudisch, A.; Ulmer, H. Cranio-maxillofacial trauma: a 10 year review of 9,543 cases with 21,067 injuries. *J Craniomaxillofac Surg.* **2003**, *31*, 51-61.
4. Subhashraj, K.; Nandakumar, N.; Ravindran, C. Review of maxillofacial injuries in Chennai, India: a study of 2748 cases. *Br J Oral Maxillofac Surg.* **2007**, *45*, 637-639.
5. Turnbull, G.; Clarke, J.; Picard, F.; Riches, P.; Jia, L.; Han, F.; Li, B.; Shu, W. 3D bioactive composite scaffolds for bone tissue engineering. *Bioact Mater.* **2018**, *3*, 278-314.
6. Xu, L.; Qin, H.; Tan, J.; Cheng, Z.; Luo, X.; Tan, H.; Huang, W. Clinical study of 3D printed personalized prosthesis in the treatment of bone defect after pelvic tumor resection. *J Orthop Translat.* **2021**, *29*, 163-169.
7. Pu, F.; Wu, W.; Jing, D.; Yu, Y.; Peng, Y.; Liu, J.; Wu, Q.; Wang, B.; Zhang, Z.; Shao, Z. Three-dimensional-printed titanium prostheses with bone trabeculae enable mechanical-biological reconstruction after resection of bone tumours. *Biomater Transl.* **2022**, *3*, 134-141.
8. Long, J.; Teng, B.; Zhang, W.; Li, L.; Zhang, M.; Chen, Y.; Yao, Z.; Meng, X.; Wang, X.; Qin, L.; Lai, Y. Preclinical evaluation of acute systemic toxicity of magnesium incorporated poly(lactic-co-glycolic acid) porous scaffolds by three-dimensional printing. *Biomater Transl.* **2021**, *2*, 272-284.
9. Luquetti, D. V.; Leoncini, E.; Mastroiacovo, P. Microtia-anotia: a global review of prevalence rates. *Birth Defects Res A Clin Mol Teratol.* **2011**, *91*, 813-822.
10. Duscher, D.; Shiffman, M. A. *Regenerative medicine and plastic surgery*. Springer Nature Switzerland: Cham, Switzerland,2019.
11. Posnick, J. C. 18 - Grafts frequently used during orthognathic surgery and for adjunctive procedures. In *Orthognathic surgery*, Posnick, J. C., ed. W.B. Saunders: St. Louis, 2014; pp 607-639.
12. Elsalanty, M. E.; Genecov, D. G. Bone grafts in craniofacial surgery. *Craniomaxillofac Trauma Reconstr.* **2009**, *2*, 125-134.
13. Pacifici, L.; F, D. E. A.; Orefici, A.; Cielo, A. Metals used in maxillofacial surgery. *Oral Implantol (Rome).* **2016**, *9*, 107-111.
14. Sun, H.; Guo, Q.; Shi, C.; McWilliam, R. H.; Chen, J.; Zhu, C.; Han, F.; Zhou, P.; Yang, H.; Liu, J.; Sun, X.; Meng, B.; Shu, W.; Li, B. CD271 antibody-functionalized microspheres capable of selective recruitment of reparative endogenous stem cells for in situ bone regeneration. *Biomaterials.* **2022**, *280*, 121243.
15. Yang, T.; Tamaddon, M.; Jiang, L.; Wang, J.; Liu, Z.; Liu, Z.; Meng, H.; Hu, Y.; Gao, J.; Yang, X.; Zhao, Y.; Wang, Y.; Wang, A.; Wu, Q.; Liu, C.; Peng, J.; Sun, X.; Xue, Q. Bilayered scaffold with 3D printed stiff subchondral bony compartment to provide constant mechanical support for long-term cartilage regeneration. *J Orthop Translat.* **2021**, *30*, 112-121.
16. Yin, H. W.; Feng, J. T.; Yu, B. F.; Shen, Y. D.; Gu, Y. D.; Xu, W. D. 3D printing-assisted percutaneous fixation makes the surgery for scaphoid nonunion more accurate and less invasive. *J Orthop Translat.* **2020**, *24*, 138-143.
17. Li, D.; Xia, Y. Electrospinning of nanofibers: reinventing the wheel? *Adv Mater.* **2004**, *16*, 1151-1170.
18. Frenot, A.; Chronakis, I. S. Polymer nanofibers assembled by electrospinning. *Curr Opin Colloid Interface Sci.* **2003**, *8*, 64-75.
19. Tuzlakoglu, K.; Bolgen, N.; Salgado, A. J.; Gomes, M. E.; Piskin, E.; Reis, R. L. Nano- and micro-fiber combined scaffolds: a new architecture for bone tissue engineering. *J Mater Sci Mater Med.* **2005**, *16*, 1099-1104.
20. Sun, B.; Long, Y. Z.; Zhang, H. D.; Li, M. M.; Duvail, J. L.; Jiang, X. Y.; Yin, H. L. Advances in three-dimensional nanofibrous macrostructures via electrospinning. *Prog Polym Sci.* **2014**, *39*, 862-890.
21. Brown, T. D.; Dalton, P. D.; Hutmacher, D. W. Melt electrospinning today: an opportune time for an emerging polymer process. *Prog Polym Sci.* **2016**, *56*, 116-166.
22. Nayak, R.; Padhye, R.; Arnold, L. 2 - Melt-electrospinning of nanofibers. In *Electrospun nanofibers*, Afshari, M., ed. Woodhead Publishing: 2017; pp 11-40.
23. Zhang, L. H.; Duan, X. P.; Yan, X.; Yu, M.; Ning, X.; Zhao, Y.; Long, Y. Z. Recent advances in melt electrospinning. *RSC Adv.* **2016**, *6*, 53400-

53414.
24. Brown, T. D.; Edin, F.; Detta, N.; Skelton, A. D.; Hutmacher, D. W.; Dalton, P. D. Melt electrospinning of poly(ε-caprolactone) scaffolds: phenomenological observations associated with collection and direct writing. *Mater Sci Eng C Mater Biol Appl.* **2014**, *45*, 698-708.
25. Sun, W.; Starly, B.; Daly, A. C.; Burdick, J. A.; Groll, J.; Skeldon, G.; Shu, W.; Sakai, Y.; Shinohara, M.; Nishikawa, M.; Jang, J.; Cho, D. W.; Nie, M.; Takeuchi, S.; Ostrovidov, S.; Khademhosseini, A.; Kamm, R. D.; Mironov, V.; Moroni, L.; Ozbolat, I. T. The bioprinting roadmap. *Biofabrication.* **2020**, *12*, 022002.
26. Holmes, A. M.; Charlton, A.; Derby, B.; Ewart, L.; Scott, A.; Shu, W. Rising to the challenge: applying biofabrication approaches for better drug and chemical product development. *Biofabrication.* **2017**, *9*, 033001.
27. Holland, I.; Logan, J.; Shi, J.; McCormick, C.; Liu, D.; Shu, W. 3D biofabrication for tubular tissue engineering. *Biodes Manuf.* **2018**, *1*, 89-100.
28. Cornelissen, D. J.; Faulkner-Jones, A.; Shu, W. Current developments in 3D bioprinting for tissue engineering. *Curr Opin Biomed Eng.* **2017**, *2*, 76-82.
29. Sahranavard, M.; Sarkari, S.; Safavi, S.; Ghorbani, F. Three-dimensional bio-printing of decellularized extracellular matrix-based bio-inks for cartilage regeneration: a systematic review. *Biomater Transl.* **2022**, *3*, 105-115.
30. Turnbull, G.; Clarke, J.; Picard, F.; Zhang, W.; Riches, P.; Li, B.; Shu, W. 3D biofabrication for soft tissue and cartilage engineering. *Med Eng Phys.* **2020**, *82*, 13-39.
31. Groll, J.; Boland, T.; Blunk, T.; Burdick, J. A.; Cho, D. W.; Dalton, P. D.; Derby, B.; Forgacs, G.; Li, Q.; Mironov, V. A.; Moroni, L.; Nakamura, M.; Shu, W.; Takeuchi, S.; Vozzi, G.; Woodfield, T. B.; Xu, T.; Yoo, J. J.; Malda, J. Biofabrication: reappraising the definition of an evolving field. *Biofabrication.* **2016**, *8*, 013001.
32. Kang, H. W.; Lee, S. J.; Ko, I. K.; Kengla, C.; Yoo, J. J.; Atala, A. A 3D bioprinting system to produce human-scale tissue constructs with structural integrity. *Nat Biotechnol.* **2016**, *34*, 312-319.
33. Murphy, S. V.; Atala, A. 3D bioprinting of tissues and organs. *Nat Biotechnol.* **2014**, *32*, 773-785.
34. Wu, Z.; Su, X.; Xu, Y.; Kong, B.; Sun, W.; Mi, S. Bioprinting three-dimensional cell-laden tissue constructs with controllable degradation. *Sci Rep.* **2016**, *6*, 24474.
35. Yu, Y.; Hua, S.; Yang, M.; Fu, Z.; Teng, S.; Niu, K.; Zhao, Q.; Yi, C. Fabrication and characterization of electrospinning/3D printing bone tissue engineering scaffold. *RSC Adv.* **2016**, *6*, 110557-110565.
36. Gao, Q.; Gu, H.; Zhao, P.; Zhang, C.; Cao, M.; Fu, J.; He, Y. Fabrication of electrospun nanofibrous scaffolds with 3D controllable geometric shapes. *Mater Des.* **2018**, *157*, 159-169.
37. Gao, Q.; Zhao, P.; Zhou, R.; Wang, P.; Fu, J.; He, Y. Rapid assembling organ prototypes with controllable cell-laden multi-scale sheets. *Bio-des Manuf.* **2019**, *2*, 1-9.
38. Moroni, L.; Burdick, J. A.; Highley, C.; Lee, S. J.; Morimoto, Y.; Takeuchi, S.; Yoo, J. J. Biofabrication strategies for 3D in vitro models and regenerative medicine. *Nat Rev Mater.* **2018**, *3*, 21-37.
39. Dalton, P. D.; Woodfield, T. B. F.; Mironov, V.; Groll, J. Advances in hybrid fabrication toward hierarchical tissue constructs. *Adv Sci (Weinh).* **2020**, *7*, 1902953.
40. Sankar, S.; Sharma, C. S.; Rath, S. N.; Ramakrishna, S. Electrospun nanofibres to mimic natural hierarchical structure of tissues: application in musculoskeletal regeneration. *J Tissue Eng Regen Med.* **2018**, *12*, e604-e619.
41. Kong, B.; Sun, W.; Chen, G.; Tang, S.; Li, M.; Shao, Z.; Mi, S. Tissue-engineered cornea constructed with compressed collagen and laser-perforated electrospun mat. *Sci Rep.* **2017**, *7*, 970.
42. Lee, B. L.; Jeon, H.; Wang, A.; Yan, Z.; Yu, J.; Grigoropoulos, C.; Li, S. Femtosecond laser ablation enhances cell infiltration into three-dimensional electrospun scaffolds. *Acta Biomater.* **2012**, *8*, 2648-2658.
43. Aquino-Martínez, R.; Angelo, A. P.; Pujol, F. V. Calcium-containing scaffolds induce bone regeneration by regulating mesenchymal stem cell differentiation and migration. *Stem Cell Res Ther.* **2017**, *8*, 265.
44. Laco, F.; Grant, M. H.; Black, R. A. Collagen-nanofiber hydrogel composites promote contact guidance of human lymphatic microvascular endothelial cells and directed capillary tube formation. *J Biomed Mater Res A.* **2013**, *101*, 1787-1799.
45. Li, H.; Cheng, F.; Robledo-Lara, J. A.; Liao, J.; Wang, Z.; Zhang, Y. S. Fabrication of paper-based devices for in vitro tissue modeling. *Bio-des Manuf.* **2020**, *3*, 252-265.
46. Moe, S. T.; Skjaak-Braek, G.; Elgsaeter, A.; Smidsroed, O. Swelling of covalently crosslinked alginate gels: influence of ionic solutes and nonpolar solvents. *Macromolecules.* **1993**, *26*, 3589-3597.
47. No authors listed. Rapid analysis of human adipose-derived stem cells and 3T3-L1 differentiation towards adipocytes using the Scepter™ 2.0 Cell Counter. *Biotechniques.* **2012**, *53*, 2.
48. Laurencin, C. T.; Ambrosio, A. M.; Borden, M. D.; Cooper, J. A., Jr. Tissue engineering: orthopedic applications. *Annu Rev Biomed Eng.* **1999**, *1*, 19-46.
49. Bridle, H.; Wang, W.; Gavriilidou, D.; Amalou, F.; Hand, D. P.; Shu, W. Static mode microfluidic cantilevers for detection of waterborne pathogens. *Sens Actuators A Phys.* **2016**, *247*, 144-149.
50. Faulkner-Jones, A.; Fyfe, C.; Cornelissen, D. J.; Gardner, J.; King, J.; Courtney, A.; Shu, W. Bioprinting of human pluripotent stem cells and their directed differentiation into hepatocyte-like cells for the generation of mini-livers in 3D. *Biofabrication.* **2015**, *7*, 044102.

Received: January 27, 2023
Revised: April 19, 2023
Accepted: June 20, 2023
Available online: June 28, 2023

Biomaterials Translational

Harnessing decellularised extracellular matrix microgels into modular bioinks for extrusion-based bioprinting with good printability and high post-printing cell viability

Hanyu Chu[1], Kexin Zhang[2], Zilong Rao[2], Panpan Song[2], Zudong Lin[1], Jing Zhou[2], Liqun Yang[1], Daping Quan[1,2,], Ying Bai[2,*]*

Key Words:
3D bioprinting; bioinks; cell viability; decellularised extracellular matrix; microgels

From the Contents

ABSTRACT

The printability of bioink and post-printing cell viability is crucial for extrusion-based bioprinting. A proper bioink not only provides mechanical support for structural fidelity, but also serves as suitable three-dimensional (3D) microenvironment for cell encapsulation and protection. In this study, a hydrogel-based composite bioink was developed consisting of gelatin methacryloyl (GelMA) as the continuous phase and decellularised extracellular matrix microgels (DMs) as the discrete phase. A flow-focusing microfluidic system was employed for the fabrication of cell-laden DMs in a high-throughput manner. After gentle mixing of the DMs and GelMA, both rheological characterisations and 3D printing tests showed that the resulting DM-GelMA hydrogel preserved the shear-thinning nature, mechanical properties, and good printability from GelMA. The integration of DMs not only provided an extracellular matrix-like microenvironment for cell encapsulation, but also considerable shear-resistance for high post-printing cell viability. The DM sizes and inner diameters of the 3D printer needles were correlated and optimised for nozzle-based extrusion. Furthermore, a proof-of-concept bioink composedg of RSC96 Schwann cells encapsulated DMs and human umbilical vein endothelial cell-laden GelMA was successfully bioprinted into 3D constructs, resulting in a modular co-culture system with distinct cells/materials distribution. Overall, the modular DM-GelMA bioink provides a springboard for future precision biofabrication and will serve in numerous biomedical applications such as tissue engineering and drug screening.

http://doi.org/10.12336/biomatertransl.2023.02.006

How to cite this article:
Chu, H.; Zhang, K.; Rao, Z.; Song, P.; Lin, Z.; Zhou, J.; Yang, L.; Quan, D.; Bai, Y. Harnessing decellularised extracellular matrix microgels into modular bioinks for extrusion-based bioprinting with good printability and high post-printing cell viability. *Biomater Transl.* **2023**, *4*(2), 115-127.

Introduction

Three-dimensional (3D) bioprinting is one of the most attractive advancing techniques that allow the construction of bio-scaffolds with complex architectures.[1] Smart design of bioinks and bioprinting process can achieve precisely controlled deposition of heterogeneous components, including cells and functional biomaterials, for versatile applications in tissue engineering and regenerative medicine.[2] Among the extensively developed bioprinting techniques, extrusion-based bioprinting is the most commonly used modality, in which pre-designed structures are obtained after continuous extrusion of bioinks through small nozzles.[3] To ensure good printability and structural fidelity, various bioinks have been developed for extrusion-based bioprinting, and most of them are hydrogels,[4] such as gelatin methacryloyl (GelMA),[5] poly(ethylene glycol) diacrylate,[6] collagen,[7] and alginate.[8] Nowadays, GelMA is the most frequently used hydrogel,

due to its relatively high viscosity, thermo-responsibility, and shear-thinning property. It also enables cell-laden bioprinting through extrusion and light-induced post-printing crosslinking.[9] However, whenever cells were directly mixed with viscous pre-gel solutions (not just GelMA or GelMA-based composites) to form bioinks, large shear stresses are inevitably induced during bioink extrusion through the narrow needles (nozzles). Large amounts of encapsulated cells may suffer unrecoverable damage or even death under shear, resulting in a highly reduced viability.[10, 11] Therefore, how to prepare a sort of bioinks that convey both good printability and well-preserved cell viability becomes one of the greatest challenges to the researchers in bioprinting-related fields, including material scientists, mechanical engineers, and even therapists.[12]

To address this issue, various forms of hydrogel-based cell carriers have been investigated for bioink development.[13] Among them, one of the smart designs uses micrometer-sized hydrogels, also termed microgels, to encapsulate cells for the preparation of extrusion-based bioinks.[14] Compared to bulk hydrogels, microgels are more suitable for cell encapsulation and 3D culture. The large surface-to-volume ratio and high porosity of the microgels effectively accelerate substance exchange, such as nutrients and oxygen delivery.[15] Besides, microgels encapsulating different cell types have been employed as building blocks in modular bioinks for establishing various co-culture and heterogeneous bioprinted systems. For example, Fang et al.[16] developed a cell-laden microgel-based biphasic bioink that enabled the construction of heterogeneous scaffolds through extrusion-based bioprinting. The bioink basically consisted of jammed GelMA microgels that resulted in a large density of encapsulated cells, and the second GelMA network ensured the connection between microgels but contributed little to the mechanical support of the bioprinted structures. Chen et al.[17] used GelMA/chitosan microspheres integrated modular bioink for 3D printing of composite scaffolds, in which the PC12 cells and RSC96 Schwann cells were co-cultured. Though the application of hydrogel microspheres was inspiring, the PC12 cells were pre-seeded on the GelMA/chitosan microspheres rather than embedded in the microgels, and axonal extension was only evident using the GelMA/chitosan microspheres supplemented with nerve growth factor. Microgels played vital roles in these two bioprinting processes, and so did them in many other research studies,[18, 19] which also lead to two major concerns about the microgel-containing bioinks. First, in most cases, the cell density shall be controlled due to versatile requirements and the complex microgel preparation processes. Hence, the second polymer network outside the microgels is required to provide more mechanical support for better printability and structural fidelity. Meanwhile, for 3D encapsulation, extrusion, and culture, tissue-specific biomaterials are highly desired for cell survival and maturation within the microgels. Urged by these strict requirements, the choices of bioink materials are key to the success of extrusion-based bioprinting.

In the previous studies, the microgels mostly consisted of hydrogels derived from natural biomaterials, including GelMA,[20] sodium alginate,[21] chitosan,[22] etc. These materials usually exhibit very low bioactivity and require additional chemical crosslinking to ensure mechanical stability. Decellularised extracellular matrices (dECMs) and their derivative hydrogels have shown their outstanding biocompatibility, processibility, and tissue-specific bioactivity, as reported in our previous studies and many others.[23] The dECMs are mostly derived from human or other mammal tissues, which preserve various structural and functional extracellular matrix (ECM) components, such as collagen, fibronectin, laminin, proteoglycans, glycoproteins, and growth factors from the native tissues. Hydrogels derived from the dECMs have been frequently used for cell encapsulation, culture, and transplantation, due to their tuneable rheological properties, ECM-like ultrastructure, and bioactive ECM components.[24] Furthermore, we have previously developed a temperature-controlled microfluidic system for the fabrication of dECM microspheres, which were free of chemical- or photo-crosslinking.[25] The ECM components effectively promoted the adhesion and proliferation of nerve cells cultured on the surface of the dECM microspheres.

On the other hand, dECM-containing bioinks have been extensively developed to endow biological functionalities into bioprinted scaffolds.[26] The simplest way to prepare the bioink was to directly blend cells, GelMA, and dECM pre-gel solution together.[27] However, the contrary temperature-sensitive rheological properties of GelMA and dECM hydrogel (GelMA gels at ~4°C before secondary photocrosslinking, and dECM hydrogel forms at ~37°C) often lead to severe phase separation and low structural fidelity after extrusion-based bioprinting. Additionally, the dECMs were pulverised into powder and employed as additives in bioinks.[28] Despite their improved mechanical and biological properties, the dECM powder often aggregates considerably and causes nozzle clogging during bioink extrusion. Taking all these experiences into account, we believe that the preformed cell-encapsulated dECM microgels (DMs) hold great promise in the preparation of functional modular bioinks for extrusion-based 3D bioprinting.

Herein, we report a sort of extrusion-based modular bioinks that consisted of two major parts: GelMA served as the continuous phase to provide good printability and structural fidelity, meanwhile, the prepared DMs served as the discrete phase that recapitalised favorable ECM-like microenvironments for the encapsulated cells (**Figure 1**). First, a cell-friendly microfluidic-based approach was developed for

* **Corresponding authors:** Daping Quan, cesqdp@mail.sysu.edu.cn; Ying Bai, baiy28@mail.sysu.edu.cn.

1 Key Laboratory for Polymeric Composite & Functional Materials of Ministry of Education, School of Chemistry, Sun Yat-sen University, Guangzhou, Guangdong Province, China; 2 Guangdong Engineering Technology Research Centre for Functional Biomaterials, Key Laboratory for Polymeric Composite & Functional Materials of Ministry of Education, School of Materials Science and Engineering, Sun Yat-sen University, Guangzhou, Guangdong Province, China

the continuous preparation of cell-laden DMs. Then, the DM-GelMA composite bioink was employed for extrusion-based 3D bioprinting. The diameters of the microgels and extrusion nozzles were correlated and optimised for better bioprinting conditions. Cell viability tests were carried out on the modular DM-bioinks with different building blocks, i.e., the cells were pre-encapsulated either in the DMs or in GelMA, respectively. Finally, as a proof-of-concept, a modular bioink consisting of human umbilical vein endothelial cells (HUVECs) containing GelMA and RSC96 Schwann cell-loaded DMs was extruded into 3D constructs, the feasibility of this bioprinted co-culture system was verified.

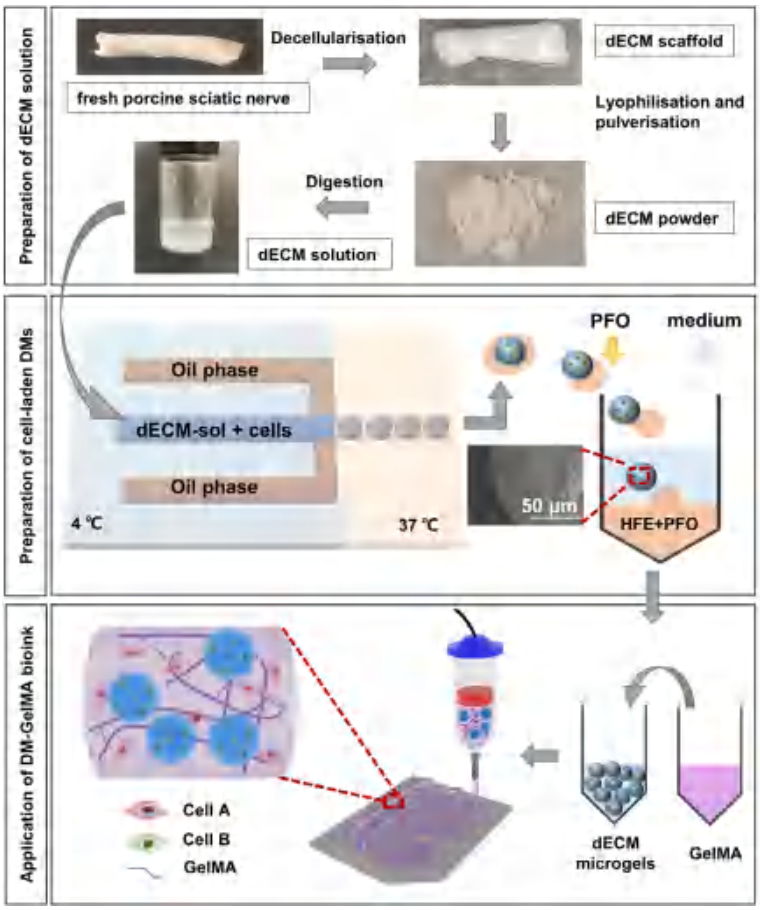

Figure 1. Schematic diagrams illustrate the preparation of the DM-GelMA bioink for extrusion-based bioprinting. The upper diagram shows the preparation of dECM solution. The middle diagram shows the temperature-controlled flow-focusing microfluidic device to prepare cell-laden DMs. The lower diagram shows the preparation of DM-GelMA composite bioink and its application in extrusion-based bioprinting. Created using 3D Max 2021. dECM: decellularised extracellular matrix; DM: decellularised extracellular matrix microgel; GelMA: gelatin methacryloyl; HFE: HFE: hexane, 3-ethoxy-1,1,1,2,3,4,4,5,5,6,6,6-d odecafluoro-2-(trifluoromethyl); PFO: 1H,1H,2H,2H-perfluoro-1-octanol.

Methods

Synthesis and characterisation of gelatin methacryloyl

GelMA was synthesised according to a previously described method with slight modifications.[29] Briefly, 10 g gelatin (Type A, 300 bloom, Sigma-Aldrich, St. Louis, MO, USA) was dissolved in 100 mL phosphate-buffered saline (PBS, Meilunbio, Dalian, China), then agitated at 60°C to obtain 10% (w/v) gelatin aqueous solution. 10 mL methacrylic anhydride (Sigma-Aldrich) was slowly added into the gelatin solution at a rate of ~0.5 mL/min under stirring at 50°C. After reaction in the dark for 3 hours, the solution was diluted with 5× PBS and then dialysed in deionised water at 37°C for 5 days, water was replaced every 12 hours. The final product was lyophilised and then stored at –20°C until use.

The resulting GelMA was examined and compared with gelatin using ^{1}H NMR (AVANCE III-400 MHz, Bruker, Zurich, Switzerland). The samples were separately dissolved at ~10 mg/mL in D_2O, and the chemical shift of each sample was measured at 25°C (pulse sequence 64 times).

Synthesis of lithium phenyl-2,4,6-trimethylbenzoylphosphinate

The photoinitiator, lithium phenyl-2,4,6-trimethylbenzoylphosphinate), was synthesised by following the protocol described.[30] Briefly, 3.2 g 2,4,6-trimethylbenzoylchloride (Sigma-Aldrich) was added dropwise to an equimolar amount of 3 g dimethylphenylphosphonate (Sigma-Aldrich) and allowed

reaction for 18 hours under continuous agitation at room temperature. 6.1 g lithium bromide (Sigma-Aldrich) was pre-dissolved in 150 mL 2-butanone (Guangzhou Reagent, Guangzhou, China), added to the mixture and then heated to 50°C. A solid precipitate formed and was placed at room temperature for 12 hours. The redundant lithium bromide was removed from the precipitate by washing with 2-butanone three times. The resulting lithium phenyl-2,4,6-trimethylbenzoylphosphinate powder was vacuum dried and stored in argon gas at room temperature.

Preparation of decellularised nerve matrix pre-gel solution

All animal experimental procedures were conducted according to the Affidavit of Approval of Animal Ethics and Welfare, which has been reviewed and approved by the Animal Ethics and Welfare Committee of Sun Yat-sen University (approval No. SYSU-IACUC-2021-B0088) in 2021. The decellularisation process was implemented by following a previously reported protocol.[27] Briefly, fresh sciatic nerves were harvested from healthy 8-month-old Landrace pigs at weight ~100 kg purchased from a local slaughter house. The nerve tissues were cut into 5-cm-long pieces, residual blood and clots were rinsed off and cleaned carefully before decellularisation. The nerve tissues were then placed in 3.0% (v/v) Triton X-100 (Sigma-Aldrich) for 12 hours, rinsed in sterile water three times, soaked in 4.0% (w/v) sodium deoxycholate (Sigma-Aldrich) for 24 hours, and rinsed by sterile water another three times. The resulting decellularised nerves were lyophilised and then treated with a solvent mixture consisting of ethanol and dichloromethane (ethanol: dichloromethane = 1:2) for 24 hours to remove residual lipids. Finally, the decellularised tissue was washed with sterile water for several times, lyophilised, and pulverised using a Thomas Wiley Mini-Mill (Thomas Scientific, Swedesboro, NJ, USA). The resulting dECM powder was digested for 5 hours in 0.1 % (w/v) pepsin with 0.01 M HCl, before centrifugation to remove the undissolved particles. The mixed solution was adjusted to pH ~7.4 using 1 M NaOH and 0.1 M HCl solutions, and 10× Dulbecco's modified Eagle medium solution was added for ionic balance. Finally, the dECM pre-gel solution was obtained and stored at 4°C until use. Before fabrication of the cell-laden dDMs, PC12 or RSC96 cells at density ~1 × 10^7 cells/mL were pre-suspended in the dECM pre-gel solution.

Cell culture

PC12 (lot No. 0481, RRID: CVCL_0481) and RSC96 (lot No. 0199, RRID: CVCL_4694) cells were purchased from Procell Life Science & Technology Company (Wuhan, China). The cells were cultured in Dulbecco's modified Eagle medium/F12 medium (Gibco, Waltham, MA, USA) with additional 10% (v/v) foetal bovine serum (Gibco) and 1% (v/v) penicillin/streptomycin (100 U/mL, Invitrogen, Carlsbad, CA, USA), respectively. HUVECs were purchased from Zhong Qiao Xin Zhou Biotechnology (Shanghai, China; DFSC-EC-01) and cultured using endothelial cell medium (Science Cell, San Diego, CA, USA) with 5% (v/v) foetal bovine serum, 1% (v/v) endothelial cell growth supplement (Science Cell), and 1% (v/v) penicillin/streptomycin. All the abovementioned cells were incubated at 37°C with 95% humidity and 5% CO_2 before use. The culture medium was refreshed every 3 days. At confluence, the cells were washed with PBS twice, detached using 0.25% trypsin-ethylenediaminetetraacetic acid (Meilunbio) for 1 minute, and counted before mixing with the prepared bioink for encapsulation and bioprinting. To better locate the cells, PC12 cells were pre-labelled with Cell Tracker Green Fluorescent Probe (20 mM, Invitrogen).

Fabrication of cell-laden microgels

Droplet-based microfluidic devices were fabricated using a previously described procedure.[25] Briefly, negative photoresist (Microchem, Westborough, MA, USA) was first spin-coated on a clean silicon wafer. After baking at 80°C for 10 minutes and 150°C for another 5 minutes, the photoresist was exposed to ultraviolet (UV) light through a photomask and then developed in a developer solution. A mixture of polydimethylsiloxane (PDMS, Sylgard 184, Dow Corning, Midland, MI, USA) consisting of PDMS base and curing agent (10:1 w/w) was poured onto the silicon wafer, degassed in a vacuum oven, and cured on a hot plate at 70°C for 5 hours. The structured PDMS chip was punched through using a miniature hole punch to introduce two 1-mm-diameter inlet wells ("I_1" and "I_2" in **Figure 2A**) and a 2-mm-diameter outlet well ("O" in **Figure 2A**). The PDMS replica was peeled off and sealed with a glass slide using oxygen plasma (30 W, PDC-MG, MING HENG, Beijing, China).

All kinds of equipments used were pre-treated with an autoclave sterilizer or UV light (wavelength ~365 nm) for 12 hours, prior to microgel preparation in a biosafety cabinet. The oil phase solution was prepared using fluorinated carbon oil (3M HFE 7500, Saint Paul, MN, USA). The drops were stabilised by a biocompatible triblock perfluorinated copolymer surfactant (0.5 % w/v, PEG-Krytox-PEG, RAN Biotech, Beverly, MA, USA), and the cell-laden dECM pre-gel solution (1 × 10^7 cells /mL) was used as the aqueous phase. The oil and aqueous phase solutions were respectively injected into inlets I_1 and I_2, and the microfluidic chip was placed on ice to maintain the temperature at ~4°C. Water-in-oil droplets were formed at the conical head and flowed out from the outlet O, which was further stabilised in water bath at 37°C. After the microgels were collected, 20% (v/v) 1H,1H,2H,2H-perfluoro-1-octanol (PFO, Aladdin, Shanghai, China) was added to destabilize the oil-water interface, and then cell culture medium was added quickly to purify the microgels without centrifugation. Finally, the cell-laden microgels were re-suspended in culture medium. The sizes of the resultant microgels were determined using an optical microscope (Eclipse TS2, Nikon, Tokyo, Japan) and ImageJ software (v1.8, National Institutes of Health, Bethesda, MD, USA; n = 100).[31] The distribution curves corresponding to different flow rate ratios were graphed. The coefficient of variation (CV, %) was calculated using the following equation,

$$CV=SD/Mean \times 100\% \quad (1)$$

where Mean denotes the averaged diameter of the DMs, and SD represents the corresponding standard deviation.

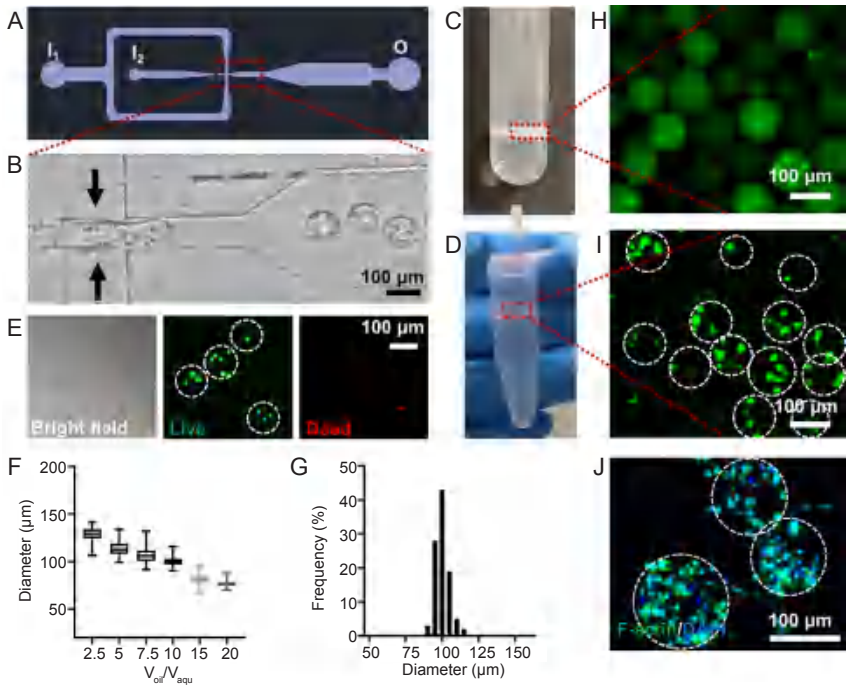

Figure 2. Preparation of the cell-laden DMs. (A) The design of the microfluidic device for high-throughput generation of microgels. Created using AutoCAD 2021. (B) Enlarged view of microfluidic chip during water-in-oil emulsification. (C, D) Photographs of DM collection after gelation (C) and PFO-based transfer into aqueous solution (D). (E) Live/dead staining showing the viability of cells encapsulated in the DMs, green: live cells, red: dead cells. (F) The diameters of the DMs were highly dependent on the flow rate ratio (Q_{oil}/Q_{aqu}) during emulsification. Data are expressed as mean ± SD. (G) Distribution of the DM diameters at Q_{oil}/Q_{aqu} = 10:1. Representative fluorescence micrographs showing the DMs containing the PC12 cells pre-labelled with Cell Tracker green fluorescent dye, when the DMs were dispersed in the (H) oil and (I) aqueous phases, respectively. (J) Fluorescence staining showed the cytoskeletal of PC12 cells encapsulated in the DMs, green: F-actin, blue: DAPI. The dashed lines circle out the DMs with pre-encapsulated PC12 cells. Scale bars: 100 μm. DAPI: 4′,6-diamidino-2-phenylindole; DMs: decellularised extracellular matrix microgels; PFO: 1H,1H,2H,2H-perfluoro-1-octanol; Q_{oil}: the flow rate of the oil phase; Q_{aqu}: the flow rate of the aqueous phase.

The number of encapsulated cells in each microgel was counted using micrographs taken by an optical microscope (Eclipse TS2, Nikon) and ImageJ software (n > 300).

Preparation of DM-GelMA composite bioink

The rinsed microgels were centrifugated at 270 G for 1 minute to remove extra fluids. Then an equal volume of 16% (w/v) GelMA and 0.6% (w/v) photoinitiator lithium phenyl-2,4,6-trimethylbenzoylphosphinate mixture was added as the second phase to obtain the final concentration of GelMA at 8% (w/v). The microgels occupied around 50% of the total volume in the DM-GelMA composite bioink. The bioink was gently blown through a pipette gun to reach complete mixing and homogeneous DM dispersion.

Rheological characterisation

Rheological measurements were performed using a Kinexus pro$^+$ rheometer (Malvern Instruments Ltd., Malvern, UK) with a plate-plate geometry (20 mm) at 1-mm gap. Viscosity measurements were carried out using a shear-rate ramp at 25°C. The rheometry test was performed in an oscillatory time-sweep mode with a plate-plate geometry at 0.1% strain, 1 Hz frequency, and 1 mm gap to monitor the kinetics of photo-induced gelation. The hydrogel precursors were first placed on a quartz plate, and UV light (365 nm, 5 mW/cm^2) was then turned on 60 seconds after the geometrical measurements had started recording.

Degradation properties of DM-GelMA bioink

Two bioinks, including the DM-GelMA and GelMA alone, were prepared into hydrogel discs with the same size, then immersed in PBS and subjected for aseptic degradation at 37°C for three weeks, respectively. After the samples were taken out, they were washed with deionised water three times, lyophilised, and weighed at different time points (1, 3, 7, 14, and 21 days), respectively. The m_0/m' ratio was used to evaluate the residual mass of each sample, where m_0 was the original dry mass, and m' was the mass of the lyophilised hydrogel at each time point.

Circularity of decellularised extracellular matrix microgels after extrusion

After extrusion through a narrow needle, the DMs might have underwent obvious deformation and loss of the standard circular shape. The circularity (C) of an enclosed area is defined and calculated using the following equation,

$$C=4\pi A/L^2 \quad (2)$$

where L denotes the perimeter, and A denotes the area. When the C value was approaching 1, the shape of the measured DM

was closer to a circle. The polydisperse DMs were extruded through needles with different inner diameters. The microgels were pre-labelled with fluorescein isothiocyanate (FITC, Macklin, Shanghai, China) for visualization of the DMs and their morphological variations. The circularities after bioink extrusion were employed to evaluate the extrudability of the DMs.

Printability

The estimation of bioink printability was implemented based on a previously reported semi-quantitative method.[32] An ideal gelation state of a bioink results in an extruded filament that demonstrates a clear morphology with smooth surface, regular grids, and square holes in the bioprinted constructs. Here, the printability (*Pr*) of an enclosed area is defined as the following,

$$Pr=\pi/4\bullet 1/C=L^2/16A \quad (3)$$

To determine the printability, optical micrographs of the bioprinted constructs were captured using a microscope (Eclipse TS2, Nikon) and analysed using ImageJ software (n = 20).

Bioprinting process

The DM-GelMA bioink was first stored in the bioink reservoir at 20°C for 25 minutes to allow transformation from an aqueous state to a pre-gel state, then extruded at pressure ~1.1 bar and printing speed ~5 mm/s using an extrusion-based 3D bioprinter (3D Bioplotter, EnvisionTEC, Gladbeck, Germany). The 10 × 10 × 1.28 mm^3 sized grids were collected on a receiving plate at 15°C and then exposed to UV irradiation (365 nm, 5 mW/cm^2) for 50 seconds. In some cases, microgels were pre-labeled with FITC for observation by a confocal laser fluorescence microscope (LSM710, Zeiss, Baden-Württemberg, Germany). PC12 cell-containing DM-GelMA bioink and GelMA bioink were bioprinted at the same cell density (5 × 10^6 cells /mL) and printing conditions (pressure ~1.1 bar and printing rate ~5 mm/s). Finally, the cell-laden 3D bioprinted constructs were transferred into a 12-well culture plate and incubated at 37°C with 95% humidity and 5 % CO_2.

RSC96 cells and HUVECs co-culture in the bioprinted scaffold

RSC96 cells and HUVECs were pre-labelled with Cell Tracker Green CMFDA (20 mM, Invitrogen) and Cell Tracker Orange CMTMR (20 mM, Invitrogen) fluorescent dyes, respectively. To prepare the modular bioink for bioprinting and co-culture of RSC96 cells and HUVECs, the RSC96-cell-encapsulated microgels were transferred to a low-adhesion culture flask, and a sufficient medium was added for suspension culture. These microgels were collected through centrifugation, and an equal volume of GelMA pre-mixed with HUVECs (2.5 × 10^6 cells/mL) was added. Fluorescence images were taken on the 3D bioprinted scaffolds using a confocal laser microscope (LSM710, Zeiss).

Cell viability and proliferation assays

Cell viability within the cell-laden microgels and 3D bioprinted structures were examined using Calcein-AM/PI Double Staining Kit (Meilunbio) by following the manufacturer's instructions. Briefly, after removing the culture medium, the samples were rinsed with PBS three times and incubated with 2 mM Calcein AM (live cell stain, green) and 4.5 mM propidium iodide (dead cell stain, red) at 37°C for 15 minutes. The samples were observed using a confocal laser scanning microscope (LSM710, Zeiss). Cell viability was calculated by dividing the number of live cells by the total cell number. After three days of culture, the cells were fixed with 4% (w/v) paraformaldehyde, washed with PBS, and incubated in PBS containing 5% (w/v) bovine serum albumin (BSA, Meilunbio) and 0.3% (v/v) Triton X-100 for an hour at 37°C. Then, the cells were incubated with Phalloidin-iFluor 488 Conjugate (Solarbio, Beijing, China) for an hour at 25°C and washed with PBS three times. The cell nuclei were stained with DAPI (Sigma-Aldrich).

Statistical analysis

Experiments were implemented using triplicate samples. Data are presented as mean ± standard deviation (SD). Statistical analyses including Student's *t*-test and one-way analysis of variance, followed by Tukey's *post hoc* analysis, were performed for two-group and multi-group comparisons, respectively. P values < 0.05 were considered statistically significant. Statistical analyses were performed using GraphPad Prism (version 9.0.0 for Windows, GraphPad Software, San Diego, CA, USA, www.graphpad.com).

Results

Fabrication and characterisation of cell-laden dECM microgels

The cell-laden DMs were primarily fabricated using a flow-focusing microfluidic device which was similar to our previously reported temperature-controlled microfluidic system,[25] but with PC12 cells pre-encapsulated in the aqueous phase (the microfluidic chip is schematically illustrated in **Figure 2A**). To reach a stable water-in-oil emulsion, the cell-laden dECM pre-gel solution continuously flowed into the microchannels through inlet I_2. In the meantime, fluorinated carbon oil containing biocompatible triblock Krytox-PEG-Krytox surfactant flowed into the microchannels through inlet I_1. Water-in-oil droplets were generated under shear flow at the intersection of oil and water channels (**Figure 2B**, and **Additional Video 1**). The encapsulated PC12 cells were easily visualised within the droplets using an optical microscope (**Figure 2B**). The cell-laden droplets were collected and formed microgels in a water bath at 37°C through temperature-dependent solution-gel transition. The resulting DMs were floating within the oil phase due to their lower density (**Figure 2C**). The addition of PFO led to a quick phase separation which successfully transferred the microgels into the aqueous culture medium (**Figure 2D**). There was no significant difference in the viability of PC12 cells before and after preparation (**Figure 2D**, and **Additional Figure 1**). It was noticed that the sizes of the microgels were highly dependent on the flow rate ratios between the oil phase (Q_{oil}) and aqueous phase (Q_{aqu}). The average diameters of the microgels were 128 ± 7, 114 ± 8, 107

± 8, 101 ± 5, 82 ± 6, and 77 ± 4 μm for Q_{oil}/Q_{aqu} = 2.5, 5, 7.5, 10, 15, and 20, respectively (**Additional Figure 2**). Generally, a greater Q_{oil}/Q_{aqu} ratio resulted in smaller microgels (**Figure 2F**). However, when Qaqu exceeded 1.0 mL/h, the cell-laden dECM pre-gel solution cannot form droplets no matter how large the Qoil was. On the other hand, though homogeneous DMs were observed generating in the microfluidic device for Qaqu less than 0.2 mL/h, the yield of products was very low. Since the sizes of cell-laden microgels are often required optimization for sufficient oxygen and nutrients exchange,[33] along with the diameter dispersity and yield of microgels. In this study, the DMs with a diameter of 101 ± 5 μm were chosen for further investigation, in which case (Q_{oil}/Q_{aqu} = 10), the sizes of the DMs followed a narrow Gaussian distribution, and the coefficient of variation was 4.7 % (**Figure 2G**).

The presence of PC12 cells pre-stained with Cell Tracker Green Fluorescent Probes was easily evident using fluorescence microscopy, which was found respectively in oil and aqueous phases during preparation (**Figure 2H** and **I**). The number of cells was vaguely counted under a microscope, which showed that 0–12 cells were found encapsulated in each DM, while most of the DMs likely contained 3–6 cells (**Additional Figure 3**). Furthermore, F-actin fluorescence staining on the DMs clearly implicated the growth of encapsulated PC12 cells (**Figure 2J**). Overall, the cell-laden DMs were successfully fabricated through emulsification in a flow-focusing microfluidic device and optimised for bioink preparation.

Preparation and characterisation of DM-GelMA bioink

Prior to DM-GelMA bioink preparation, the cell-laden DMs required centrifugation for volume control. However, it was noticed that the centrifugation-induced shear stress can cause damage to the encapsulated cells. Herein, the duration of centrifugation was investigated and optimised for cell survival. Live/dead staining showed that cell viability decreased with prolonged centrifugation (**Additional Figure 4**). But when the centrifugation was too short (i.e., half a minute), most of the microgels remained in the supernatant. To prepare the DM-GelMA composite bioink, centrifugation at 270 G for just one minute was chosen for guaranteed DM compaction and maximised cell viability (89.1 ± 3.0%). The compact DMs were gently blended with homemade GelMA solution (NMR characterisation; **Additional Figure 5**) at volume ratio (DM: GelMA) = 1:1, resulting in the DM-GelMA composite bioink with GelMA concentration at 8% (w/v). The rheological properties of the DM-GelMA composite were assessed to investigate the changes in mechanical properties, and compared to GelMA hydrogel at the same concentration. It was noted that the viscosity of the DM-GelMA composite hydrogel decreased with increasing shear rate, implicating the preservation of shear-thinning property from GelMA hydrogel which enables nozzle-based extrusion (**Figure 3A**). Furthermore, in-situ photo-rheometry tests were performed to evaluate the mechanical properties in response to photocrosslinking. UV light (365 nm, 5 mW/cm^2) was turned on one minute after the rheology test had begun, gel points of both DM-GelMA and GelMA appeared immediately upon irradiation (**Figure 3B**). It was interesting to notice that the DM-GelMA composite hydrogel exhibited a slightly larger storage modulus than that of GelMA hydrogel alone, but resulted in much less storage modulus than GelMA after photocrosslinking (**Figure 3C**). To assess the degradation performance of GelMA and DM-GelMA hydrogels *in vitro*, both specimens were immersed in PBS. It was evident that the dry weights of both hydrogels dropped rapidly for the first three days, then underwent slow degradation. The final residual mass of the DM-GelMA composite hydrogel was 53.0 ± 5.1%, and that was 61.9 ± 2.1% for the GelMA hydrogel after 21 days of PBS immersion.

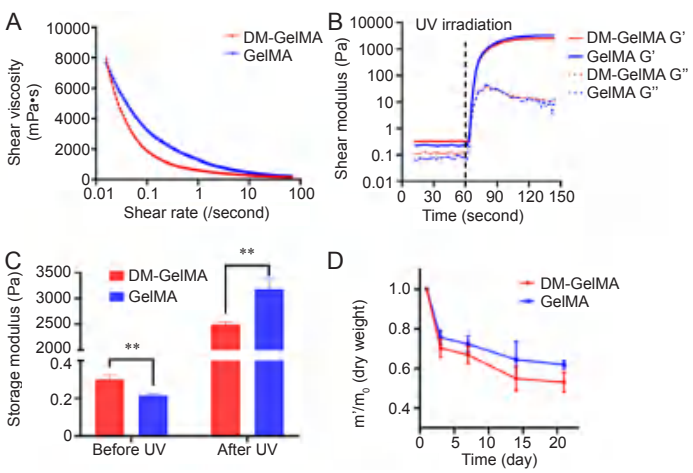

Figure 3. Rheological properties of the DM-GelMA composite hydrogel. (A) Rheology assessments showed shear-thinning behaviors evident in both DM-GelMA and GelMA hydrogels. (B) The shear moduli of both DM-GelMA and GelMA hydrogels, UV light was turned on 60 seconds after the rheology test had begun. G' (solid lines): storage modulus, G" (dashed lines): loss modulus. (C) Storage moduli of both DM-GelMA and GelMA hydrogels before and after UV photocrosslinking. Data are presented as means ± SD. $^{**}P < 0.01$ (Student's *t*-test). (D) Degradation of both DM-GelMA and GelMA hydrogels presented as the ratio of residual mass during 3 weeks of PBS immersion. m_0: the original dry mass, *m*': the mass of the lyophilised hydrogel at each time point. DM: decellularised extracellular matrix microgel; GelMA: gelatin methacryloyl; PBS: phosphate buffered saline; UV: ultraviolet.

Extrusion of DM-GelMA bioink

In this study, the FITC-labeled DMs with varying sizes were extruded through needles with different inner diameters, respectively. First, the DM-GelMA hydrogels containing polydisperse DMs were ejected from different needles. It was noted that the DM sizes had their own upper limits to ensure continuous extrusion without clotting or jamming, which were all slightly larger than the inner diameters of corresponding needles (**Figure 4A**). This is most likely due to the elasticity of the microgels and energy dissipation through shear-induced deformation.

For the DM-GelMA hydrogels containing monodisperse DMs with ~100 μm in diameter, needles with three different inner diameters (Φ = 110 μm, 210 μm, and 410 μm) were assessed for extrusion-based 3D printing, respectively. The morphology change of the ejected microgels was used to determine the optimised needle size. In most cases, the DMs within the composite hydrogel underwent deformation after extrusion, more or less, apart from their original circular shape (depicted in **Figure 4B**). The circularity (*C*) of each extruded DM was calculated to evaluate the extrudability through different needles. Whenever *C* is closer to 1, the morphology of that DM was nearly spherical. It was evident that the circularities of the extruded DMs were approximately 1.05, when needles with an inner diameters of 210 and 410 μm were used (**Figure 4C**). However, both average circularities and their deviation changed significantly after the DM-GelMA hydrogel were ejected from 110-μm needles. These results indicated that the nozzle-induced shear can be considered harmless, when the inner diameter of the needle was more than twice as much as the size of the DMs.

Even though the utilization of needles with inner diameter of either 210 μm or 410 μm caused little damage to the DMs, the microgel distribution was varied after extrusion (**Figure 4D**). The density of DMs found in the extruded filament through 210-μm needles is much lower than that extruded from 410-μm needles (**Figure 4E**). Furthermore, serious stagnation and disfluency often occurred during continuous extrusion using 210-μm needles, which led to poor structural fidelity.

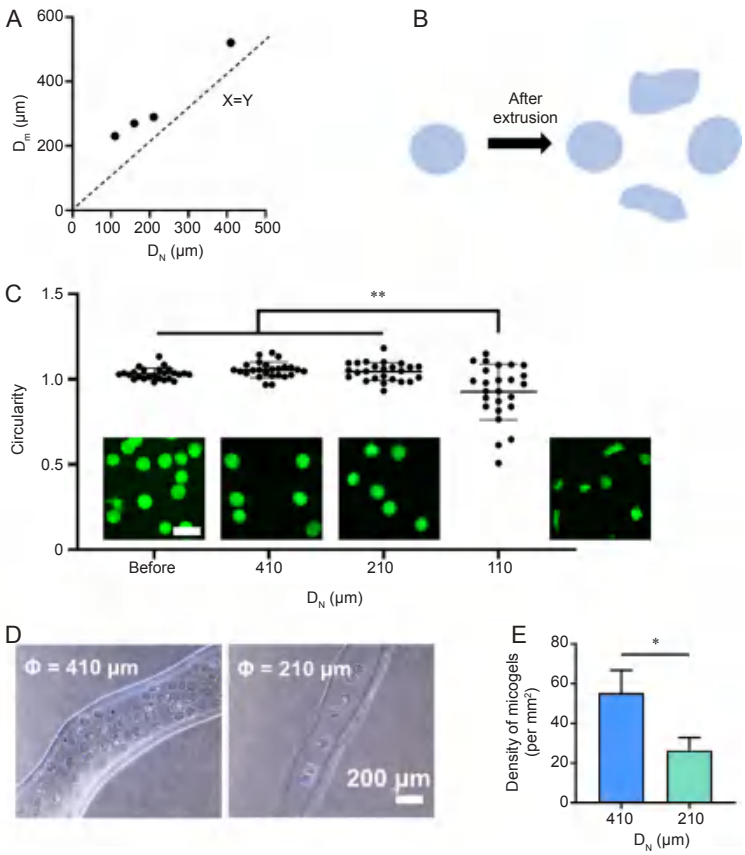

Figure 4. Extrusion of the DM-GelMA hydrogel and preservation of DM morphology. (A) The relationship between different sized needles and their corresponding maximum extrudable DM sizes. DN is the inner diameter of the needles, and Dm is the maximum size of the DMs. The dashed line represents a specific condition when the inner diameter of the needle is equal to the DM size. (B) The schematic diagram illustrates the changes in microgel morphology after extrusion. Created using Microsoft PowerPoint 2020. (C) The circularity of DMs post-extrusion using different sized needles, and representative fluorescence micrographs show the extruded microgels pre-labelled with FITC. Scale bars: 200 μm. Data are expressed as the mean ± SD. $^{**}P < 0.01$ (one-way analysis of variance followed by Tukey's *post hoc* analysis). (D) The 3D bioprinted filaments extruded from 410- and 210-μm needles, respectively. (E) The density of microgels in the 3D bioprinted filaments using 410- and 210-μm needles. Data are expressed as the mean ± SD. $^{*}P < 0.05$ (Student's *t*-test). DM: decellularised extracellular matrix microgel; FITC: fluorescein isothiocyanate; GelMA: gelatin methacryloyl.

Printability of DM-GelMA bioinks

To evaluate the printability of the DM-GelMA bioink, 100-μm monodisperse DMs were pre-mixed with GelMA solution, and then subjected to an extrusion-based bioprinter using 410-μm needles. It was noted that the DM-GelMA composite was extruded continuously and smoothly into cylindrical filaments, exhibiting a proper-gelation condition (**Figure 5A**). The composite hydrogel was 3D printed into standard grid frameworks consisting of at least four layers without obvious interlayer mismatch (**Figure 5B** and **C**). The multilayer filaments were well-distinguished using optical microscopy (**Figure 5D**), and no severe deformation or delamination was evident in the 3D construct, indicating a considerable structural fidelity. Meanwhile, it was noted that most of the FITC-labelled DMs remained spherical and nicely embedded within the bioprinted filaments (**Figure 5E**). No significant microgel collapse or damage was observed. Finally, a previously reported semi-quantitative approach was used for the estimation of the bioink printability.[32] The calculated printability (P_r) values of the DM-GelMA hydrogel were in the range of 1.0–1.1 (**Figure 5F**), indicating that the 3D printed holes displayed similar shapes that were comparable to regular squares (P_r = 1). These results confirmed that the DM-GelMA composite bioink exhibited good printability and structural fidelity in extrusion-based bioprinting.

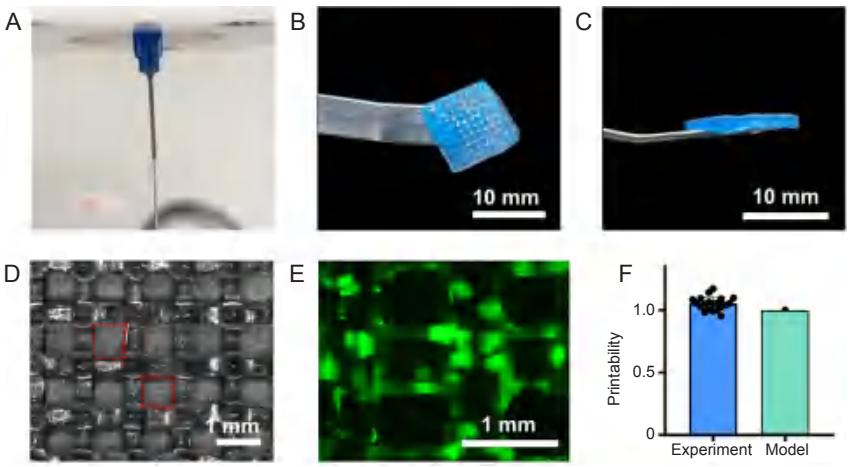

Figure 5. Printability of the DM-GelMA bioink. (A) The DM-GelMA hydrogel was extruded continuously and smoothly, showing a proper-gelation condition for 3D printing. The (B) top-view and (C) side-view of a representative 3D printed grid mesh using DM-GelMA hydrogel. (D) The grid framework 3D printed by DM-GelMA hydrogel, observed by optical microscopy. (E) A representative fluorescence micrograph showed the FITC-labelled DMs (green) embedded in the 3D printed construct. Scale bar: 10 mm (B, C) and 1 mm (D, E). (F) The P_r of the DM-GelMA bioink ("Experiment") compared with a regular square shape ("Model", P_r = 1), analysed accordingly to a previously reported semi-quantitative method. 3D: three-dimensional; DM: decellularised extracellular matrix microgel; FITC: fluorescein isothiocyanate; GelMA: gelatin methacryloyl; P_r: printability.

Cell viability in modular DM-GelMA bioinks

To prepare a sort of modular bioinks, PC12 cells were either pre-mixed with GelMA solution and then blended with the DMs alone to form the DM/(GelMA + Cells) bioink, or pre-encapsulated in the DMs then mixed with GelMA to form (DM + Cells)/GelMA bioink. The PC12 cells were 3D cultured in both bioinks for 4 days, and compared with those directly encapsulated in the GelMA hydrogel at the same concentration (8% w/v, denoted as GelMA + Cells bioink). It was encouraging to note that both DM containing bioinks (DM/(GelMA + Cells) and (DM + Cells)/GelMA) exhibited high cell viability (> 90%), while that of the GelMA + Cells bioink was less than 80% (**Figure 6A** and **B**).

Besides the 3D culture, post-printing cell viability is of great importance in extrusion-based bioprinting. Live/dead staining was implemented after the extrusion-based bioprinting using the DM-GelMA bioink with PC12 cells pre-encapsulated in the DMs (i.e., the (DM + Cells)/GelMA bioink) and compared with the GelMA bioink (i.e., the GelMA + Cells bioink). Dramatic difference in post-printing cell viability was clearly evident between these two bioinks (**Figure 6C**). Statistically, the viability in the DM-GelMA bioink was 86.3 ± 3.2%, which was almost twice as much as that of the GelMA bioink (43.4 ± 3.9%), by following the same bioprinting conditions that basically consisting of hydrogel extrusion and photocrosslinking (**Figure 6D**).

3D bioprinted DM-GelMA scaffolds with heterogeneous cells/materials distribution

In the experimental realization, the RSC96 Schwann cells were pre-loaded in the DMs, while the HUVECs were pre-mixed with GelMA pre-gel solution, then gently blended together to form heterogeneous modular bioink for extrusion-based bioprinting (**Figure 7A**). Since the RSC96 cells and HUVECs were pre-stained with green and orange Cell Tracker Fluorescent Probes, respectively, they were easily visualised in the bioprinted filaments using laser scanning confocal microscopy (**Figure 7B**). Furthermore, 3D confocal micrographs showed homogeneous distribution of green RSC96 cells embedded in the microgels, while the orange HUVECs were also distributed evenly outside the microgels (**Figure 7C**). As a result, a modular 3D co-culture system was successfully constructed owing to the utilization of DM-GelMA composite bioink.

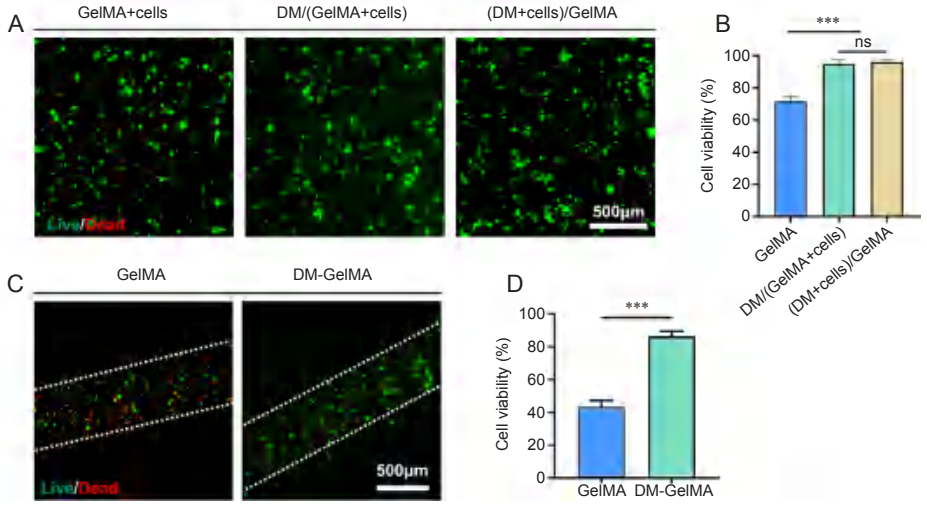

Figure 6. Cell viability in the modular bioinks. (A) Representative fluorescence micrographs after live/dead staining on the PC12 cell-encapsulated bioinks and 3D cultured for 4 days. "GelMA+Cells" represents the bioink that PC12 cells were directly mixed with GelMA solution. "DM/(GelMA+Cells)" represents the bioink consisting of prepared DMs and PC12-cell-encapsulated GelMA solution. "(DM+Cells)/GelMA" denotes the bioink prepared by mixing PC12-cell-encapsulated DMs and GelMA solution. Green: live cells; red: dead cells. (B) Cell viability of the PC12 cells within the abovementioned bioinks based on the fluorescence images shown in A. Data are expressed as the mean ± SD. ***P < 0.001 (one-way analysis of variance followed by Tukey's *post hoc* analysis). (C) Representative fluorescence micrographs after live/dead staining on the bioprinted filaments using cell-laden GelMA and DM-GelMA bioinks, respectively. Green: live cells; red: dead cells. Scale bars: 500 μm. (D) Post-printing cell viability based on the fluorescence images shown in C. Data are expressed as the mean ± SD. ***P < 0.001 (Student's t-test). DM: decellularised extracellular matrix microgel; GelMA: gelatin methacryloyl; ns: no significance.

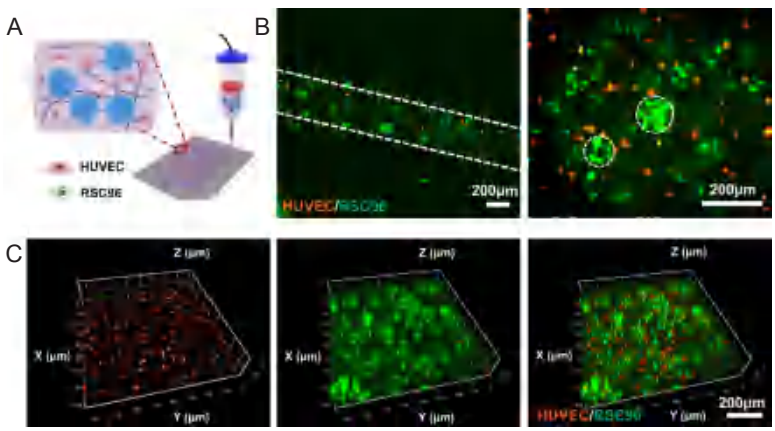

Figure 7. 3D bioprinting of multiscale DM-GelMA bioink for RSC96 cells and HUVECs co-culture. (A) Schematic illustration of extrusion-based bioprinting using HUVECs and RSC96 cell-laden DM-GelMA bioink. Created with 3D Max 2021. (B, C) 2D views (B) and 3D views (C) of the bioprinted 3D constructs using the cell-laden DM-GelMA composite bioink, characterised by confocal laser fluorescence microscopy. RSC96 cells and HUVECs were pre-stained with green and orange Cell Tracker Fluorescent Probes, respectively, prior to cell encapsulation. Scale bars: 200 μm. 2D: two-dimensional; 3D: three-dimensional; DM decellularised extracellular matrix microgel; GelMA: gelatin methacryloyl; HUVEC: human umbilical vein endothelial cell.

Discussion

Nowadays, microfluidic emulsification technique is widely used in the preparation of cell-laden microgels, due to the well-controlled particle size and cell loading capacity. In our microfluidic approach for high-throughput DM production, the oil/aqueous interface was stabilised by surfactant which inhibited emulsion coalescence. However, the DMs had to be exchanged into aqueous medium for cell culture. Therefore, PFO was employed to replace the fluorinated surfactant on the surface of the microgels and reduce the stability of oil-aqueous interface,[34] leading to a much faster phase separation. Once the oil-aqueous interface was destabilised, the cell culture medium was added quickly to purify the microgels without centrifugation. Further live/dead staining assay showed that this PFO-based method effectively shortened the time for cells' exposure to harsh oil reagents, and protected them from high

mechanical stresses caused by centrifugation that is frequently used in traditional methods.[35] Furthermore, the conditions for dECM gel formation (pH = 7, 37°C) were physiologically friendly to cells. The abovementioned processes contributed to the high cell viability in the DMs, in addition to the intrinsic bioactivities of the dECM.

The biodegradability and degradation rate are important parameters to evaluate bioinks, in terms of their feasibility in biomedical applications. The DM-GelMA hydrogel degraded slightly faster than GelMA, since dECM hydrogels often undergo fast degradation.[36] Despite that, the DM-GelMA composite hydrogel remained relatively stable within three weeks. After ejection from the nozzle and collected on the receiving plate, the GelMA solution formed an initial shape at a relatively low temperature owing to the thermosensitivity of gelatin. This initial structure was then reinforced by photocrosslinking. The results from *in-situ* crosslinking test showed that the DM-GelMA hydrogel reached a completely crosslinked state within 50 seconds until the bioprinted structure was fixed, implicating that it can serve as a suitable bioink for extrusion-based bioprinting. The photo-crosslinked DM-GelMA bioink exhibited less storage modulus than that of the GelMA bioink. We conjecture that this was due to the embedded microgels with much smaller mechanical strength compared to the photo-crosslinked GelMA, which presented as many "defects" within the GelMA hydrogel network.

The needle sizes are crucial for structural fidelity and cell survival in nozzle-based bioprinting,[37] especially for those using microgel-based bioinks. When the nozzle tip is too fine, high shear stress can induce severe damage to the microgels and their inner cells.[18] On the other hand, much larger needles lead to poor resolution of the bioprinted structures. Ideally, the microgels should remain intact after extrusion bioprinting. While, the selection of needle sizes should take both post-printing cell viability and structural fidelity into consideration. Based on our experimental observation during bioprinting, we speculated that some extent of DM jamming happened at either end of the nozzle, causing uneven distribution of the DMs within the extruded filaments or even clotting in the 210-μm needles. However, such jamming effect was not observed when the needles with 410-μm inner diameter were used, since the nozzle was wide enough to allow the smooth and continuous flow of DM-GelMA bioink during extrusion.

High cell viability is essential for the extrusion-based cell-laden bioprinting,[11] which is mainly determined by the suitable 3D microenvironment provided by hydrogels and their protection during nozzle ejection. The post-printing viability of the DM-GelMA bioink was almost twice as much as that of the GelMA bioink, which revealed that the DMs effectively protected the encapsulated cell from shear damage. Meanwhile, the addition of DMs played a vital role in facilitating cell survival in the bioinks, attributed to the prominent bioactivity of the dECM components for cell accommodation and the large specific area provided by the microgels for mass exchange. Both effects contributed to the greatly elevated cell viability through extrusion-based bioprinting.

Finally, most tissues and organs consist of various cell types and their corresponding ECM microenvironment that work synergistically for specific biological functions in human body. For instance, Schwann cells play a central role in peripheral nerve regeneration due to their secretion of various cytokines (e.g., nerve growth factor) and remyelination.[38] Meanwhile, angiogenesis occurs alongside neurogenesis, the growing blood vessels provide nutrients and oxygen for nerve cell metabolism.[39] As a proof-of-concept, the DM-GelMA bioink was employed as a modular system to integrate both RSC96 Schwann cells and HUVECs in the same 3D bioprinted scaffold. Meanwhile, the prepared DMs also preserve various ECM components from native nerve tissues that can effectively promote neurite growth and remyelination.[40, 41] Compared with the traditional methods which directly mix different cell types, The DM-GelMA bioink-based co-culture system exhibited much better control of the cell/material compositions and bioprinted structures. Considering the numerous cell combinations, cell-cell interactions, and tissue-specific dECM hydrogels that can easily replace any of the modules in the bioink, this sort of multi-modular composite bioinks holds great promise in future bioprinting and tissue engineering.

In summary, a modular DM-GelMA composite bioink was successfully developed and applied for extrusion-based bioprinting. First, the cell-laden DM module was continuously fabricated using a cell-friendly microfluidic-based strategy. Upon integrating cell-laden DMs into GelMA, the composite bioink provided both bioactive microenvironment and cell protection from nozzle-induced shear damage, resulting in highly enhanced post-printing cell viability. Moreover, using the optimised DM sizes and needle sizes, the DM-GelMA bioink exhibited good printability and convenient bioprinting conditions. Finally, as a proof-of-concept, the modular bioink consisted of RSC96 cell-encapsulated DMs and HUVEC-loaded GelMA was used for 3D bioprinting, a co-culture system was obtained in a 3D printed construct. We believe that this type of modular bioinks enables bioprinting for multi-component and multi-functional tissue fabrication with precisely controlled cells and materials localization. In the future, *in vivo* validations are highly desired for versatile applications of the DM-GelMA modular bioinks in regenerative medicine.

Author contributions

Validation, investigation, visualization: HC, KZ, PS, ZL; methodology: ZR, JZ, LY; formal analysis: HC; writing - original draft: HC; writing - review & editing: ZR, YB; conceptualization, project administration, supervision, funding acquisition: DQ, YB. All authors approved the final version of this manuscript.

Financial support

This work was supported by National Natural Science Foundation of China, Nos. 32171353, 52073314, Guangdong Key Areas Research and Development Program, No. 2020B1111150003, Guangdong Basic and Applied Basic Research Foundation, No. 2022A1515011388, Science and Technology Projects of Guangzhou, No. 202002020078.

Acknowledgement

None.

Conflicts of interest statement

The authors declare no conflict of interest.

Open access statement

This is an open access journal, and articles are distributed under the terms of the Creative Commons Attribution-NonCommercial-ShareAlike 4.0

License, which allows others to remix, tweak, and build upon the work non-commercially, as long as appropriate credit is given and the new creations are licensed under the identical terms.

Additional files

Additional Video 1: Preparation of the cell-laden DMs by microfluidic emulsification.

Additional Figure 1: Cell viability of the PC12 cells encapsulated in the microgels.

Additional Figure 2: The micrographs and the distribution of the diameters of the microgels for Q_{oil}/Q_{aqu} = 2.5, 5, 7.5, 10, 15, and 20, respectively.

Additional Figure 3: The number of cells encapsulated in each microgel and its corresponding frequency of appearance.

Additional Figure 4: The viability of encapsulated PC12 cells decreased with increasing centrifugation time.

Additional Figure 5: ^{1}H-NMR characterisation of gelatin and GelMA.

1. Daly, A. C.; Prendergast, M. E.; Hughes, A. J.; Burdick, J. A. Bioprinting for the biologist. *Cell.* **2021**, *184*, 18-32.
2. Derakhshanfar, S.; Mbeleck, R.; Xu, K.; Zhang, X.; Zhong, W.; Xing, M. 3D bioprinting for biomedical devices and tissue engineering: A review of recent trends and advances. *Bioact Mater.* **2018**, *3*, 144-156.
3. Gungor-Ozkerim, P. S.; Inci, I.; Zhang, Y. S.; Khademhosseini, A.; Dokmeci, M. R. Bioinks for 3D bioprinting: an overview. *Biomater Sci.* **2018**, *6*, 915-946.
4. Unagolla, J. M.; Jayasuriya, A. C. Hydrogel-based 3D bioprinting: A comprehensive review on cell-laden hydrogels, bioink formulations, and future perspectives. *Appl Mater Today.* **2020**, *18*, 100479.
5. Ying, G.; Jiang, N.; Yu, C.; Zhang, Y. S. Three-dimensional bioprinting of gelatin methacryloyl (GelMA). *Bio-des Manuf.* **2018**, *1*, 215-224.
6. Bandyopadhyay, A.; Mandal, B. B.; Bhardwaj, N. 3D bioprinting of photo-crosslinkable silk methacrylate (SilMA)-polyethylene glycol diacrylate (PEGDA) bioink for cartilage tissue engineering. *J Biomed Mater Res A.* **2022**, *110*, 884-898.
7. Lee, J. M.; Suen, S. K. Q.; Ng, W. L.; Ma, W. C.; Yeong, W. Y. Bioprinting of collagen: considerations, potentials, and applications. *Macromol Biosci.* **2021**, *21*, e2000280.
8. Jia, J.; Richards, D. J.; Pollard, S.; Tan, Y.; Rodriguez, J.; Visconti, R. P.; Trusk, T. C.; Yost, M. J.; Yao, H.; Markwald, R. R.; Mei, Y. Engineering alginate as bioink for bioprinting. *Acta Biomater.* **2014**, *10*, 4323-4331.
9. Gao, Q.; Niu, X.; Shao, L.; Zhou, L.; Lin, Z.; Sun, A.; Fu, J.; Chen, Z.; Hu, J.; Liu, Y.; He, Y. 3D printing of complex GelMA-based scaffolds with nanoclay. *Biofabrication.* **2019**, *11*, 035006.
10. Busch, R.; Strohbach, A.; Pennewitz, M.; Lorenz, F.; Bahls, M.; Busch, M. C.; Felix, S. B. Regulation of the endothelial apelin/APJ system by hemodynamic fluid flow. *Cell Signal.* **2015**, *27*, 1286-1296.
11. Xu, H. Q.; Liu, J. C.; Zhang, Z. Y.; Xu, C. X. A review on cell damage, viability, and functionality during 3D bioprinting. *Mil Med Res.* **2022**, *9*, 70.
12. Adhikari, J.; Roy, A.; Das, A.; Ghosh, M.; Thomas, S.; Sinha, A.; Kim, J.; Saha, P. Effects of Processing parameters of 3D bioprinting on the cellular activity of bioinks. *Macromol Biosci.* **2021**, *21*, e2000179.
13. Luan, C.; Liu, P.; Chen, R.; Chen, B. Hydrogel based 3D carriers in the application of stem cell therapy by direct injection. *Nanotechnol Rev.* **2017**, *6*, 435-448.
14. Highley, C. B.; Song, K. H.; Daly, A. C.; Burdick, J. A. Jammed microgel inks for 3D printing applications. *Adv Sci (Weinh).* **2019**, *6*, 1801076.
15. Daly, A. C.; Riley, L.; Segura, T.; Burdick, J. A. Hydrogel microparticles for biomedical applications. *Nat Rev Mater.* **2020**, *5*, 20-43.
16. Fang, Y.; Guo, Y.; Ji, M.; Li, B.; Guo, Y.; Zhu, J.; Zhang, T.; Xiong, Z. 3D printing of cell-laden microgel-based biphasic bioink with heterogeneous microenvironment for biomedical applications. *Adv Funct Mater.* **2022**, *32*, 2109810.
17. Chen, J.; Huang, D.; Wang, L.; Hou, J.; Zhang, H.; Li, Y.; Zhong, S.; Wang, Y.; Wu, Y.; Huang, W. 3D bioprinted multiscale composite scaffolds based on gelatin methacryloyl (GelMA)/chitosan microspheres as a modular bioink for enhancing 3D neurite outgrowth and elongation. *J Colloid Interface Sci.* **2020**, *574*, 162-173.
18. Xin, S.; Deo, K. A.; Dai, J.; Pandian, N. K. R.; Chimene, D.; Moebius, R. M.; Jain, A.; Han, A.; Gaharwar, A. K.; Alge, D. L. Generalizing hydrogel microparticles into a new class of bioinks for extrusion bioprinting. *Sci Adv.* **2021**, *7*, eabk3087.
19. Feng, Q.; Li, D.; Li, Q.; Li, H.; Wang, Z.; Zhu, S.; Lin, Z.; Cao, X.; Dong, H. Assembling microgels via dynamic cross-linking reaction improves printability, microporosity, tissue-adhesion, and self-healing of microgel bioink for extrusion bioprinting. *ACS Appl Mater Interfaces.* **2022**, *14*, 15653-15666.
20. Zhao, X.; Liu, S.; Yildirimer, L.; Zhao, H.; Ding, R.; Wang, H.; Cui, W.; Weitz, D. Injectable stem cell-laden photocrosslinkable microspheres fabricated using microfluidics for rapid generation of osteogenic tissue constructs. *Adv Funct Mater.* **2016**, *26*, 2809-2819.
21. An, C.; Liu, W.; Zhang, Y.; Pang, B.; Liu, H.; Zhang, Y.; Zhang, H.; Zhang, L.; Liao, H.; Ren, C.; Wang, H. Continuous microfluidic encapsulation of single mesenchymal stem cells using alginate microgels as injectable fillers for bone regeneration. *Acta Biomater.* **2020**, *111*, 181-196.
22. Riederer, M. S.; Requist, B. D.; Payne, K. A.; Way, J. D.; Krebs, M. D. Injectable and microporous scaffold of densely-packed, growth factor-encapsulating chitosan microgels. *Carbohydr Polym.* **2016**, *152*, 792-801.
23. Xu, Y.; Zhou, J.; Liu, C.; Zhang, S.; Gao, F.; Guo, W.; Sun, X.; Zhang, C.; Li, H.; Rao, Z.; Qiu, S.; Zhu, Q.; Liu, X.; Guo, X.; Shao, Z.; Bai, Y.; Zhang, X.; Quan, D. Understanding the role of tissue-specific decellularized spinal cord matrix hydrogel for neural stem/progenitor cell microenvironment reconstruction and spinal cord injury. *Biomaterials.* **2021**, *268*, 120596.
24. Kim, B. S.; Das, S.; Jang, J.; Cho, D. W. Decellularized extracellular matrix-based bioinks for engineering tissue- and organ-specific microenvironments. *Chem Rev.* **2020**, *120*, 10608-10661.
25. Lin, Z.; Rao, Z.; Chen, J.; Chu, H.; Zhou, J.; Yang, L.; Quan, D.; Bai, Y. Bioactive decellularized extracellular matrix hydrogel microspheres fabricated using a temperature-controlling microfluidic system. *ACS Biomater Sci Eng.* **2022**, *8*, 1644-1655.
26. Abaci, A.; Guvendiren, M. Designing decellularized extracellular matrix-based bioinks for 3D bioprinting. *Adv Healthc Mater.* **2020**, *9*, e2000734.
27. Wang, T.; Han, Y.; Wu, Z.; Qiu, S.; Rao, Z.; Zhao, C.; Zhu, Q.; Quan, D.; Bai, Y.; Liu, X. Tissue-specific hydrogels for three-dimensional printing and potential application in peripheral nerve regeneration. *Tissue Eng Part A.* **2022**, *28*, 161-174.
28. Kim, M. K.; Jeong, W.; Lee, S. M.; Kim, J. B.; Jin, S.; Kang, H. W. Decellularized extracellular matrix-based bio-ink with enhanced 3D printability and mechanical properties. *Biofabrication.* **2020**, *12*, 025003.
29. Li, X.; Chen, S.; Li, J.; Wang, X.; Zhang, J.; Kawazoe, N.; Chen, G. 3D culture of chondrocytes in gelatin hydrogels with different stiffness. *Polymers (Basel).* **2016**, *8*, 269.
30. Fairbanks, B. D.; Schwartz, M. P.; Bowman, C. N.; Anseth, K. S. Photoinitiated polymerization of PEG-diacrylate with lithium phenyl-2,4,6-trimethylbenzoylphosphinate: polymerization rate and cytocompatibility. *Biomaterials.* **2009**, *30*, 6702-6707.

31. Schneider, C. A.; Rasband, W. S.; Eliceiri, K. W. NIH Image to ImageJ: 25 years of image analysis. *Nat Methods.* **2012**, *9*, 671-675.
32. Ouyang, L.; Yao, R.; Zhao, Y.; Sun, W. Effect of bioink properties on printability and cell viability for 3D bioplotting of embryonic stem cells. *Biofabrication.* **2016**, *8*, 035020.
33. Gal, I.; Edri, R.; Noor, N.; Rotenberg, M.; Namestnikov, M.; Cabilly, I.; Shapira, A.; Dvir, T. Injectable cardiac cell microdroplets for tissue regeneration. *Small.* **2020**, *16*, e1904806.
34. Akartuna, I.; Aubrecht, D. M.; Kodger, T. E.; Weitz, D. A. Chemically induced coalescence in droplet-based microfluidics. *Lab Chip.* **2015**, *15*, 1140-1144.
35. Zheng, Y.; Wu, Z.; Khan, M.; Mao, S.; Manibalan, K.; Li, N.; Lin, J. M.; Lin, L. Multifunctional regulation of 3D cell-laden microsphere culture on an integrated microfluidic device. *Anal Chem.* **2019**, *91*, 12283-12289.
36. Xu, J.; Fang, H.; Zheng, S.; Li, L.; Jiao, Z.; Wang, H.; Nie, Y.; Liu, T.; Song, K. A biological functional hybrid scaffold based on decellularized extracellular matrix/gelatin/chitosan with high biocompatibility and antibacterial activity for skin tissue engineering. *Int J Biol Macromol.* **2021**, *187*, 840-849.
37. Ning, L.; Yang, B.; Mohabatpour, F.; Betancourt, N.; Sarker, M. D.; Papagerakis, P.; Chen, X. Process-induced cell damage: pneumatic versus screw-driven bioprinting. *Biofabrication.* **2020**, *12*, 025011.
38. Rao, Z.; Lin, Z.; Song, P.; Quan, D.; Bai, Y. biomaterial-based schwann cell transplantation and Schwann cell-derived biomaterials for nerve regeneration. *Front Cell Neurosci.* **2022**, *16*, 926222.
39. Ogunshola, O. O.; Antic, A.; Donoghue, M. J.; Fan, S. Y.; Kim, H.; Stewart, W. B.; Madri, J. A.; Ment, L. R. Paracrine and autocrine functions of neuronal vascular endothelial growth factor (VEGF) in the central nervous system. *J Biol Chem.* **2002**, *277*, 11410-11415.
40. Zou, J. L.; Liu, S.; Sun, J. H.; Yang, W. H.; Xu, Y. W.; Rao, Z. L.; Jiang, B.; Zhu, Q. T.; Liu, X. L.; Wu, J. L.; Chang, C.; Mao, H. Q.; Ling, E. A.; Quan, D. P.; Zeng, Y. S. Peripheral nerve-derived matrix hydrogel promotes remyelination and inhibits synapse formation. *Adv Funct Mater.* **2018**, *28*, 1705739.
41. Chen, S.; Du, Z.; Zou, J.; Qiu, S.; Rao, Z.; Liu, S.; Sun, X.; Xu, Y.; Zhu, Q.; Liu, X.; Mao, H. Q.; Bai, Y.; Quan, D. Promoting neurite growth and schwann cell migration by the harnessing decellularized nerve matrix onto nanofibrous guidance. *ACS Appl Mater Interfaces.* **2019**, *11*, 17167-17176.

Received: June 4, 2023
Revised: June 15, 2023
Accepted: June 20, 2023
Available online: June 28, 2023